Electrochemical Society

Vol. 99,

UNIV. OF MICHIGAN
APR 8 1952
EAST ENGINEERING
LIBRARY

1902—FIFTIETH ANNIVERSARY—1952

Electronics Issue I

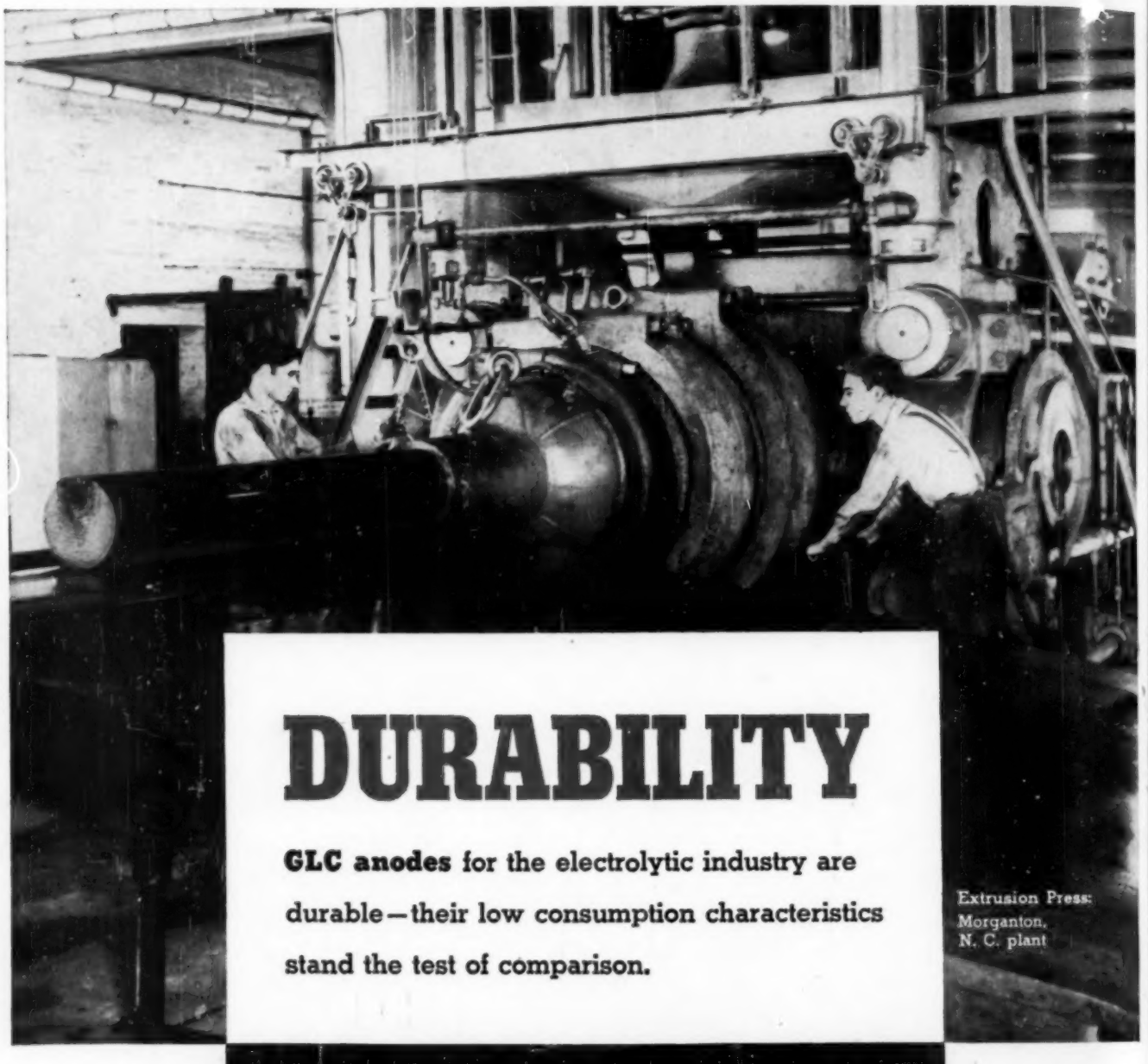

DURABILITY

GLC anodes for the electrolytic industry are durable—their low consumption characteristics stand the test of comparison.

Extrusion Press:
Morganton,
N. C. plant

Plants:
Niagara Falls, N. Y.
Morganton, N. C.

Great Lakes Carbon Corporation

GLC

ELECTRODE DIVISION · NIAGARA FALLS, N. Y.

Sales Offices:
Niagara Falls, N. Y.
New York, N. Y.
Chicago, Ill.
Pittsburgh, Pa.

Sales Representatives:
Birmingham, Ala.
Wilmington, Cal.

PRODUCTS OF GREAT LAKES CARBON CORPORATION

Electrode Division
Graphite anodes. Graphite and amorphous carbon electrodes. Carbon and graphite specialties.

Oil and Gas Division
Crude petroleum and natural gas.

Carbon Division
Petroleum coke. Calcined petroleum coke. Industrial carbons.

Dicalite Division
Diatomaceous silica for filter-aids, fillers and insulating uses.

Perlite Division
Perlite lightweight aggregates and products for the building, oil, foundry and other industries. Perlite ore.

Merchant Coke Plant
Premium foundry and industrial coke. Coke co-products.

Journal of the

Electrochemical Society

APRIL, 1952 VOLUME 99 • NUMBER 4

CONTENTS

Anniversary Features

The Electronics Division of the Society—Editorial. *John W. Marden* 77C
History of the Electronics Division of The Electrochemical Society. *John W. Marden* 79C
Growth of the Luminescence Section. *Rudolph Nagy* 81C

Technical Papers

Cadmium Chlorophosphate Phosphors. *Robert W. Wollentin, C. K. Lui Wei, and Rudolph Nagy* 131
Calcium Zinc Silicate Phosphor. *Rudolph Nagy, C. K. Lui Wei, and R. W. Wollentin* 137
The Zinc Silicate Phosphors Fluorescing in the Yellow and Red. *H. G. Pfeiffer and G. R. Fonda* 140
The Function of Oxygen in Zinc Sulfide Phosphors. *F. A. Kroeger and J. A. M. Dikhoff* 144
Zinc-Magnesium Oxide and Zinc-Magnesium Sulfide Phosphors. *Arthur L. Smith* 155
The Excitation Spectra of Various Silicate Phosphors. *Alexander J. Oszy* 159
Liquid Settled Luminescent Screens. *S. Pakswer and P. Intiso* 164
The Mechanism of the Cathodic Hydrogen Evolution Reaction. *J. O'M. Bockris and E. C. Potter* 169

Current Affairs

Plans Now Complete for Philadelphia Meeting 85C
Technical Program for Meeting 85C
An Open Letter to the Membership 90C
News Notes 90C
Section News 92C
Personals 92C
New Members 93C
Literature from Industry 94C
Highlights of the Board of Directors' Meeting 96C
Recent Patents 98C
Employment Situation 98C

EDITORIAL STAFF

R. M. BURNS, *Chairman*

NORMAN HACKERMAN, *Technical Editor* RUTH G. STERNS, *Assistant Editor* F. L. LAQUE *Business Manager*
CECIL V. KING, *Associate Editor* MARY F. MURRAY, *Assistant Editor* U. B. THOMAS, *News Editor*

DIVISIONAL EDITORS: M. A. STREICHER, *Corrosion*; ABNER BRENNER, *Electrodeposition*; N. C. CAHOON, *Battery*; H. C. FROELICH, *Electronics*; W. C. GARDINER, *Industrial Electrolytic*; S. J. SINDEBAND, *Electrothermic*; R. R. RALSTON, *Electric Insulation*; L. B. ROGERS, *Theoretical*; SHERLOCK SWANN, JR., *Electro-Organic*

REGIONAL EDITORS: JOSEPH A. SCHULEIN, *Pacific Northwest*; J. C. SCHUMACHER, *Los Angeles*; O. W. STOREY, *Chicago*; G. W. HEISE, *Cleveland*; PAUL S. BRALLIER, *Niagara Falls*; OLIVER OSBORN, *Houston*; EARL A. GULBRANSEN, *Pittsburgh*; J. W. CUTHBERTSON, *Great Britain*; T. L. RAMA CHAR, *India*

ADVERTISING: Richard Rimbach Associates—James Condon. 133 Marlborough St., *Boston;* Richard Rimbach, Jr., 551 Fifth Ave., *New York;* William J. Gallagher. 3701 N. Broad St., *Philadelphia;* C. F. Goldcamp, 921 Ridge Ave., *Pittsburgh;* Harold Haskett, 360 N. Mich. Ave., *Chicago;* James R. Wright, 411 N. Tenth St., *St. Louis;* M. D. Pugh. 2721 N. Marengo Ave., *Altadena* (*Los Angeles*).

Published monthly by The Electrochemical Society, Inc., Mt. Royal and Guilford Aves., Baltimore 2, Md., combining the JOURNAL and TRANSACTIONS OF THE ELECTROCHEMICAL SOCIETY. Editorial Office: 235 W. 102nd St., New York 25, N. Y. Business Office: Mt. Royal and Guilford Aves., Baltimore 2, Md., or 235 W. 102nd St., New York 25, N. Y. Statements and opinions given in articles and papers in the JOURNAL OF THE ELECTROCHEMICAL SOCIETY are those of the contributors, and The Electrochemical Society assumes no responsibility for them. Subscription: $8.50 to members, $12.00 to nonmembers. Single copies $1.00 to members, $1.25 to nonmembers. Copyright 1952 by The Electrochemical Society Inc. Entered as second-class matter November 15, 1947, at the Post Office at Baltimore, Md., under the act of August 24, 1912.

Electrons probe the future

1 Electron micrograph of an alloy of aluminum, nickel, cobalt and iron. Magnification 20,000 diameters.

2 Cooled from high temperature in a magnetic field, the alloy becomes a powerful, permanent magnet. Note changed structure. Black bars reveal formation of precipitate parallel to the applied field. Each bar is a permanent magnet.

3 A Bell scientist adjusts electron diffraction camera. Electrons are projected on the specimen at glancing angles. They rebound in patterns which tell the arrangement of the atoms . . . help show how telephone materials can be improved.

4 Diffraction pattern of polished germanium reveals minute impurities which would degrade the performance of a Transistor.

In 1927, Bell Laboratories physicists demonstrated that moving electrons behave like light waves, and thus launched the new science of electron optics.

Now, through the electron beams of the electron microscope and electron diffraction camera, scientists learn crucial details about the properties of metals far beyond the reach of optical microscopes or chemical analysis.

At the Laboratories, electron beams have revealed the minute formations which produce the vigor of the permanent magnets used in telephone ringers and magnetron tubes for radar. The same techniques help show what makes an alloy hard, a cathode emit more electrons and how germanium must be processed to make good Transistors.

This is the kind of research which digs deep *inside* materials to discover how they can be made better for your telephone system . . . and for the many devices which the Laboratories are now developing for national defense.

BELL TELEPHONE LABORATORIES

Improving telephone service for America provides careers for creative men in scientific and technical fields.

Cadmium Chlorophosphate Phosphors[1]

ROBERT W. WOLLENTIN, C. K. LUI WEI, AND RUDOLPH NAGY

Research Department, Westinghouse Electric Corporation, Bloomfield, New Jersey

ABSTRACT

An investigation of cadmium chlorophosphate phosphor was undertaken to determine the possibilities of its use in the production of fluorescent lamps. Under 2537 Å excitation this phosphor fluoresces a yellowish pink with a peak of emission at 5900 Å. Studies were made of the effect of substitutions of cations for cadmium on the output, emission, excitation, and interlattice spacing of the phosphor. Acceptable commercial lamps can be made with a number of modifications of cadmium chlorophosphate phosphor.

INTRODUCTION

Several authors have reported on the emission and structural characteristics of the apatite phosphors (1–4). The greatest interest has been given to calcium, barium, and strontium halophosphates doubly activated by manganese with antimony, tin, lead, arsenic, bismuth, or uranium. Comparatively little interest has been shown in cadmium chlorophosphates (5, 6) activated by manganese alone. These phosphors generally have a narrow fluorescence spectrum with the peaks of emission ranging from 5880 Å to 6100 Å.

The present paper describes some of the spectral and structural characteristics as well as the performance in fluorescent lamps of a variety of cadmium chlorophosphate phosphors.

EXPERIMENTAL

The process of phosphor preparation consisted of intimately mixing cadmium oxide, diammonium acid phosphate, manganese chloride, and a chloride of one or more of the group, cadmium, barium, strontium, magnesium, and zinc. The mixtures were fired, in covered fused silica containers, in a Globar furnace under a normal air atmosphere at temperatures ranging from 600°C for the barium-containing samples to 850°C for the normal cadmium-containing samples. The time of firing was standardized at 30 minutes for 30 gram batches to 90 minutes for 300 gram batches. The samples were refired until no further increase in plaque brightness could be gained by reheating. No special quenching procedure was employed. The samples were allowed to cool to room temperature with the covers left on. A 0.5 mole excess of phosphate over that required to form cadmium orthophosphate was found helpful in all instances in deriving maximum efficiencies and reproducible results. Therefore, all formulations include a 0.5 mole excess of phosphate per 3.0 moles of cadmium, or a total of 7.5 moles of phosphate for the 9.0 moles of cadmium in the starting compositions.

A recording spectroradiometer, employing a Beckman monochromator, photomultiplier tube, and a Brown electronic recorder, was used to obtain all spectral distribution curves. The mechanical slit width of the monochromator was maintained at 0.15 mm for all samples. The resultant curves, with the mercury lines removed, were corrected for photomultiplier sensitivity and adjusted to a peak value of 100.

All of the x-ray diffraction studies on cadmium chlorophosphates were made with a North American Philips, Geiger counter, x-ray spectrometer. Copper, chromium, and iron tubes were used as the source of x-ray radiation.

The excitation measurements were made with a recording spectroradiometer previously described, using a hydrogen discharge lamp and monochromator as the ultraviolet source. The phosphor powders were coated on the outer surface of a cylinder of Corning 704 glass which surrounded the photomultiplier. The photocurrent induced by the fluorescence of the phosphor was recorded as a function of the exciting wavelength. Correction for the energy distribution of the hydrogen source was made.

Relative brightness values were obtained on a plaque of the powdered material exposed to 2537 Å radiation. The emission was detected by a photronic cell corrected to eye sensitivity, and a sensitive galvanometer.

Fluorescent lamp data were obtained on 40-watt fluorescent lamps manufactured on factory equipment. The lamps were subjected to the usual test cycle of three hours on, twenty minutes off for one hundred hours of burning.

RESULTS

The chlorides of magnesium, cadmium, barium, strontium, and zinc were introduced in various molar proportions to a base material of tertiary cadmium

[1] Manuscript received September 17, 1951. This paper prepared for delivery before the Washington Meeting, April 8 to 12, 1951.

phosphate and manganese according to the general formulation: $3Cd_3(PO_4)_2 \cdot X(MCl_2):0.2Mn$ where M is any of the afore-mentioned cations and X is varied from 0 to 5.0 moles. Fig. 1 and 2 show the results of these additions on relative brightness. The mole proportions referred to throughout this work are in terms of starting compositions and do not necessarily reflect the actual compositions of the finished phosphors, since no chemical analyses were made to determine end products. Maxima in the curves occur over a range of 1 to 3 moles of the chlorides per three moles of tertiary cadmium phosphate. Zinc chloride produces the sharpest peak at

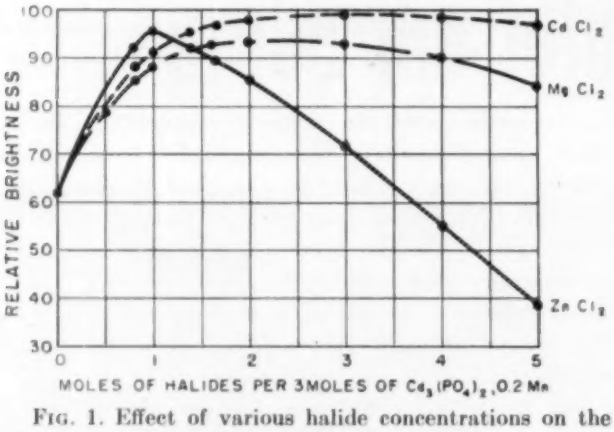

FIG. 1. Effect of various halide concentrations on the relative brightness of cadmium chlorophosphate.

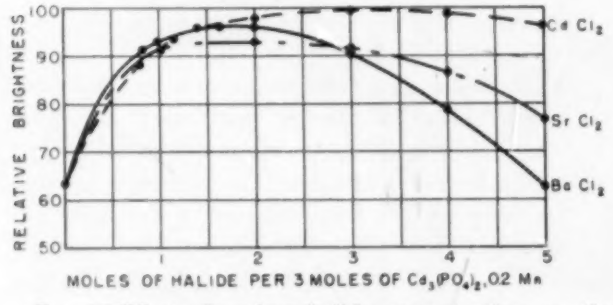

FIG. 2. Effect of various halide concentrations on the relative brightness of cadmium chlorophosphate.

one mole. The other cations all display peaks at greater than 1 mole. Cadmium chloride, for example, peaks at about 3.0 moles, while magnesium, barium, and strontium chlorides show poorly defined but recognizable peaks at 2.0 moles. It is interesting to note the variable tolerance of the phosphor for an excess of the chlorides. Apparently large amounts of cadmium chloride over that necessary to yield the apatite x-ray diffraction pattern may be present without serious effect, while excessive zinc chloride should be avoided as indicated by the rapid decrease in relative brightness with increasing zinc content.

The effect of the simultaneous addition of two or more cations on relative brightness is illustrated in Fig. 3. The diagram represents all possible combinations of strontium, barium, and zinc in a basic formula which for convenience may be represented by: $3Cd_3(PO_4)_2:2(Sr, Zn, Ba)Cl_2:0.2Mn$, where the sum of the total chlorides always equals 2 moles. Plaque brightness measurements are superimposed on points indicating the compositions of the phosphors tested. As is evidenced by the chart, slightly higher powder brightnesses were obtained toward the lower center of the diagram corresponding to starting compositions containing low strontium and relatively higher barium and zinc proportions. The firing temperature of 750°C was employed in the preparation of all the phosphors represented in the chart. A deviation of the order of 50°C or more from 750°C would result in either sintering of the high barium compositions or serious underfiring of

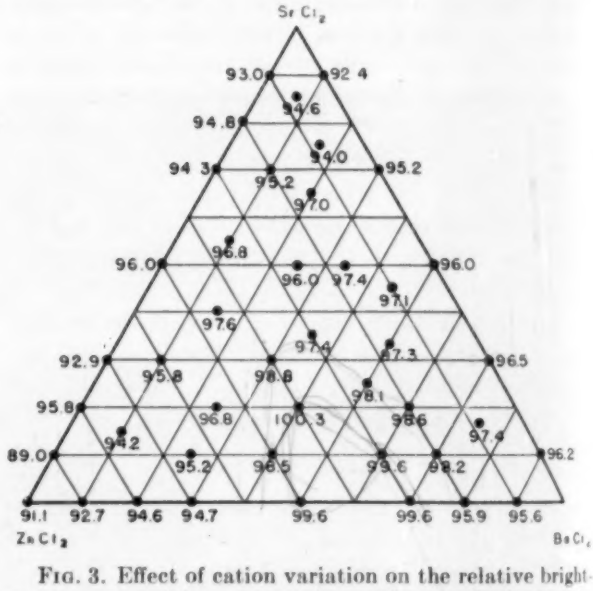

FIG. 3. Effect of cation variation on the relative brightness in a general formulation of $3Cd_3(PO_4)_2 \cdot 2(Sr,Zn,Ba)Cl_2$: 0.2 Mn, fired at 750°C.

the high strontium containing formulations. Each of the mixtures was refired for periods of 30 minutes until the relative brightness of the resultant phosphors remained constant.

The optimum concentration of manganese varies with the specific cation chosen to replace cadmium. When manganese chloride is added to cadmium orthophosphate, Fig. 4, a broad maximum in the brightness curve occurs between 0.6 and 0.7 moles of manganese chloride per three moles of cadmium orthophosphate. However, when manganese chloride is introduced into compositions containing two moles of barium chloride or three moles of strontium chloride per three moles of cadmium orthophosphate, somewhat sharper peaks are obtained with 0.1 moles of manganese chlorides for the former and 0.2 moles for the latter. In the presence of the chlorides of magnesium, cadmium, and zinc, the optimum con-

centration of manganese chloride is essentially the same as in the strontium containing phosphor.

The spectral distributions, under 2537 Å excitation, of a cadmium chlorophosphate ($3Cd_3(PO_4)_2 \cdot CdCl_2$:0.2 Mn), a zinc beryllium silicate and a calcium halophosphate as used in the production of 3500K white are presented in Fig. 5. The peak of emission of the cadmium chlorophosphate, curve

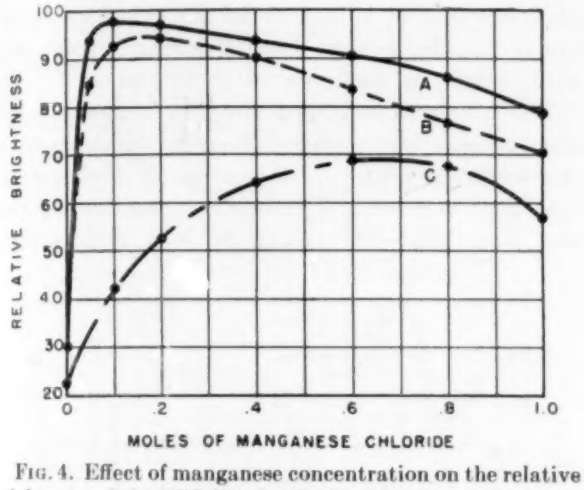

FIG. 4. Effect of manganese concentration on the relative brightness of A—$3Cd_3(PO_4)_2 \cdot 2BaCl_2$:Mn, B—$3Cd_3(PO_4)_2 \cdot 3SrCl_2$:Mn, C—$3Cd_3(PO_4)_2$:Mn.

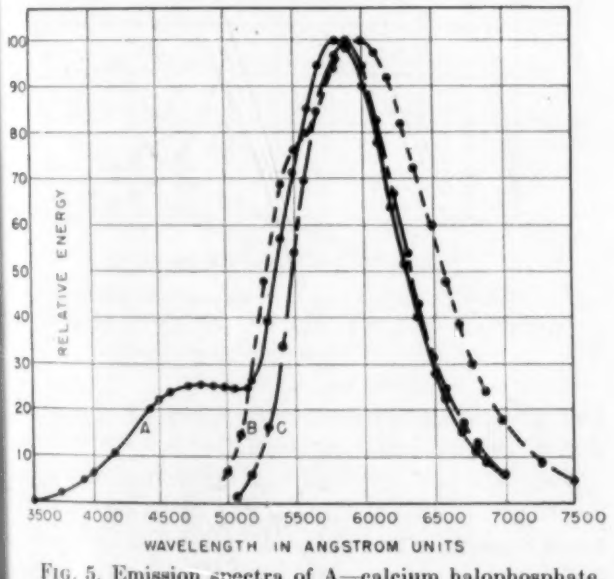

FIG. 5. Emission spectra of A—calcium halophosphate, B—zinc beryllium silicate, C—cadmium chlorophosphate.

C, is located at approximately 5900 Å and falls between the peaks for calcium halophosphate and zinc beryllium silicate. The red portion of the cadmium chlorophosphate emission closely parallels that of calcium halophosphate, curve A, while the shorter wavelength side is markedly deficient in the blue and green. This deficiency in color necessitates the use of auxiliary phosphors in producing satisfactory white light in fluorescent lamp applications.

The position of the emission peak of cadmium chlorophosphate varies with the manganese content and the specific cation replacing cadmium. For example, increasing the strontium chloride content causes a gradual shift of the emission toward longer wavelengths. Fig. 6 shows the shift in the emission obtained by increasing strontium chloride to three moles in a base material of $3Cd_3(PO_4)_2$:$X$$SrCl_2$:1.0 Mn. This shift brings the longer wavelength emission to coincide fairly closely with the corresponding portion of the zinc beryllium silicate emission curve B, Fig. 5. The variation of the manganese content from 0.1 to 1.5 moles, Fig. 7, in a basic formulation of $3Cd_3(PO)_2 \cdot 3SrCl_2$:$X$Mn, resulted in a gradual shift of the emission peak, a total of 200 Å toward longer wavelengths. A similar effect was noted in

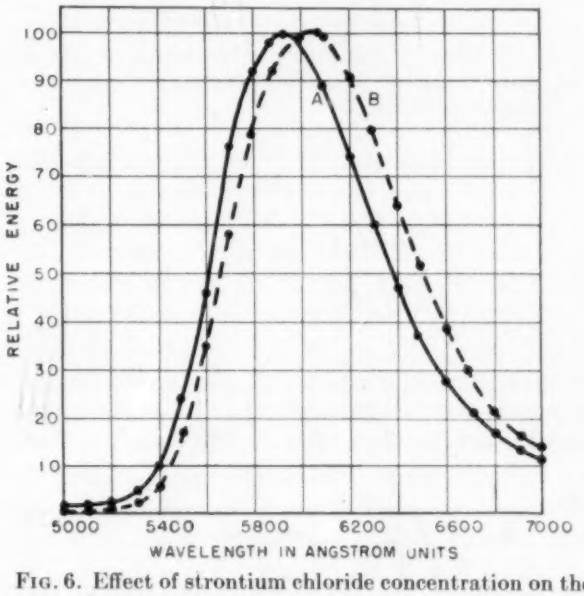

FIG. 6. Effect of strontium chloride concentration on the spectral distribution of cadmium chlorophosphate. A—$3Cd_3(PO_4)_2$:1 $MnCl_2$, B—$3Cd_3(PO_4)_2 \cdot 3SrCl_2$:1 $MnCl_2$.

barium-containing cadmium chlorophosphates, but to a much lesser extent. Increasing the manganese in a formulation of $3Cd_3(PO_4)_2 \cdot 2BaCl_2$:Mn from 0.1 to 1.5 moles Mn produced a total shift of 40 Å toward the longer wavelengths. Samples containing magnesium, cadmium, and zinc did not show the shift on increasing manganese.

Table I presents some of the emission peaks obtained in cadmium chlorophosphate phosphors. In addition to those listed, magnesium and zinc chlorides, when present in apatite proportions with 0.2 moles Mn, gave emission peaks and distributions nearly identical to the cadmium chloride-containing phosphor of Table I.

It appears characteristic of the cadmium chlorophosphate phosphors to display double peaks in the excitation curve, Fig. 8 and 9. The major peak at 2300 Å is common to all, while the minor peak

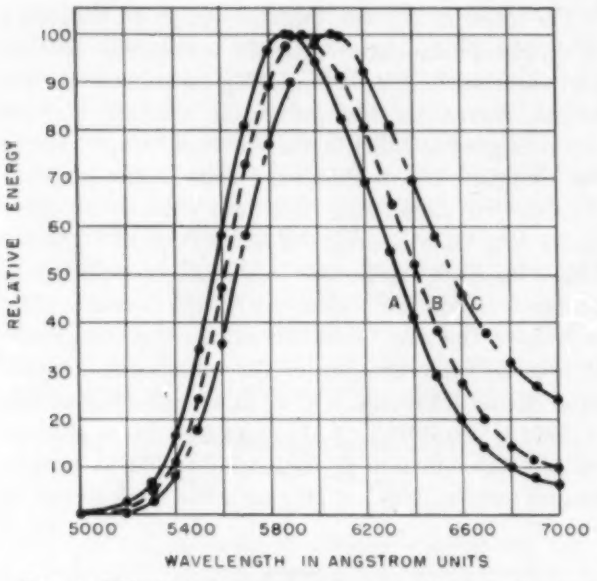

FIG. 7. Effect of manganese concentration on the spectral distribution of $3Cd_3(PO_4)_2 \cdot 3SrCl_2$:Mn, A—0.1 Mn, B—0.5 Mn, C—1.5 Mn.

TABLE I. *Emission peaks of cadmium chlorophosphate phosphors prepared at 800°C*

Composition	Emission peak (Å)
$3Cd_3(PO_4)_2 \cdot CdCl_2$:0.2Mn	5890
$3Cd_3(PO_4)_2 \cdot BaCl_2$:0.1Mn	5900
$3Cd_3(PO_4)_2 \cdot BaCl_2$:1.0Mn	5940
$3Cd_3(PO_4)_2 \cdot 3SrCl_2$:0.2Mn	5860
$3Cd_3(PO_4)_2 \cdot 3SrCl_2$:1.0Mn	6080
$3Cd_3(PO_4)_2 \cdot 0.6MgCl_2 \cdot 0.4ZnCl_2$:0.2Mn	5940

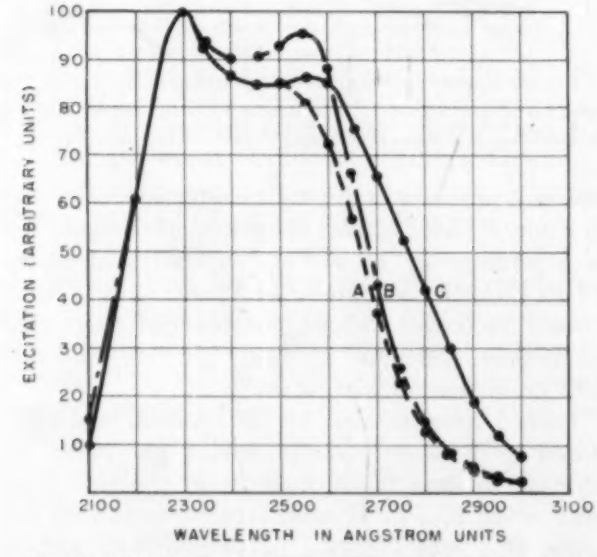

FIG. 8. Excitation spectra of cadmium chlorophosphates. A—$3Cd_3(PO_4)_2 \cdot BaCl_2$:0.2 Mn, B—$3Cd_3(PO_4)_2 \cdot CdCl_2$:0.2 Mn, C—$3Cd_3(PO_4)_2 \cdot BaCl_2$:1.0 Mn.

varies in position and height with the cation replacing cadmium and the manganese content. The shift in excitation toward the longer wavelengths obtained by increasing the manganese content, Fig. 8, is quite marked. Fig. 8 also presents the excitation spectrum of $3Cd_3(PO_4)_2 \cdot CdCl_2$:0.2Mn which shows the relatively high secondary peak at about 2550 Å and the steeper slope of the long wavelength side. The substitution of zinc chloride for cadmium chloride does not alter the excitation curve, while magnesium chloride results in an excitation spectrum essentially the same as for the barium-containing phosphor of Fig. 8, and strontium chloride, Fig. 9, causes a definite shift toward longer wavelengths with increasing amounts of strontium.

The interlattice spacings and x-ray diffraction line intensities of our samples of cadmium chlorophosphate correspond to the data given by McKeag and Randall (5). According to their analysis this material has a chemical formulation of $3Cd_3(PO_4)_2 \cdot CdCl_2$,

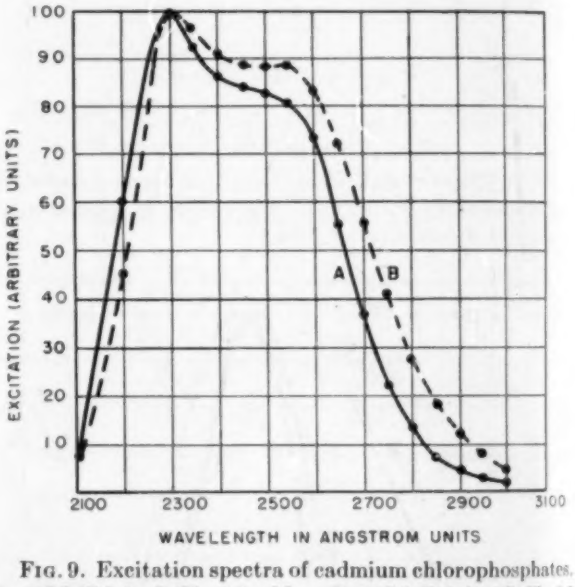

FIG. 9. Excitation spectra of cadmium chlorophosphates. A—$3Cd_3(PO_4)_2 \cdot SrCl_2$:0.2 Mn, B—$3Cd_3(PO_4)_2 \cdot 3SrCl_2$:0.2 Mn.

and an apatite structure with $a_0 = 9.6$ Å, $c_0 = 6.45$ Å and an axial ratio 0.667.

The data derived from our diffraction measurements proved that the interaction of 3 moles of cadmium phosphate and one mole or more of cadmium, barium, magnesium, zinc, strontium, and manganese, alone or in combination, led to the formation of the apatite type lattice structure. When manganese chloride is used in the absence of other chlorides, as little as 0.6 mole per 3.0 moles of cadmium orthophosphate has been found to yield the apatite lattice structure.

In the substitution of magnesium, zinc, strontium, and barium chlorides for cadmium chloride in the above formulation, strontium produced the greatest expansion of lattice spacings, while magnesium produced a moderate amount of contraction.

Three moles of barium chloride gave a slight expansion while zinc chloride in all proportions showed no change. Increasing the manganese content of the phosphor results in a contraction of the lattice spacing. These alterations of lattice spacings indicate substitutional solid solutions of the added elements. All of the substituted phosphors contained small amounts of ortho- or pyrophosphates of the corresponding elements.

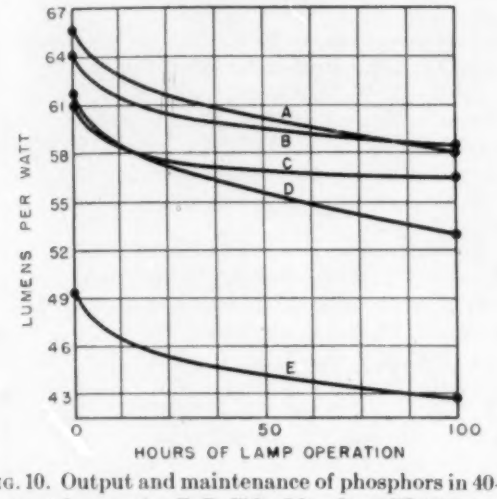

FIG. 10. Output and maintenance of phosphors in 40-watt fluorescent lamps. A—$ZnBeSiO_4$:Mn, B—$3Cd_3(PO_4)_2 \cdot 2MgCl_2$:0.2 Mn, C—$3Cd_3(PO_4)_2 \cdot 2SrCl_2$:0.2 Mn, D—$3Cd_3(PO_4)_2 \cdot 2BaCl_2$:0.2 Mn, E—$3Cd_3(PO_4)_2 \cdot ZnCl_2$:0.2 Mn.

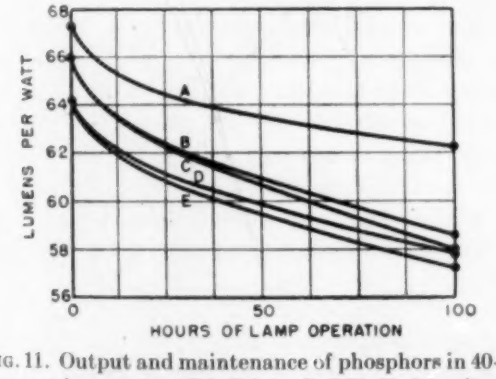

FIG. 11. Output and maintenance of phosphors in 40-watt fluorescent lamps. A—$3Cd_3(PO_4)_2 \cdot CaFCl$:Sb:Mn, B—$3Cd_3(PO_4)_2 \cdot 2CdCl_2$:0.2 Mn, C—$ZnBeSiO_4$:Mn, D—$3Cd_3(PO_4)_2 \cdot 2MgCl_2$:0.2 Mn, E—3500K white blend of Zn_2SiO_4:Mn, $MgWO_4$, and $3Cd_3(PO_4)_2 \cdot 0.6MgCl_2 \cdot 0.4ZnCl_2$: 0.2 Mn.

The performance in 40-watt fluorescent lamps of a number of these phosphors is recorded in Fig. 10 and 11. For comparison purposes, 3500K white calcium halophosphate and zinc beryllium silicate lamps are included. Cadmium chlorophosphate gave 66.0 lumens per watt at zero hours compared to 49.5 to 64.5 lumens per watt for the substituted cadmium chlorophosphate. A 3500K white blend of zinc silicate, magnesium tungstate, and a cadmium chlorophosphate, i.e., $3Cd_3(PO_4)_2 \cdot 0.6MgCl_2 \cdot 0.4ZnCl_2$:0.2 Mn produced an average of 64.4 lumens per watt at zero hour and a maintenance of 89 per cent, Fig. 11. Slightly higher maintenance is indicated for the strontium and magnesium substitutions than for the zinc-magnesium combination used in the above-mentioned blend, but the higher lumen values for the latter offset the slight superiority in maintenance.

Discussion

The foregoing data have served to corroborate existing data on the formation of the apatite structure in the reaction between cadmium chloride and cadmium orthophosphate. It has also been shown that the reaction between cadmium orthophosphate and the chlorides of magnesium, barium, zinc, and strontium leads to the formation of the apatite structure. However, in all instances extra lines are present in the x-ray patterns indicating the formation of small amounts of unwanted compounds. When cadmium chloride is used, a small amount of what may be cadmium pyrophosphate is formed. Strontium, barium, and zinc chlorides all form orthophosphates, while magnesium forms a small amount of magnesium pyrophosphate.

The relative brightness of these phosphors is not always maximum with the three to one mole ratio of cadmium phosphate to halide as prevalent in the normal apatite structure. Except in the substitution of zinc chloride, all of the other permissible cations are required to be present in one or more moles excess in the prefired mixture. It is believed that this excess may function in at least three ways. The formation of extraneous phosphates has already been mentioned. Another portion is accounted for in the actual substitution of these cations for cadmium but a portion may also serve to flux the reaction since in all instances increasing amounts of the chlorides effectively decrease the melting point of the mixtures.

The data on x-ray diffraction, excitation spectra, and emission indicate that manganese occupies a position in the cadmium halophosphate lattice similar to the position of manganese in calcium halophosphate. Increasing proportions of manganese in the barium and strontium substituted cadmium chlorophosphates produce a contraction of the lattice spacing as would be expected by a comparison of the ionic radii of cadmium and manganese, proving that manganese enters in substitutional solid solution for the cations. The increase in manganese is also accompanied by an emission shift toward longer wavelengths.

The performance of these phosphors in 40-watt fluorescent lamps operated at 420 milliamperes varies with the specific cation substituted for cadmium. McKeag and Randall (7) reported an efficiency of

25 lumens per watt from fluorescent lamps coated with cadmium chlorophosphate and operated at a current density of 20 ma/cm². Randall (8) obtained 30 lumens per watt from cadmium phosphate activated by manganese. In our tests on standard 40-watt fluorescent lamps, cadmium chlorophosphate yielded 66 lumens per watt at zero hours, that dropped to 88.5 per cent of that value in 100 hours. Magnesium chloride and the combined magnesium-zinc chloride substitution for cadmium chloride lead to slightly lower zero hour lumens per watt but slightly higher maintenance. These results compare favorably with zinc beryllium silicates. Furthermore, blends of these cadmium chlorophosphates have equaled the performance of blends of zinc beryllium silicates. While it is true that the cadmium chlorophosphates are still inferior to the present day calcium halophosphate, in lumens and maintenance, there are some advantages to be gained in color since it is possible to derive phosphors among the cadmium chlorophosphates with emission as saturated in red as zinc beryllium silicate, by the proper choice of cation and manganese content.

ACKNOWLEDGMENT

The authors wish to express their appreciation to the North American Philips Company for the use of their Geiger counter, x-ray spectrometer, and particularly to Miss Margaret Berry for her assistance.

Any discussion of this paper will appear in a Discussion Section, to be published in the December 1952 issue of the Journal.

REFERENCES

1. A. H. McKeag and P. W. Ranby (To the General Electric Co., Ltd.), British Pat. 578,192 (1942).
2. R. Nagy, R. W. Wollentin, and C. K. Lui, *J.* (*and Trans.*) *Electrochem. Soc.*, **95**, 187 (1949).
3. H. G. Jenkins, A. H. McKeag, and P. W. Ranby, *J.* (*and Trans.*) *Electrochem. Soc.*, **96**, 1 (1949).
4. K. H. Butler and C. W. Jerome, *J. Electrochem. Soc.*, **97**, 265 (1950).
5. A. H. McKeag and J. T. Randall (To the General Electric Co., Ltd.), British Pat. 495,706 (1937).
6. H. P. Rooksby and A. H. McKeag, *J. Gen. Elec. Co., England*, **17**, No. 2, 89 (1950).
7. A. H. McKeag and J. T. Randall (To the General Electric Co.), U. S. Pat. 2,191,351 (1940).
8. J. T. Randall (To the Canadian General Electric Co., Ltd.), Canadian Pat. 419,532 (1944).

Calcium Zinc Silicate Phosphor[1]

RUDOLPH NAGY, C. K. LUI WEI, AND R. W. WOLLENTIN

Westinghouse Electric Corporation, Bloomfield, New Jersey

ABSTRACT

Partial substitution of zinc for calcium in lead-activated calcium silicate phosphor shifted the peak of emission from 3350 Å to 3450 Å. X-ray analysis indicated that the new phosphor had a tetragonal structure similar to the mineral hardystonite, rather than the monoclinic or triclinic calcium silicate. This phosphor, when made into "black-light" fluorescent lamps, equaled the performance of calcium cerium phosphate phosphor.

INTRODUCTION

A preliminary investigation of various ultraviolet emitting phosphors indicated that calcium silicate activated with lead probably could be used as a substitute for calcium cerium phosphate, a "black-light" phosphor. Froelich (1) has shown calcium silicate to have an emission near 3400 Å. However, the ultraviolet energy output as measured by excitation of zinc sulfides is only about 60 per cent of calcium cerium phosphate. Since both the peak emission and output of some of these phosphors can be altered by proper variation of the constituents, a program was initiated to determine if an improvement could be made in this manner. A calcium silicate phosphor would be ideal from the manufacturing point of view because both calcium and silica are abundant and are relatively inexpensive. Preliminary experimentation indicated that a replacement of a portion of calcium in calcium silicate by zinc shifted the emission spectrum of this phosphor to longer wavelengths. This paper describes the preparation and properties of a new calcium zinc silicate phosphor activated with lead.

EXPERIMENTAL

Preparation of Phosphor

Zinc was substituted in various molar ratios for calcium in calcium silicate to determine the optimum proportion of each. Lead activator was added as PbF_2 and kept constant at 0.019 moles for each mole of calcium silicate. The zinc oxide, calcium carbonate, silica, and lead fluoride were mixed by ballmilling. The phosphor was heated in covered silica crucibles in an electric furnace for two hours at 1000°C. The ultraviolet luminescence was compared with calcium cerium phosphate taken as 100, by exposing a plaque of the phosphor to 2537 Å radiations and measuring the visible fluorescence of a ZnS·Cu phosphor excited by the ultraviolet emission of the phosphor under test. Fig. 1 shows that maximum luminescence is obtained with a ratio of two moles of calcium for every mole of zinc.

To determine the optimum amount of silica a series of phosphors was made in which the mole ratio of cation to silica was varied between 3:2 to 3:4. The plaque luminescence was maximum as seen in Fig. 2 when the ratio of the cation and anion was about equal. Since with most silicates it is desirable to use a slight excess of silica to obtain the maximum output, all subsequent formulas were made with 3.4 moles silica for every 3 moles of cation.

Various compounds of lead were also tested to determine the best method of introducing the activator. Lead oxide, lead fluoride, lead carbonate, and lead nitrate were used in various amounts from 0.06 to 0.48 mole per cent of lead for each mole of calcium silicate. Lead fluoride was preferred to the other lead compounds in that it reduced the time of firing of the sample. The highest plaque output was obtained with 0.3 mole per cent of lead which is approximately 1.0 per cent of lead by weight of calcium zinc silicate.

X-Ray Diffraction

To determine phosphor structure, x-ray diffraction studies of different compositions were made using powder technique and iron K_α radiation. The x-ray diffraction pattern of the new calcium zinc silicate phosphor, (B) Fig. 3, does not correspond to either the α (C) or β (D) form of calcium silicate described by Fonda and Froelich (2) or to zinc silicate (A). A search of the ASTM card index indicates that the interlattice spacings correspond to melilite, a group of minerals having a tetragonal structure and a general formula $Ca_2R\ Si_2O_7$, where R may be Mg, Al, Fe, Mn, or Zn. Matching the lines with the Hull and Davey charts, the present phosphor also has a tetragonal structure. A comparison of the x-ray data of these calcium silicates is given in Table I. A rare mineral of this composition and structure is found in nature and is known as "hardystonite."

[1] Manuscript received September 17, 1951. This paper prepared for delivery before the Washington Meeting, April 8 to 12, 1951.

Excitation

The excitation spectra of the calcium silicates were determined with a Beckman monochromator and a hydrogen discharge lamp as the ultraviolet source. The phosphor powders were coated on the outer surface of a cylinder of Corning 704 glass which surrounded an RCA 1P22 photomultiplier. The photocurrent produced by the fluorescence of the phosphor was then recorded as a function of the exciting wavelength by a Brown electronic potentiometer. After proper correction for the energy distribution of the hydrogen source, the relative excitation was plotted as shown in Fig. 4. Calcium zinc silicate (A) has two peaks, one at 2350 Å and the other at 2550 Å. This excitation curve corresponds more nearly to the α form of calcium silicate (B) than to the low temperature form β calcium silicate (C); however, it is different from either of them.

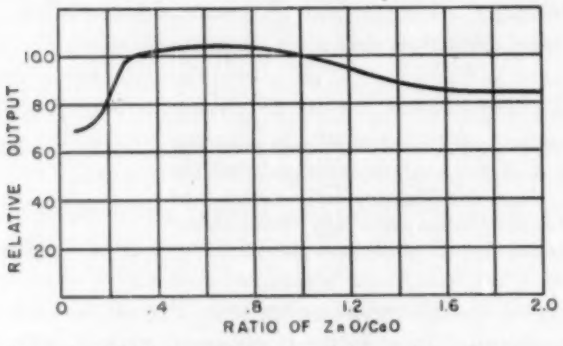

FIG. 1. Relative output of calcium zinc silicate with various ratios of zinc to calcium compared to calcium cerium phosphate as 100 for 2537 Å excitation.

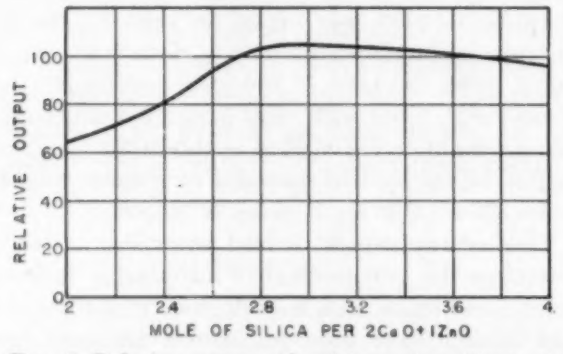

FIG. 2. Relative output of calcium zinc silicate, lead activated, with different mole ratios of silica to calcium plus zinc oxides compared with calcium cerium phosphate as 100 for 2537 Å excitation.

TABLE I. *A comparison of lattice spacings (d/n) and intensities (I) of calcium zinc silicate, melilite, and wollastonite structures*

$Ca_2Zn(SiO_3)_3$·Pb Phosphor		$Ca_2Mg(SiO_3)_2$ Melilite-ASTM II 1719		$CaSiO_3$·Pb* Wollastonite		Ca Silicate* Wollastonite	
d/n	*I*	*d/n*	*I*	*d/n*	*I*	*d/n*	*I*
3.64	4	3.62	4	3.80	0.5	3.95	1.9
						3.80	0.7
3.36	3	3.35	2	3.43	1.9	3.50	2.4
3.13	7	3.14	6	3.25	10.0	3.30	3.0
2.91	10	3.00	6			3.09	1.9
2.80	1	2.81	10	2.81	7.2	2.97	10.0
2.46	3	2.43	5	2.47	2.3	2.80	1.0
		2.37	5	2.35	0.5	2.5	2.9
2.21	1	2.28	5	2.16	0.3	2.35	2.4
2.02	2	2.02	6	2.12	0.4	2.29	2.5
		1.93	6	1.99	7.4	2.19	2.6
1.85	1	1.81	4	1.84	1.5	1.91	0.5
1.74	10	1.75	8	1.70	1.3	1.82	1.6
1.64	1	1.62	2	1.63	1.3	1.74	0.6
1.61	1	1.59	2	1.54	0.8	1.72	1.6
1.54	2	1.53	2	1.48	1.5	1.60	0.6
1.51	2	1.51	6	1.40	0.6	1.54	0.7
1.44	2	1.43	6	1.30	0.5	1.37	0.6

* G. R. FONDA AND H. C. FROELICH, *J. (and Trans.) Electrochem. Soc.*, **93**, 116 (1948).

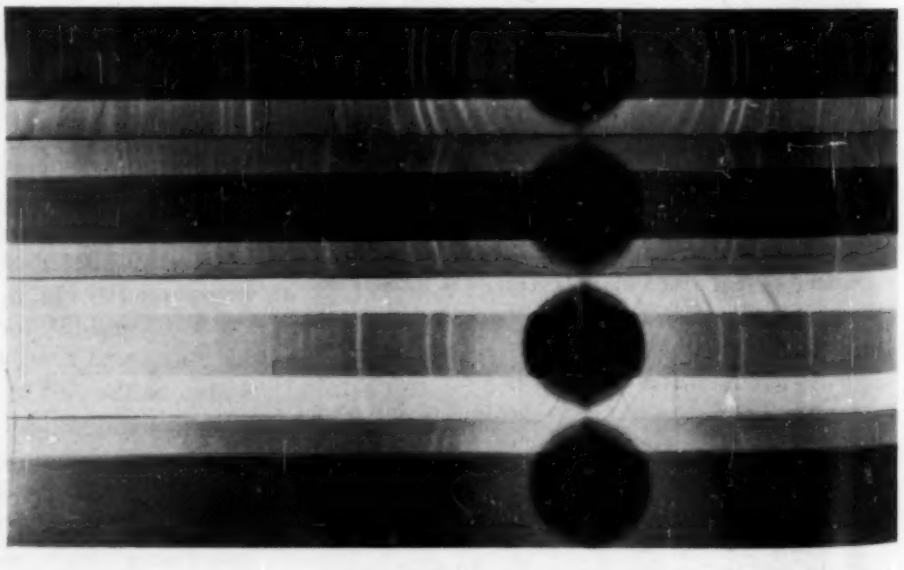

FIG. 3. X-ray diffraction patterns of: A. Zinc silicate · Mn; B. Calcium zinc silicate · Pb; C. α Calcium silicate · Pb; D. β Calcium silicate · Pb.

Emission Spectra

The emission spectra of the calcium silicate phosphors excited by 2537 Å radiation were made with a recording spectroradiometer. It will be seen from Fig. 5 that the spectral distribution of the calcium zinc silicate (A) has a peak at about 3450 Å which is at a longer wavelength than either the α or β calcium silicate (C and D). Thus, the emission of this phosphor will more nearly correspond to the excitation peak of the sulfides and can account for the apparent higher efficiency of calcium zinc silicate as a "black-light" phosphor.

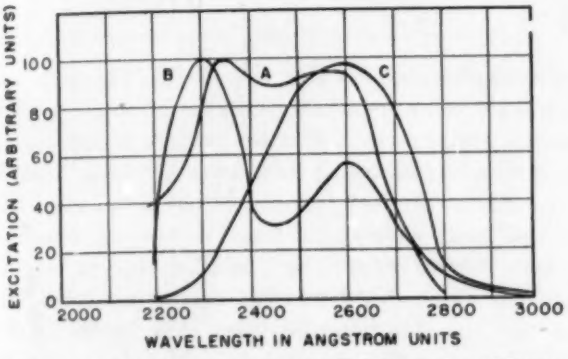

FIG. 4. Excitation spectra: A. Calcium zinc silicate · Pb; B. α Calcium silicate · Pb; C. β Calcium silicate · Pb.

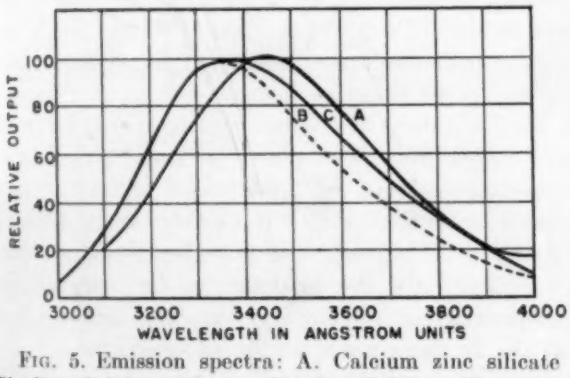

FIG. 5. Emission spectra: A. Calcium zinc silicate · Pb; B. α Calcium silicate · Pb; C. β Calcium silicate · Pb.

DISCUSSION

The substitution of one-third of the calcium by zinc in lead-activated calcium silicate produces a new phosphor as evidenced by x-ray diffraction patterns, excitation and emission spectra. X-ray evidence indicates the compound has the structure of hardystonite, $Ca_2Zn(SiO_2)_3$. Warren (3) has analyzed this compound by x-rays and found that the zinc atoms are coordinated by four oxygens and calcium by eight oxygens. The zinc tetrahedral groups are in the center and corners of the calcium groups. Warren's analysis also indicates that the silicon tetrahedrals are linked giving Si_2O_7 groups. He believed that there were two silicon atoms for two calcium and one zinc atom. Berman (4) has made a chemical analysis of hardystonite, apparently from some other source, and found that there are three atoms of silicon in each molecule which is in the same ratio as found in the present phosphor.

The apparent higher "black-light" output of the calcium zinc silicate phosphor can be attributed to the shift of the emission to longer wavelengths which are nearer to the peak of the excitation spectra of the zinc sulfides and organic dyes normally used to gauge the relative efficiencies of such phosphors. Unlike the gradual shift of emission wavelengths obtained by the incorporation of beryllia in zinc silicate, manganese activated, or zinc in calcium phosphate, thallium activated, the substitution of zinc in calcium silicate, lead activated, causes an abrupt transition to longer wavelengths; this probably results from the change in crystal configuration from the monoclinic pseudo-wollastonite to tetragonal hardystonite.

The excitation and emission spectra of the calcium silicates can also be attributed to the change in the crystal configuration as can be seen from Fig. 4 and 5. Lead-activated calcium silicate prepared either by the method of Studer, *et al.* (5), or Schulman, *et al.* (6), but heated at 1120°C, gave only β calcium silicate which had an excitation peak at 2600 Å and an emission peak with 2537 Å excitation at about 3350 Å. The α calcium silicate has a double excitation peak with one maximum at 2300 Å and the other at 2600 Å. The emission spectrum of α calcium silicate has a peak at 3350 Å. These results would indicate that Schulman, *et al.* (6), worked only with α calcium silicate while Studer, *et al.* (5), had both the α and β form depending upon the temperature of firing. There is, however, some discrepency as to the position of both the excitation and emission curves of the various types of calcium silicates so that it would appear that more fundamental work on this subject is necessary.

Any discussion of this paper will appear in a Discussion Section, to be published in the December 1952 issue of the JOURNAL.

REFERENCES

1. H. C. FROELICH, *J. (and Trans.) Electrochem. Soc.*, **93**, 101 (1948).
2. G. R. FONDA AND H. C. FROELICH, *J. (and Trans.) Electrochem. Soc.*, **93**, 114 (1948).
3. B. E. WARREN, *Z. Krist.*, **74**, 131 (1930).
4. H. BERMAN, *Am. Mineral.*, **14**, 389 (1929).
5. F. J. STUDER AND G. R. FONDA, *J. Optical Soc. Am.*, **39**, 655 (1949).
6. J. H. SCHULMAN, R. J. GINTHER, AND C. C. KLICK, *J. Electrochem. Soc.*, **97**, 123 (1950).

The Zinc Silicate Phosphors Fluorescing in the Yellow and Red[1]

H. G. Pfeiffer and G. R. Fonda[2]

Research Laboratory, General Electric Company, Schenectady, New York

ABSTRACT

The spectral emission at room temperature and at 80°K of yellow and red fluorescing zinc orthosilicates prepared in various ways has been determined The glassy state of the red phosphor has been confirmed. The yellow phosphor has been found to have some degree of crystallinity but its spectral emission is affected only slightly by the degree of crystallinity as determined by x-ray diffraction.

Introduction

Eleven years ago one of us published his results on the formation of zinc silicate phosphors emitting fluorescence of abnormal colors (1). When prepared at a low temperature, such as 850°C, from a mixture of zinc oxide, silica, and a manganese salt with an inert material and with a flux of potassium chloride to catalyze the reaction, a product was obtained which fluoresced yellow. It did not exhibit the x-ray diffraction pattern of zinc orthosilicate. Oddly enough, it showed the pattern of the inert material cristobalite, when an excess of precipitated silica had been added; quartz, when all of the silica including the excess was in the form of ground quartz; and zinc oxide, when an excess of zinc oxide had been used. In all cases the same yellow fluorescence resulted.

The experiment of Schleede and Gruhl (2) was also repeated, by fusing a mixture of zinc oxide and silica with manganese as activator and chilling with a blast of air. This yielded a phosphor emitting the same yellow fluorescence. The diffraction pattern showed only the lines of cristobalite. The pattern presented by Schleede and Gruhl was inadequately reproduced but gave evidence that it was likewise the pattern of cristobalite.

When the fused mass was abruptly quenched, by plunging into water, the product was found to fluoresce red, a result which is also in accord with an experiment by Schleede and Gruhl. The diffraction pattern showed only a few weak lines, but was so badly darkened that it denoted the presence of much general, scattered radiation. It was concluded that the product was so finely grained that it could be called amorphous. Rooksby and McKeag also investigated these two methods for preparing the abnormal phosphors of zinc silicate (3). The high temperature yellow-emitting phosphor obtained by them shows a clear x-ray diffraction pattern of lines, rather complicated because of their unusually large number. The 850°C product, on the other hand, exhibits a diffuse pattern and, at least in the reproduction, shows fewer lines. They ascribe this to smaller particle size and conclude that the pattern is the same as the high temperature form. The presence of a certain amount of noncrystalline material is denoted by the amount of diffuse scattering, but they believe that the phosphor has the same structure as that of the high temperature form. They interpret this structure as that of a novel compound of zinc oxide and silica, an allotropic modification of zinc orthosilicate, and call it β-zinc orthosilicate.

They obtained also some high temperature products which fluoresced red. The small amounts of crystalline material indicated in their diffraction patterns were attributed by them either to zinc oxide or cristobalite. They conclude that their work produces no evidence for the existence of the red-emitting phosphor as an allotropic crystalline form of zinc silicate. In this respect we are in agreement.

The disagreement between the x-ray results of Fonda and those of Rooksby and McKeag made further x-ray work desirable to see if the difference could be resolved. At the same time a more extensive investigation of the emission spectra of these compounds was undertaken.

Experimental

A series of yellow fluorescing zinc silicate phosphors were prepared using quartz, flint or precipitated silica as the source of silica. Table I shows some typical preparations.

Emission Spectra

The spectral distribution of the fluorescence emitted by the phosphors prepared from fusion under excitation by 2537 Å is given in Fig. 1 and 2. The

[1] Manuscript received November 30, 1951. This paper prepared for delivery before the Cleveland Meeting, April 19 to 22, 1950.

[2] Consultant, General Electric Company.

emission of the two phosphors prepared at 850°C was found to be essentially identical with that of the yellow-emitting phosphor #3 formed by fusion.

TABLE I

Phosphor*	$ZnO:SiO_2$	Form of SiO_2	Firing	Fluorescence
1	1 2	pptd SiO_2	40 min 850°C	Yellow
2	1 4	Quartz	40 min 850°C	Yellow
3	1.8 1	pptd	Fused and chilled	Yellow
4	1 1	pptd	Fused and quenched	Red

* All phosphors contain 0.6% Mn.

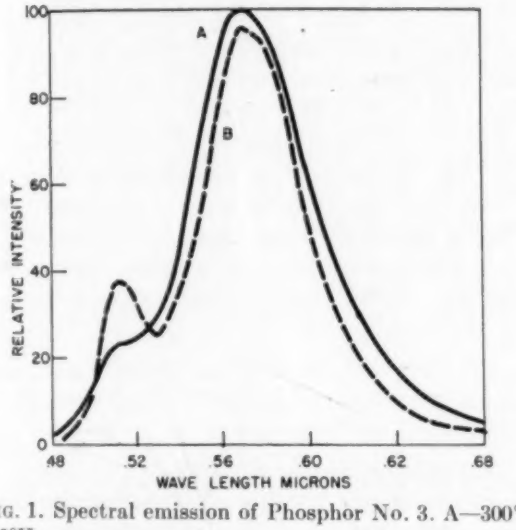

FIG. 1. Spectral emission of Phosphor No. 3. A—300°K, B—80°K.

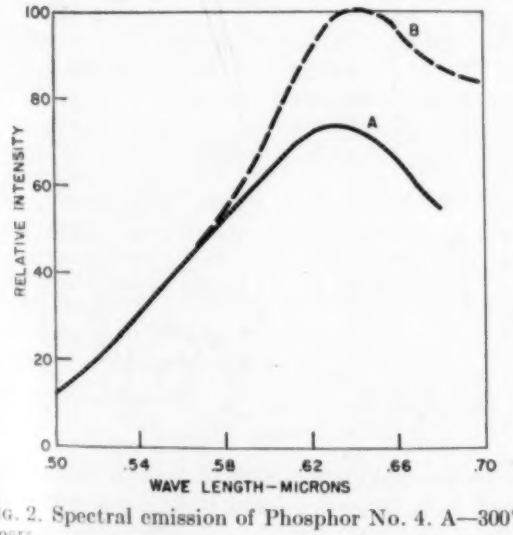

FIG. 2. Spectral emission of Phosphor No. 4. A—300°K, B—80°K.

In the case of all three yellow-emitting phosphors, measurements of the emission at liquid air temperature developed a sharp subsidiary peak at 5140 Å. A more extensive investigation was therefore undertaken, with the aim of ascertaining more about this shorter wave emission.

Preparations were made with the extremely fine particle silica which is now available in the form of Mallinckrodt's "Special Bulky." It proved to be so much more reactive than the precipitated silica available in the earlier preparations that it was necessary to lower the temperature of preparation from 850° to 800°C or lower. Mixtures were made in proportions of 1.8 moles SiO_2 to one mole ZnO. They contained, as before, 15 per cent potassium chloride which was washed out after firing.

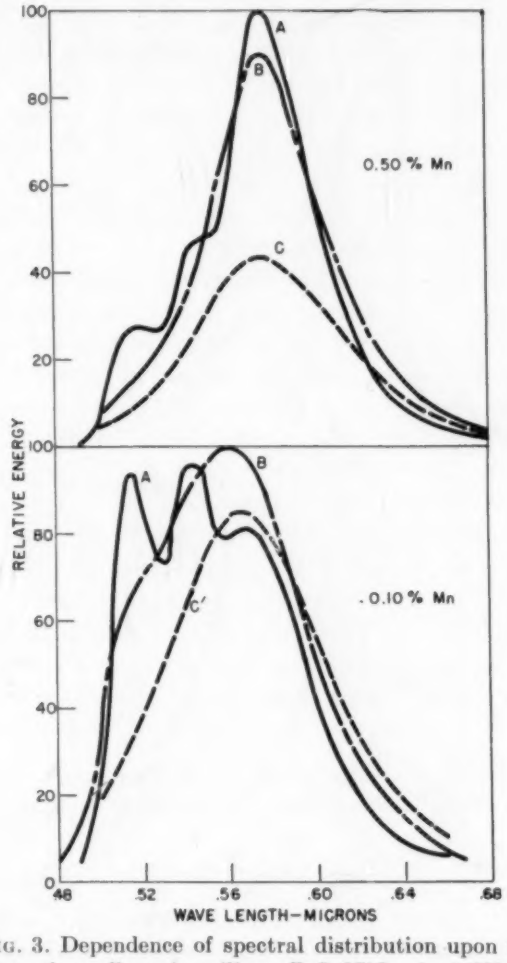

FIG. 3. Dependence of spectral distribution upon temperature for yellow zinc silicate $ZnO \cdot 2SiO_2$. A—80°K, B—298°K, C—480°K, C'—475°K.

The first group of experiments was made to find how the shorter wave emission depended upon the manganese concentration. As is evident from the curves of Fig. 3, the shorter wave emission occurs as two bands whose peaks are at 5150 Å and 5440 Å. They are intensified by a reduction in manganese concentration. They are also intensified, with reference to the yellow emission band at 5800 Å, by a reduction in temperature, a result which is in agreement with observations by Shrader (4). Such an effect of temperature is contrary to what normally happens with a single-activated phosphor whose

emission comprises more than one band. It is therefore probable that the yellow-emitting zinc silicate phosphor possesses two types of centers, one giving rise to the 5800 Å band and a second one which is responsible for the emission of the shorter wavelength doublet at low temperatures and low manganese concentration.

The phosphor with 0.5 per cent Mn, in which the 5800 Å band predominates, showed a brightness at room temperature which was 50 per cent of the green zinc silicate under 2537 Å excitation and which was

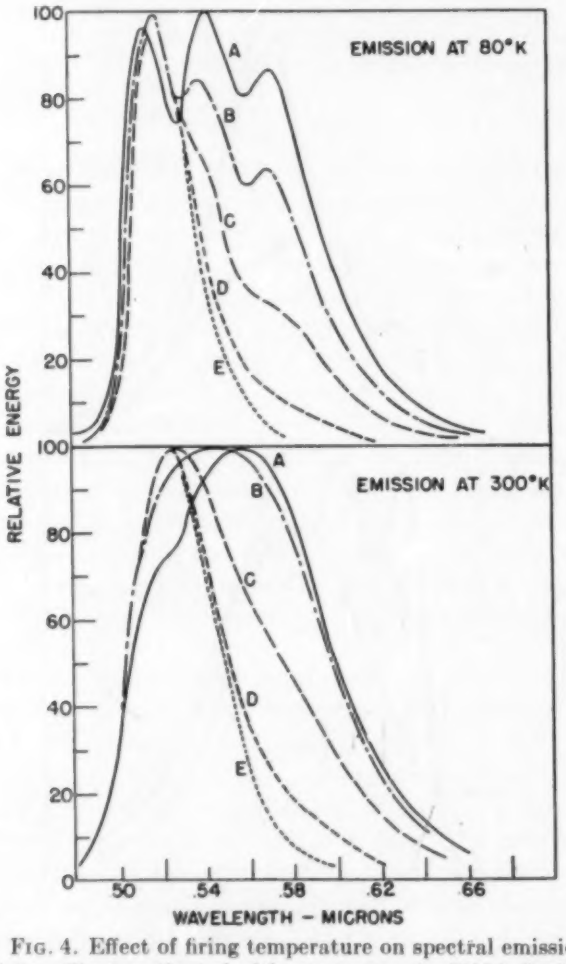

FIG. 4. Effect of firing temperature on spectral emission of zinc silicate activated with manganese. A—700° to 750°C, B—800°C, C—850°C, D—900°C, E—1200°C (no flux). The phosphors ($ZnO \cdot (1.8)SiO_2$) contain 0.1% Mn.

nearly as bright under cathode ray excitation. Its decay constant was greater than that for the green zinc silicate having the same manganese concentration.

The second group of experiments was made with the aim of investigating the structure as disclosed by diffraction patterns of phosphors prepared at various temperatures ranging from 700° to 1200°C. The low manganese concentration of 0.1 per cent Mn was used in order that the changes in relative intensity of all three emission bands at 5800 Å, 5440 Å, and 5150 Å might be followed. At the same time, the development of the green band at 5250 Å, characteristic of the normal orthosilicate, could be observed. The extent of formation of the normal orthosilicate could thereby be demonstrated in two ways: by the appearance of its emission band and by the alteration in the diffraction pattern.

TABLE II

hkl	d obs	d calc	d R + McK	I_{obs}	hkl	d obs	d calc	d R + McK	I_{obs}
101	7.39	7.37		¼	314	1.910	1.913	1.918	1
201	5.07	5.04		¼	503	1.896	1.898		¼
					521	1.875	1.878	1.880	1
102	4.33	4.35	4.39	1	105	1.846	1.845	1.855	½
211	4.09	4.07	4.10	2	522	1.772	1.774		¼
300	4.00	3.99	4.04	5	711		1.770		
112	3.88	3.87		1	414	1.743	1.741		½
202	3.67	3.68	3.703	2	215	1.723	1.726		½
301	3.64	3.67	3.646	3	701				
220	3.46	3.46	3.502	3	531	1.682	1.683	1.686	2
					603		1.680		
221	3.166	3.165	3.238	4	620	1.658	1.661	1.660	½
302	3.041	3.034	3.067	2	621	1.634	1.635	1.635	6
113	2.831	2.838	2.846	6	523		1.633		
203	2.753	2.762		1				1.596?	
320		2.747			613	1.577	1.575	1.580	1
213	2.567	2.565		½	622	1.563	1.565		½
402	2.518	2.520	2.531	1	711		1.564		½
411		2.517	2.403?		006	1.557	1.556	1.559	½
303	2.467	2.455	2.454	6	540	1.534	1.533	1.531	½
322	2.367	2.368	2.398	1	541	1.514	1.513	1.517	7
004	2.347	2.335		½	800	1.497	1.497	1.488	5
330	2.300	2.304	2.313	1	720	1.461	1.463		2
104		2.291			335	1.449	1.451		1
331	2.238	2.238	2.250	1	306		1.451		
421	2.200	2.199	2.210	1	721	1.443	1.445	1.446	3
511	2.096	2.099	2.114	4	425		1.441		
422	2.044	2.038	2.053	2	632	1.435	1.436		½
304	2.017	2.015	2.022	3	802	1.429	1.425	1.430	2
413	1.999	2.001		½	226	1.419	1.419	1.420	4
600		1.996		½	810	1.403	1.402	1.406	2
512	1.959	1.954	1.967	1	444	1.392	1.389	1.394	½
601		1.952			550	1.384	1.383		½
224	1.940	1.933	1.947	1	551	1.370	1.368	1.371	2
431	1.925	1.926		¼	641	1.358	1.359		½
					633		1.358		

$a_0 = 13.86$ Å.
$c_0 = 9.34$ Å.

The spectral distribution of typical phosphors selected from those prepared within the temperature range of 700°–1200°C is shown in Fig. 4. At the upper limit of the temperature range, the emission of the product formed at 1200°C from the mixture of one mole ZnO with 1.8 moles SiO_2 is identical with the emission of the normal green orthosilicate, prepared likewise at 1200°C from a mixture of 1.8 moles ZnO with one mole SiO_2.

From inspection of these spectral distribution

curves, it is evident that the product formed at 700°–750°C is predominantly the yellow-emitting phosphor. Not only is the 5800 Å band prominent, but so likewise is the 5150 Å band, and no evidence appears of the green orthosilicate band at 5250 Å. At 800°C and above, however, the 5250 Å band becomes perceptible and finally predominant. It is well defined in Curves C and D at 25°C, a temperature at which the doublet bands, 5150 Å and 5440 Å, are largely suppressed. At liquid air temperature, the peak is observed at 5200 Å. This serves to denote the presence of some yellow-emitting silicate, even in the product formed at 900°C. The extension of the curve on the long wavelength side confirms this conclusion. The spectral emission proved much more sensitive to the presence of the yellow form than the x-ray diffraction patterns. The reason for this will be seen below.

Several yellow fluorescing phosphors were examined by x-ray diffraction. The optical spectra of these phosphors were practically identical but the x-ray diffraction patterns were strikingly different. Several of the preparations showed no pattern at all but a few gave the very complex pattern reported by Rooksby and McKeag. The phosphors which were fused and chilled gave the most extensive x-ray pattern. Quartz or cristobalite patterns were found in those phosphors with an excess of silica.

The small effect that the crystallinity had on the optical spectrum indicates that it is only the immediate environment of the activator ion that determines the character of the emission.

Ortho zinc silicate is hexagonal (5) with $a_0 = 13.92$ Å, and $c_0 = 9.33$ Å corresponding to $c/a = 0.67$. The yellow fluorescing phosphors were examined optically. Some of the preparations showed no crystallinity. Other preparations had small crystals *ca.* 10 μ in diameter mixed with amorphous matter. The crystals looked rhombohedral with an axial ratio of 0.65. When viewed under ultraviolet light the small crystals fluoresced yellow proving that the fluorescence was not due to the amorphous components of the phosphor.

It was possible to index the complex powder pattern (56 lines) on the basis of a slightly reduced zinc orthosilicate lattice. The calculated d values were based on $a_0 = 13.86$ Å, $c_0 = 9.34$ Å, and $c/a = 0.67$ (Table II). Some of the lines prohibited by a rhombohedral structure show up, however, indicating a real change in structure.

The agreement of our pattern and that of Rooksby and McKeag was quite good. Crystals for single crystal x-ray diffraction patterns to determine the unit cell with certainty could not be obtained. On the basis of the powder data, the structure of the yellow fluorescing zinc orthosilicate is closely related to that of the normal zinc orthosilicate.

The optical and x-ray evidence show that the active regions in this phosphor are small enough so that they do not have to give an x-ray pattern and yet the occasional presence of x-ray patterns indicated that some ordering greater than atomic dimensions is present in the yellow phosphor. In Fonda's earlier preparations these ordered domains were enclosed in the silica matrix. Rooksby and McKeag prepared their phosphors under such conditions as to promote growth of larger regions.

At least three types of structures in the zinc orthosilicate phosphors may then be recognized: (*a*) the green fluorescing definitely crystalline phosphor, (*b*) the yellow fluorescing phosphor with some order extending for at least several unit cells, and (*c*) the red fluorescing phosphor which is a glass.

The x-ray diffraction evidence indicates that the yellow phosphor is a distorted form of the normal green zinc orthosilicate. This distortion seems to have a definite structure or limits of distortion of its own. If this were not so it would be possible to prepare a continuous series of phosphors from the green to the red.

Any discussion of this paper will appear in a Discussion Section, to be published in the December 1952 issue of the JOURNAL.

REFERENCES

1. G. R. FONDA, *J. Phys. Chem.*, **44**, 851 (1940).
2. A. SCHLEEDE AND A. GRUHL, *Z. Elektrochem.*, **29**, 411 (1923).
3. H. P. ROOKSBY AND A. H. MCKEAG, *Trans. Faraday Soc.* **37**, 308 (1941).
4. R. E. SHRADER, *J. Optical Soc. Am.*, **39**, 699 (1949).
5. W. SCHUTZ, *Z. physik. Chem.*, **B31**, 298 (1936).

The Function of Oxygen in Zinc Sulfide Phosphors[1]

F. A. Kroeger and J. A. M. Dikhoff

Philips Research Laboratories, N. V. Philips' Gloeilampenfabrieken, Eindhoven, Netherlands

ABSTRACT

At 1200°C ZnS and ZnO form solid solutions of the composition ZnS—1 mole per cent ZnO and ZnO—0.3 mole per cent ZnS. The incorporation of ZnO in ZnS causes the appearance of a new absorption band and, in the presence of activators, of new fluorescence bands displaced about 150 Å toward longer wavelengths with respect to the original bands. These effects are explained by the assumption of separate oxygen levels 0.1 ev above the full band and of new centers consisting of associated pairs of oxygen and activator ions. The formation of such pairs is explained on the basis of the principle of compensation of volume. This principle also explains the favorable effect of oxygen on the intensity of fluorescence. It is found to be the logical complement of the principle of compensation of charge introduced earlier in connection with the incorporation of ions of a certain valency in a base lattice consisting of ions of a different valency.

It is shown that oxygen gives rise to characteristic traps and has further a marked effect in combination with fluxes.

The optical properties of ZnO-xZnS are briefly described and explained along similar lines.

Introduction

Zinc sulfide phosphors made in the presence of oxygen differ in many of their properties from similar phosphors made with exclusion of oxygen. Thus zinc sulfide activated with copper and made with the addition of a chloride flux shows only a moderate green afterglow, but a strong and persistent afterglow is observed when 1–2 per cent ZnO is added before firing (1). Comparison of the thermoluminescence of these products shows that the latter have a strong glow peak above room temperature while with the former this peak is very weak. Refiring with sulfur destroys the extra glow peak (2).

Oxygen influences the spectral distribution of the luminescence in two ways. It affects the position of separate sub-bands and it affects the relative intensities of the various sub-bands. Examples of the first effect are given by Rothschild (3) for ZnS-Cu and by Smith (4) for ZnS-Ag. In all cases oxygen shifts the bands 100–150 Å toward longer wavelengths.[2] The second effect has been found with ZnS-Cu made with NaCl as a flux. In this case addition of ZnO was found to lead to a green luminescent product while a similar product made without ZnO showed fluorescence in the blue copper band (6).

Finally, oxygen has been reported to increase the intensity of fluorescence when the phosphors are prepared with halide fluxes; however, moderate intensities are also attained for preparations with oxygen but without such fluxes (4, 9). This point is particularly important. As shown previously, ZnS can be activated by Ag, Cu, or Au only when the samples are fired in the presence of compounds containing the monovalent anions Cl^-, Br^-, or I^- (5, 7, 8) or trivalent cations (9) and this has been explained on the basis of the assumption that only in the presence of such ions can Ag, Cu, or Au be incorporated in the ZnS lattice. The reason is that the activators are present as ions rather than as atoms. In the case of silver this means that silver must be incorporated as Ag_2S. Incorporation of Ag_2S in ZnS requires either the formation of a sulfur vacancy for each two Ag^+ ions added, or the occupation of interstitial sites by half of the silver ions. Both effects cause a large increase in the free energy of the system and, therefore, the solubility will be extremely low. These complications are avoided, and the solubility is accordingly increased, when the lack of charge due to the substitution of divalent zinc by monovalent silver is compensated by a simultaneous replacement of an equivalent amount of divalent sulfur by monovalent halogens, or of divalent zinc by trivalent cations. The observations by Smith (4) indicate that oxygen slightly increases the solubility of Ag in ZnS without the aid of compensation of charge. This effect is particularly noticeable with methods of excitation in which the centers are not directly excited and for which accordingly the concentration of centers giving a reasonable intensity of luminescence may be low (cathode rays).

The effects of oxygen must be explained either

[1] Manuscript received June 14, 1951. This paper prepared for delivery before the Washington Meeting, April 8 to 12, 1951.

[2] This effect is observed with products of one crystal modification; it is therefore not due to a transition from wurtzite to sphalerite (3, 5).

by the incorporation of oxygen in the sulfide lattice, leading to the formation of solid solutions of ZnS-ZnO; by the variation of oxidation-reduction equilibria of the ZnS itself or of the activators; or to a combination of these two effects. Incorporation of extra oxygen in the interlattice may be excluded because the space available in the interlattice is much too small to house the large oxygen ions. If solid solutions occur they must be expected to be of the normal type, in which part of the sulfur is replaced by oxygen at the same normal lattice positions. The nature of the reactions between sulfides and oxygen or oxides may be understood from the following:

In certain oxides a reaction may occur with oxygen such that the proportion of cations to anions present in the system is decreased. In this process the charge of the cations is increased (they are oxidized), as for example in

$$Sn^{2+}O^{2-} + \tfrac{1}{2}O_2 \rightarrow Sn^{4+}O_2^{2-}. \qquad (I)$$

This is an oxidation, either of the solid system as a whole, or of the cations. In a partially reduced system, oxygen similarly decreases the degree of reduction and causes the compound to become stoichiometric,

$$Zn^{2+}O^{2-}\cdot\delta Zn^0 + \frac{\delta}{2}O_2 \rightarrow (1+\delta)Zn^{2+}O^{2-}\cdot \qquad (II)$$

Similarly if the system contains different kinds of cations, the oxygen may oxidize only one of them; for instance,

$$Mg_2TiO_4\cdot x Mn^{2+}O^{2-} + \frac{x}{2}O_2 \rightarrow Mg_2TiO_4\cdot x Mn^{4+}O_2^{2-}\cdot \qquad (III)$$

It has often been assumed that the type of reaction mentioned above is also predominant in reactions between a *sulfide* and oxygen, and that oxygen therefore would tend to oxidize the sulfide. As first pointed out by Schleede (10) this is not the case: oxygen reacts with a sulfide primarily to form SO_2, thus,

$$Zn^{2+}S^{2-} + \delta O_2 \rightarrow (1-\delta)\,Zn^{2+}S^{2-}\cdot\delta Zn^0 + \delta SO_2. \qquad (IV)$$

The oxygen therefore acts as a *reducing* agent for the sulfide[3]. As it is known, however, that heating of ZnS with oxygen finally leads to stoichiometric ZnO, apparently equation (IV) does not describe the entire process, but only the initial phase of it.

This initial phase predominates as long as the concentration of the excess zinc and the pressure of the SO_2 evolved is not too high. With an increase in the concentration of reduced ZnS and the pressure of SO_2, the rate of the reducing reactions (IV) is decreased while the rate of an oxidizing reaction similar to (II) is increased[4],

$$Zn^{2+}S^{2-}\cdot\delta Zn^0 + \frac{\delta'}{2}O_2 \rightarrow ZnS\cdot(\delta-\delta')Zn^0 + \delta' ZnO. \qquad (V)$$

Eventually reaction (V) must occur together with (IV); but, as long as ZnS is present, (V) will never overtake (IV). Therefore the solid will always remain reduced. The ZnO formed in reaction (V) may partly or totally dissolve in the ZnS phase, leading to

$$Zn^{2+}(S_{(1-\delta')}\,O_{\delta'})^{2-}\cdot(\delta-\delta')\,Zn^0.$$

Effects similar to those discussed so far for the treatment of a sulfide with oxygen will also occur upon reaction of a sulfide with an oxide; for instance ZnS with ZnO,

$$Zn^{2+}S^{2-} + \left(\frac{2\delta}{3}+x\right)Zn^{2+}O^{2-} \rightarrow \left(1-\frac{\delta}{3}\right)Zn^{2+}S^{2-}{}_{(1-x)}\,O_x^{2-}\cdot\delta Zn^0 + \frac{\delta}{3}SO_2\cdot \qquad (VI)$$

Incidentally it may be emphasized that the same reaction makes S_2 or sulfides a reducing agent for ZnO. Therefore equation (VI) may be extended to cover the entire composition range, indicating the formation of reduced solid solutions both at the ZnS side and at the ZnO side of the system;

$$Zn^{2+}S^{2-} + Zn^{2+}O^{2-} \rightarrow Zn^{2+}(S,O)^{2-}\cdot\delta Zn^0 + Zn^{2+}(O,S)^{2-}\cdot\gamma Zn^0 + \frac{\delta+\gamma}{3}SO_2\cdot \qquad (VII)$$

As long as both sulfur and oxygen ions are present in the solid, each phase must remain reduced[5]. Only when one of them has disappeared, as may happen after a prolonged treatment with S_2 or O_2, will it be possible to obtain the stoichiometric compounds ZnS or ZnO.

So far we have discussed only the principles of reductions and of the formation of solid solutions, separately or in combination. In the past the extent to which these effects occur and their importance to the optical field have not always been clear. For example, the assumption that the shifting of the position of the fluorescence bands is due to a reduction

[3] Another example of the reducing effect of oxygen on a sulfide is given by PbS, the treatment of which with oxygen causes a stoichiometric excess of lead (11).

[4] For ZnS heated in an open crucible, the SO_2 pressure is determined by the partial pressure of the SO_2 remaining between the particles of the powder.

[5] This conclusion holds quite generally, independent of whether that state in which both S^{2-} and O^{2-} ions are present is reached by reactions of type (VII) or of type (V).

of the sulfide seems to find support in the observations by Rothschild (3), who found that preparation in the presence of zinc dust affected the properties of the phosphors in the same way as preparation with addition of ZnO. Sulfur, on the other hand, which of course must be expected to have an oxidizing influence on the sulfide, suppressed the effects of both agents. This, however, is not convincing; in the first place zinc dust always contains a considerable amount of oxide. Furthermore, the ZnS used almost certainly contained some ZnO or $Zn(OH)_2$ (4). Either of these is transformed into ZnS when the preparation is carried out with addition of sulfur but remains unchanged upon firing with zinc dust.

In the present paper we shall try to find the explanation for the effect of oxygen in the various cases. To this end we shall investigate the influence of oxygen on pure ZnS, on activated ZnS made without fluxes, and on activated ZnS made with fluxes.

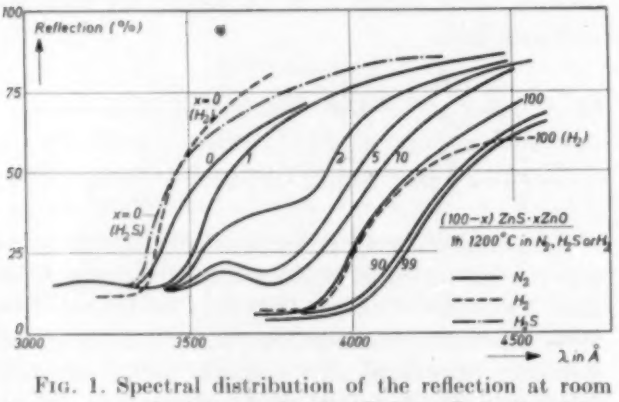

FIG. 1. Spectral distribution of the reflection at room temperature of mixtures of $(100-x)$ZnS + xZnO after firing for one hour at 1200°C in an atmosphere of N_2, H_2, or H_2S. The figures on the curves refer to the value of x.

EXPERIMENTAL PROCEDURES AND RESULTS

ZnS-ZnO

Intimate mixtures of ZnS and ZnO containing these substances in various proportions were heated at 1200°C, a temperature which is sufficiently high to guarantee crystallization without addition of fluxes. The samples were placed in narrow quartz tubes and nitrogen was used as a protecting atmosphere. The ZnS used was made by precipitation with H_2S from a purified aqueous solution of $ZnSO_4$. The ZnO was a commercial product, Analar (analytical reagent grade), made by Hopkins and Williams Ltd., England. The properties of the fired product depend on its composition. At the ZnS side of the binary system the products are white. Pure ZnO is equally white. Mixtures of ZnO-ZnS rich in ZnO are greenish yellow.

Absorption characteristics of the samples were determined by means of reflection measurements (Fig. 1). ZnS fired in N_2 shows an absorption edge at 3400 Å. Products made with addition of 1 mole per cent ZnO show an edge at 3500 Å. As ZnS normally contains some ZnO it must be expected that the value found for ZnS fired in N_2 is not the one characteristic of pure ZnS. ZnS fired in H_2S and thus transformed into really pure ZnS actually shows an edge at a slightly shorter wavelength; viz., 3350 Å. While samples containing more than 2 mole per cent ZnO show indications of an edge at 3500 Å, a new edge appears near 3900 Å. The position of this edge shifts slightly toward longer wavelengths with increasing ZnO content up to 4000 Å at 99 mole per cent ZnO. From 99 to 100 mole per cent ZnO the edge recedes to 3850 Å, the value for pure ZnO (12, 13). These results indicate that we have two phases: a ZnS phase and a ZnO phase, the former with edges at 3350 and 3500 Å, and the latter with edges at 3850 and 4000 Å. X-ray analysis supports this view. Pure ZnS and samples of 99ZnS-1ZnO show the diffraction lines of ZnS; pure ZnO and 99ZnO-1ZnS show the lines of ZnO. Products of intermediate composition show the diffraction patterns of ZnS and ZnO superimposed.

A precise determination of the lattice dimensions was carried out by L. J. M. van Weert in this laboratory, using the back-reflection technique. The results are summarized in Table I. The lattice dimensions of pure ZnS and ZnO depend slightly on the material used, probably due to minute quantities of contaminations present in varying amounts (ZnS, batches A and B). For a given batch of ZnS, the addition of ZnO causes the unit cell to contract. Addition of ZnS to ZnO, on the other hand, causes the ZnO cell to expand. Such effects are to be expected when solid solutions of ZnS-ZnO are formed. Reduction leading to an excess of zinc above the stoichiometric composition should, however, cause an increase in the lattice dimensions for both cases (14).

If we assume that solid solutions of ZnS-ZnO are formed, their composition can be calculated by applying Vegard's law. In Table I the values calculated from the a and c axes are given separately, together with their average. It is found that ZnS dissolves approximately 1 mole per cent ZnO, while ZnO dissolves about 0.3 mole per cent ZnS. These values are in good agreement with those found from the composition at which the diffraction lines of the ZnO and ZnS phases begin to appear together (Table I, third column) or from the composition at which the long wavelength edges attributed to the ZnO phase begin to appear (Fig. 1).

In order to decide whether the variation in the

absorption spectrum accompanying the incorporation of ZnO in ZnS and of ZnS in ZnO is directly due to the formation of solid solutions of ZnS-ZnO, or to an additional reduction according to the reactions described in the introduction, we submitted pure ZnS and ZnO to a strong reducing influence by heating at 1200°C in hydrogen. ZnS does not change its reflection. ZnO becomes slightly yellowish; its reflection curve shows a slight decrease in the long-wave region, but the position of the edge remains unchanged (Fig. 1). Therefore it must be concluded that the variations in the absorption spectrum, when passing from ZnS to ZnS − 1 mole per cent ZnO and from ZnO to ZnO − 0.3 mole per cent ZnS, are due to the incorporation of oxygen or sulfur and not to excess zinc caused by reducing effects.

These results may seem to contradict those obtained with ZnO by Mollwo and Stöckmann (15), who found a displacement of the absorption edge upon reduction. These authors, however, prepared their samples by burning zinc in a flame, and under these conditions the excess of zinc was extremely large (~0.5 mole per cent). Reheating at a high temperature (1000°C) caused the edge to shift back to its normal position, and the authors attributed this effect to the evaporation of the excess of zinc[6]. As our experiments were carried out at a higher temperature, extra zinc possibly formed must have evaporated to a still greater extent, and accordingly there was no appreciable deviation from stoichiometry. The long-wave tail in the absorption spectrum indicates, however, that a trace of zinc in excess was still present in the lattice.

The products of the binary system ZnS-ZnO were also investigated for luminescence upon excitation by $\lambda = 2537$ Å. Pure ZnS, heated either in H_2S or H_2, is nonluminescent at room temperature but shows an ultraviolet fluorescence with a maximum at 3360 Å at −180°C. This is the band long recognized as the fundamental fluorescence of ZnS (16). Products containing small amounts of ZnO (e.g., 1 mole per cent) are usually also nonluminescent at room temperature: at liquid air temperature they show a band with a maximum at 3640 Å; i.e., immediately next to the new absorption edge at 3500 Å (Fig. 2). Some samples of ZnS − 1 mole per cent ZnO show a weak blue luminescence at room temperature in a band with a maximum at 4550 Å. Apparently this is the band of self-activated ZnS. As this band is extremely weak and does not appear in all cases we are

TABLE I. *Lattice constants of the* ZnS *and* ZnO *phases in the system* ZnS-ZnO, *and the limits of mutual solubility of* ZnS *and* ZnO *at 1200°C*

Composition of starting material	Conditions of firing	Phases observed	Unit cell dimensions of the main phase		Composition of the main phase (100 − x) ZnS − xZnO		Average solubility in %
			a	c	$(x)_a$	$(x)_c$	
ZnS(batch A)	0.5 hr,1200°C,H_2S	ZnS	3.8233	6.2668	0	0	1
ZnS(batch A)	0.5 hr,1200°C,N_2	ZnS	3.8263	6.2625	−0.5 (!)	0.4	
99 ZnS(batch A) + 1 ZnO	0.5 hr,1200°C,N_2	ZnS	3.8180	6.2516	0.92	1.43	
98 ZnS(batch A) + 2 ZnO	0.5 hr,1200°C,N_2	ZnS+ZnO	3.8183	6.2514	0.88	1.45	
95 ZnS(batch A) + 5 ZnO	0.5 hr,1200°C,N_2	ZnS+ZnO	3.8172	6.2503	1.06	1.55	
ZnS(batch B)	0.5 hr,1200°C,H_2S	ZnS	3.8240	6.2612	0	0	
ZnS(batch B)	0.5 hr,1200°C,SO_2+O_2	ZnS	3.8189	6.2485	0.89	1.0	
ZnO	0.5 hr,1200°C,N_2+H_2	ZnO	3.2496	5.2063	100	100	
ZnO	0.5 hr,1200°C,N_2	ZnO	3.2496	5.2057	100	100	
99 ZnO + 1 ZnS	0.5 hr,1200°C,N_2	ZnO	3.2514	5.2096	99.69	99.66	0.3
98 ZnO + 2 ZnS	0.5 hr,1200°C,N_2	ZnO+ZnS	3.2513	5.2090	99.71	99.71	
95 ZnO + 5 ZnS	0.5 hr,1200°C,N_2	ZnO+ZnS	3.2514	5.2094	99.69	99.68	
90 ZnO + 10 ZnS	0.5 hr,1200°C,N_2	ZnO+ZnS	3.2514	5.2089	99.69	99.73	

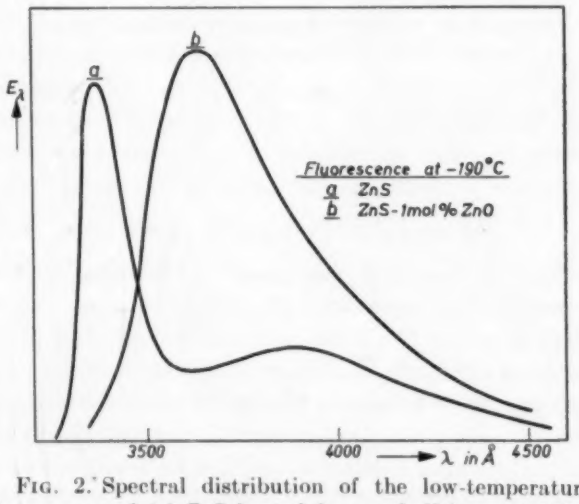

FIG. 2. Spectral distribution of the low-temperature fluorescence of (*a*) ZnS heated for one-half hour at 1200° C in H_2S, and (*b*) of ZnS-1 mole per cent ZnO heated for one-half hour at 1200°C in N_2.

[6] Faivre (14) observed the same for CdO.

not quite certain whether it is caused by contamination with halogen ions or trivalent cations, or whether it is truly promoted by the ZnO[7]. Products of ZnO — 1 mole per cent ZnS show a moderately strong green fluorescence in a broad band with a maximum at 5050 Å. Under the conditions of the experiment sulfide-free ZnO does not show this green luminescence but only the ultraviolet fundamental fluorescence of ZnO with a peak at 3880 Å (16). ZnO, heated in H_2 at 1200°C, however, is strongly fluorescent in a green band with a peak at 5050 Å, exactly identical with the band found with ZnO-ZnS. This is the band generally attributed to a stoichiometric excess of zinc; apparently the small concentration of extra zinc causing the weak long-wave absorption mentioned above is sufficient to account for the strong green luminescence shown by this sample.

The fact that ZnO fired in N_2 does not show the green fluorescence, while ZnO + ZnS fired under the same conditions does show it, indicates that the presence of the sulfide favors reduction, probably by the reaction described in the introduction. Thomsen (17) has observed the same effect, but this author interprets it in a different way, ascribing the green luminescence to sulfur incorporated in the ZnO. Although we have seen that ZnO actually dissolves some ZnS under these conditions, this cannot explain the green luminescence, for precisely the same green luminescence appears in partially reduced ZnO prepared by oxidation of spectroscopically pure zinc metal which is definitely free of sulfur.

Solid solutions of ZnS-ZnO can also be made by heating ZnS in an atmosphere containing oxygen (O_2, air, $SO_2 + O_2$)[8] or by heating ZnO in a sulfurizing atmosphere (H_2S, S_2, $N_2 + CS_2$). All properties of samples obtained in this way proved to be the same as those of samples of a corresponding composition prepared in the manner first described.

Activated ZnS Prepared without Fluxes

Oxygen-free ZnS was made by heating precipitated ZnS for one hour at 1100°C in a current of H_2S. Starting from this material, oxygen-free phosphors containing Ag, Cu, or Au were made by adding aqueous solutions of $Ag(NO_3)$, $Cu(NO_3)_2$, or $AuCl_3$ in normal concentrations ($\sim 10^{-5}$ gram atom per mole ZnS), drying, and heating for one-half hour at 1100°–1300°C in an atmosphere of H_2S or H_2S + HCl. Luminophors containing oxygen were made from similar mixtures containing 1 mole per cent of ZnO. In this case the firing was carried out in nitrogen. The luminescence properties were investigated upon excitation by $\lambda = 3650$ Å.

All oxygen-free products fired in H_2S were found to be nonluminescent. Oxygen-free products fired in H_2S-HCl are strongly luminescent in the bands characteristic of the activators, as previously found (5, 7, 8).

Products containing oxygen and fired in N_2 show a weak luminescence in bands characteristic of the activators. The spectral distributions of the luminescence are similar to those of the oxide-free phosphors, but all bands are shifted over ~ 150 Å toward longer wavelengths. The direction of the shift is the same as observed by Rothschild (3) and Smith (4), but the magnitude of the shift is even greater.

Table II gives a survey of the maxima of the fluorescence bands of the various products. The table also includes figures for the blue band of self-activated ZnS. For the case of silver as activator, the reflectivity was also measured and compared with that of corresponding products without silver. The results are shown in Fig. 3. The difference in the position of the absorption edge for products with and without ZnO is of the same order as the difference between the maxima of the fluorescence bands. The activated products show next to the fundamental bands a long-wave absorption band extending from 3500 to 4000 Å. This band is due to the centers of luminescence (5): it is extremely weak for nonfluorescent samples prepared by firing in H_2S (curve *c*); it is somewhat stronger in the weakly luminescent ZnS — 1 mole per cent ZnO-Ag (curve *d*), and has maximum strength in the strongly luminescent ZnS-Ag (Cl) (curve *e*). This proves that the concentration of centers in ZnS — 1 mole per cent ZnO-Ag is much lower than that in ZnS-Ag (Cl), as is also indicated by the difference in the intensity of the fluorescence. Obviously in the former product only a fraction of the silver added is incorporated in the proper way to form a center. Therefore, although oxygen promotes the formation of centers, it does so to a much smaller extent than halogens.

With copper-activated phosphors prepared in this way the results are similar. In this case the situation is complicated, however, by the appearance of two copper bands, one in the green and one in the blue. Just as has been found for phosphors prepared in the presence of halogen or trivalent cations (3, 7, 8, 9), the green band appears at relatively low, and

[7] In a recent paper, Bube (33) describes the appearance of the blue band of self-activated ZnS for products fired at a high temperature without fluxes. It is stated that the samples are entirely free of halogen ions. It would be of interest to know whether they are also free of trivalent cations. In any case it is fairly certain that the products did contain oxygen, as is indicated by the glow curves of ZnS-Cu, prepared in the same way, which reveal the high temperature glow peak characteristic of oxygen.

[8] Contrary to what is reported in the literature (18, 4), pure SO_2 does not transform ZnS into ZnO. Whenever this reaction occurs it is due to traces of O_2 or SO_3.

the blue band at relatively high, concentrations. The concentration at which the color changes over, however, is different for the various cases, and is much lower for ZnS − 1 mole per cent ZnO-Cu than for ZnS-Cu prepared in H_2S-HCl. This is demonstrated in Fig. 4 where the ratio $R = I_{green}:I_{blue}$ is plotted against the copper content[9]. In order to prevent complications due to energy transfer from blue to green centers, the curve is based on measurements of the spectral distributions carried out at −190°C.

For ZnS-Cu made by firing in H_2S-HCl it has been shown (8) that the proportion between the green Cu^+ and the blue Cu_2^+ centers is governed by an equilibrium which is determined by two factors: the stabilization of Cu^+ in the lattice by the simultaneous incorporation of Cl^- (compensation of charge) and the reduction of Cu^+ to Cu_2^+. The first factor favors the green centers, the second the blue. In ZnS-ZnO-Cu the first function is taken over by the oxide; but, as we have seen for the case of ZnS-ZnO-Ag, only to a small extent. On the other hand,

TABLE II

System	Temperature and atmosphere of preparation		Fluorescence			Absorption		
			Peak position		Wave number difference for products with and without ZnO	Absorption edge		$\Delta\nu$
			λ(Å)	ν(cm^{-1})		λ(Å)	ν(cm^{-1})	
	°C							
ZnS	1200	H_2S	3360	29760		3345	29900	
ZnS-1% ZnO	1200	N_2	3640	27470	2290	3500	28575	1325
ZnS	1100	70H_2S−30HCl	4455	22445				
ZnS-1% ZnO	1100	H_2	4550	22000	445			
ZnS-1% ZnO-5% NaCl	1100	N_2	4500	22220	225			
ZnS-5.10^{-5}Ag	1200	90H_2S−10HCl	4300	23250		3340	29950	
ZnS-1% ZnO-5.10^{-5}Ag	1200	N_2	4500	22220	1030	3500	28575	1375
ZnS-1% ZnO-2% NaCl-5.10^{-5}Ag	1200	N_2	4400	22730	420			
ZnS-1% NaCl-3.10^{-6}Cu	1100	N_2	5140	19455				
ZnS-1% ZnO-7.10^{-6}Cu	1100	N_2	5280	18940	515			
ZnS-1% ZnO-1% NaCl-7.10^{-6}Cu	1100	N_2	5200	19230	225			
ZnS-5.10^{-5}Au	1200	N_2+HCl	5260	19010				
ZnS-1% ZnO-5.10^{-5}Au	1200	N_2	5430	18415	595			

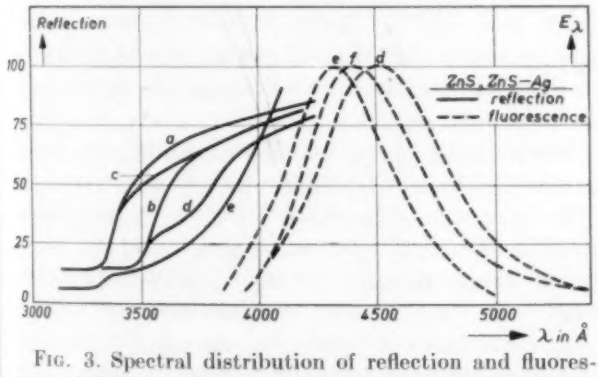

FIG. 3. Spectral distribution of reflection and fluorescence of ZnS and ZnS-Ag made under various conditions. The fluorescence was excited by λ = 3650 Å. All measurements were carried out at room temperatures. *a*) ZnS fired for ½ hr at 1200°C in H_2S; *b*) ZnS − 1 mole per cent ZnO fired for ½ hr at 1200°C in N_2; *c*) ZnS − 5 ·10^{-5}Ag fired for ½ hr at 1200°C in H_2S; *d*) ZnS − 1 mole per cent ZnO − 5·10^{-5} Ag fired for ½ hr at 1200°C in N_2; *e*) ZnS − 5·10^{-5} Ag (+ 2 per cent NaCl) fired for ½ hr at 1200°C in N_2; *f*) ZnS − 1 mole per cent ZnO − 5·10^{-5} Ag (+2 per cent NaCl) fired for ½ hr at 1200°C in N_2.

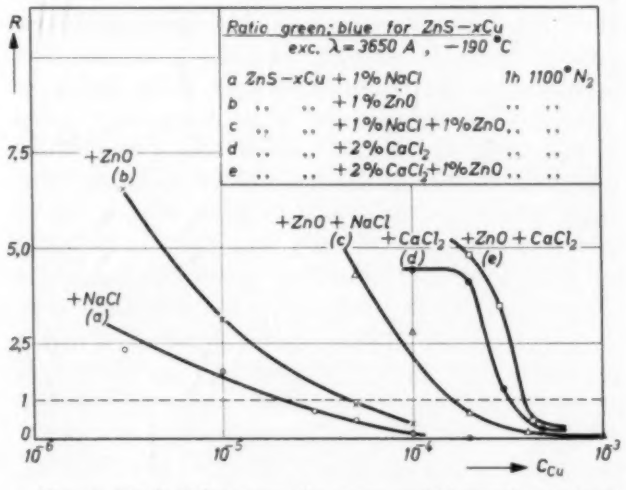

FIG. 4. Ratio *R* between the green and blue sub-bands of ZnS-Cu containing various amounts of copper and prepared in different ways.

[9] The measurements have not been extended to the extremely low copper concentrations at which the blue fluorescence due to self-activation becomes predominant (7).

a reducing influence is exerted by reactions between sulfide and oxide of the type described in the introduction; for this case they may be

$$4Cu_2S + 2Cu_2O \rightarrow 3Cu_4S + SO_2.$$

The weakness of the stabilization, together with this reduction of the copper, tends to decrease the concentration at which copper is still present predominantly as green centers.

Activated Systems Prepared with Halide Fluxes

The influence of ZnO on phosphors made with halide fluxes was investigated by comparing phosphors made with and without addition of 1 mole per cent ZnO. The fluxes were added in a concentration of 2 per cent, and the firing was carried out at 1200°C for one-half hour.

For silver-activated products made with NaCl or $CaCl_2$ as flux, the intensity of the fluorescence is not markedly affected by the presence of ZnO. The maximum of the fluorescence of the products without oxygen is situated at the same position as for products made in H_2S-HCl; the maximum for products containing ZnO, however, is situated ~100 Å toward longer wavelengths, i.e., intermediate between that of the oxygen-free samples and of the samples made with ZnO but without fluxes (Fig. 3). For copper-activated products similar shifts of the position of the sub-bands are observed. Apart from this, the proportion between the green and blue copper bands is strongly dependent on the flux used and on the presence of ZnO. With NaCl, for instance, the fluorescence is predominantly green at extremely low copper concentrations, but at medium concentrations the fluorescence turns blue. The same is the case for products made without NaCl but with addition of ZnO. Simultaneous addition of NaCl and ZnO, however, shifts the green-blue cross-over point to much higher concentrations (Fig. 4). $CaCl_2$ causes green to occur up to much higher concentrations, and addition of ZnO has hardly any effect in this case. These results show that Grillot, *et al.* (6), were wrong in concluding that the green–blue ratio is not dependent on the copper concentration. There evidently is such a dependence, just as for all other ways in which copper phosphors may be prepared. The differences between the various methods of preparation are of a quantitative rather than a qualitative nature.

The explanation of these differences and of the effect of ZnO must involve at least the following factors:

1. The stabilization of monovalent copper in the lattice by the simultaneous incorporation of chlorine ions. This requires a reaction between the copper compound added and the flux, and therefore at least part of the differences between the various fluxes may be attributed to differences in the free energy of this reaction.

2. The distribution of the activator over the solid ZnS phase and the molten flux.

3. The distribution of ZnO over these two phases possibly resulting in an influence on the distribution of the activator (19).

4. Reduction due to a reaction between sulfide and oxide leading to the formation of SO_2.

An exact treatment, however, is extremely difficult and is not attempted here.

Thermoluminescence

Samples prepared with addition of ZnO show a much stronger and longer phosphorescence than those made without oxygen. Glow curves of samples activated by Ag, Cu, or Au were obtained, after excitation by $\lambda = 3650$ Å at liquid air temperature, upon heating the sample at a rate of 2° per second. The luminescence of the silver-activated phosphor was measured through a blue filter (Schott BG 12), and that of the green copper and gold bands through a yellow filter (Schott OG 5). The samples made with $CaCl_2$ as a flux, but without ZnO, have a single glow peak below room temperature, with a maximum at −80°C. ZnS-Cu and ZnS-Au made with or without a chloride flux, but with addition of 1 mole per cent ZnO, show three peaks, viz., at −100°, −25° to −50°, and +52°C. The peak above room temperature is responsible for the strong phosphorescence at room temperature. ZnS-ZnO-Ag(Cl) shows only the two lower peaks.

The identity of the high temperature glow peak found with Au and Cu proves that the traps responsible for it cannot be characteristic of copper alone (2). It might be, of course, that Cu and Au cause exactly identical traps, but this is not very probable considering that the centers of luminescence formed by these ions are not identical. It seems preferable to assume that the traps are formed by the oxygen itself.

The appearance of the high-temperature glow peak with Cu and Au, but the absence of this peak with Ag, can then be explained on the basis of the Schön-Klasens theory of hole migration (20, 21). According to this theory, it is assumed that holes formed in the center levels may be freed from these levels into the full band above a certain critical temperature determined by the separation between the center level and the band. Once the hole is liberated it may move to killer centers always present in the lattice and may recombine there, without radiation, with an electron from the conduction band [or from the killer center itself (22, 23)]. For Cu and Au the separation between the center level and the full

band is so great that the temperature at which holes are liberated lies above that at which the electrons are liberated from the oxygen traps, and accordingly these electrons combining with the holes in the luminescence centers give rise to luminescence. For Ag, however, the reverse is the case; before the electrons are free, the holes have moved from the activator centers to the killer centers, and most of the light is lost. The weak phosphorescence still observed is due to a small fraction of holes which have not yet been liberated or which have been retrapped at luminescence centers in the course of the process. A more elaborate account of the glow properties of ZnS phosphors, including a direct proof of the existence of deep oxygen traps in ZnS-xZnO-Ag, will be given by Hoogenstraaten of this laboratory.

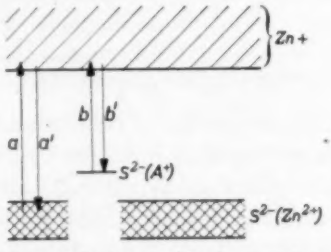

FIG. 5. Band model of an oxide-free activated ZnS phosphor (ZnS-A).

DISCUSSION

Fluorescence and Absorption

The fluorescence and absorption of sulfide phosphors is usually discussed with the aid of an orbital energy diagram in which the energy of the various levels is defined by the energy necessary to take an electron from a particular orbit out of the crystal and bring it to a point infinitely far away (21). Such a scheme is shown in Fig. 5. If it is assumed that zinc sulfide is built up of divalent ions (which does not quite correspond to reality, but which offers an easy approach), then the full band must be attributed to sulfur ions (S^{2-} band), the empty band to zinc ions (Zn^+ band), while the center levels are due to sulfur perturbed by the presence of a monovalent activator ion (Ag^+, Cu^+, Au^+, Zn^+) at an adjacent site (9)[10, 11]. Fluorescence and absorption correspond to transitions between the full and empty levels. Transitions a and b correspond to the fundamental absorption of ZnS and to the absorption of an activator center, while the reverse transitions a' and b' correspond to the fundamental fluorescence and to the activator fluorescence, respectively.

Formation of solid solutions causes a variation of the spectra for two reasons: in the first place the relative positions of various levels on the energy scale vary because of variations in the unit-cell dimensions; in the second place the incorporated ions have specific effects. The first influence is such that expansion of the lattice causes a decrease of the separation between levels of positive and negative ions, due to a decrease of the electrostatic interaction. Accordingly, the fluorescence and absorption bands shift toward the long-wave side.

In the case of ZnS-ZnO the incorporation of 1 mole per cent ZnO in ZnS causes a slight contraction of the ZnS lattice, which should result in a shift of the absorption edge towards shorter wavelength similar to what is found upon cooling. However, a variation in the opposite direction is observed. Moreover, the magnitude of the effect is greater than would be expected for the slight variation of the cell dimensions actually observed [compare, for instance, with the shift of the absorption edge of CdS upon compression (24)]. Therefore the effect must be due to a specific influence of the oxygen. The simplest way to explain this effect is to assume that oxygen gives rise to separate O^{2-} levels above the S^{2-} band (Fig. 6). The separation between the O^{2-} levels and the full band, as found from the difference between the position of the absorption edges of ZnS and ZnS — 1 mole per cent ZnO, amounts to ~0.1 ev. This separation is much smaller than the difference between the energies gained in taking an electron from free O^{2-} (8.93 ev) and free S^{2-} (7 ev). This is because of the fact that in the lattice the surrounding ions exert a stronger repulsion on the large S^{2-} than on the smaller O^{2-} ions.

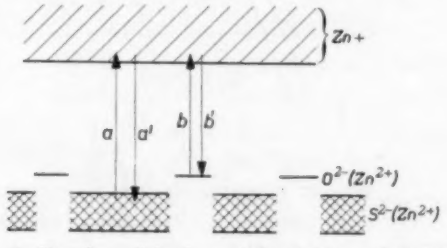

FIG. 6. Band model of a solid solution of ZnS-ZnO

The oxygen levels have a meaning only at the sites at which the oxygen is present. The sulfur band, on the other hand, has no meaning at such sites. In Fig. 6 this has been indicated by interrupting the full band at the points at which the oxygen levels are drawn. In this model the normal ZnS absorption band with an edge at 3350 Å corresponds to transition a, the absorption band of ZnS-ZnO with an edge at 3500 Å corresponding to transition

[10] In the figures the symbols inside parentheses indicate the cation occupying a site next to the anion to which the levels are attributed.

[11] Halogens and trivalent cations aid in the incorporation of the activator according to the principle of charge compensation, but they do not belong to the centers (9).

b. The low-temperature fluorescence bands observed with ZnS and ZnS-ZnO (Fig. 2) correspond to the reverse transitions (a' and b'), though of course with a correction according to the Franck-Condon principle. The same argument leading to separate O^{2-} levels in the case of ZnS-xZnO leads to the assumption of separate S^{2-} levels in ZnO-xZnS. In this case the repulsion of the large S^{2-} ions is so great that the S^{2-} levels are situated even above the O^{2-} band.

For ZnS − 1 mole per cent ZnO containing an activator A = Ag^+, Cu^+, or Au^+, two kinds of center levels are to be expected, viz., levels S^{2-} (A^+) and levels O^{2-} (A^+) due, respectively, to sulfur and oxygen ions next to the activator ions (Fig. 7). As the concentration of sulfur far exceeds that of oxygen, a random distribution of O^{2-} and A would result in far more levels of the first than of the second kind. Yet experiment shows that the fluorescence of ZnS − 1 mole per cent ZnO − A is mainly due to radiation from O^{2-} (A^+) centers. Self-absorption does not suffice to explain this effect; although

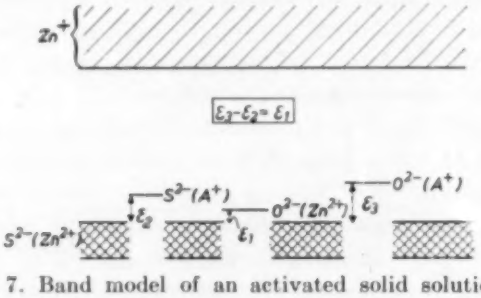

FIG. 7. Band model of an activated solid solution of ZnS-ZnO-A.

the absorption band of O^{2-} (A^+) centers partly covers the wavelength range of the S^{2-} (A^+) fluorescence band, it seems unlikely that reabsorption would be sufficiently strong to suppress the short-wave band to the extent observed. As the maximum of the spectral distributions is not markedly changed by cooling to liquid air temperature, the effect cannot be due to migration of holes from S^{2-} (A^+) to the O^{2-} (A^+) levels, followed by recombination of electrons and holes in the latter. Therefore the only possibility left seems to be to assume that the activator and oxygen ions are not distributed at random but tend to associate with each other, as was similarly found for Sm^{3+} and O^{2-} in CaS-CaO-Sm and SrS-SrO-Sm (25)[12, 13]. The differences in the peak position of the luminescence bands for products containing ZnO and made with and without fluxes (Fig. 3, Table II) may be explained by an unequal distribution of oxygen over the sample.

When an activated ZnS phosphor is made with addition of ZnO but without halide fluxes, the fluorescence originates only from those parts of the sample where oxygen is present and the fluorescence is mainly in the O^{2-} (A) band. When a halide flux like NaCl is present, however, the activator can also be incorporated at parts where ZnO is not present or is present in a smaller concentration. Therefore a sample of ZnS-xZnO-A(NaCl) contains both S^{2-} (A) and O^{2-} (A) levels and accordingly the fluorescence is a superposition of the displaced and the undisplaced activator bands. This explains the intermediate position of the bands observed in these cases.

The Principle of Compensation of Volume

The presence of oxygen-activator pairs in a concentration exceeding that corresponding to a random distribution requires an attraction between oxygen and the activator. This attraction probably results from the fact that while the monovalent activator ions are without exception larger than the divalent zinc ions forming the lattice, the oxygen ions are smaller than the sulfur ions. When the activator and oxygen ions are incorporated far from each other, the total stress in the system is roughly the sum of the stresses due to the separate ions. Upon incorporation at adjacent sites, however, the volume deficiency of oxygen is partly compensated by the volume excess of the activator leading to a smaller stress and consequently to a smaller free energy.

This explains at the same time how oxygen can promote the formation of luminescence centers in ZnS. Because of the large size of the activator ions and the complications accompanying the incorporation of monovalent cations, the solubility of the sulfide of the activator in ZnS is exceedingly low, unless special provisions of some sort are made. One of these, according to the principle of charge compensation, consists in the simultaneous incorporation of monovalent anions (halogens) or trivalent cations. Another, according to what may be called the principle of volume compensation, consists in the simultaneous incorporation of the small

[12] In the same way Cr^{3+} seems to associate with Be^{2+} in Al_2O_3-BeO (26).

[13] In the case of the unactivated sulfide containing ZnO, the fluorescence is likewise characteristic of the new levels introduced by the oxygen (Fig. 2). This obviously cannot be explained by association effects. Here, however, self-absorption is much stronger than in the case of the activated sulfide. This is because all of the O^{2-} ions (1 mole per cent) may take part in the absorption whereas with the activated sulfide the maximum amount of O^{2-} ions which can be involved in a self-absorption process is equal to the activator concentration (0.01 mole per cent). It seems quite likely, then, that the absorption bands connected with this larger amount of oxygen can absorb the short-wave ZnS bands to an important extent and thus account for their suppression in Fig. 2.

oxygen ions at sites adjacent to the activator ions. Comparing the intensity of luminescence of phosphors made by applying these two principles separately, one sees that the former is by far the more effective. Nevertheless, compensation of volume alone increases the solubility of the activator sufficiently to cause a detectable luminescence. In this case, since neutrality of the crystal must be maintained, incorporation of the monovalent activator must be accompanied by the formation of sulfur vacancies or one half of the activator ions must occupy interstitial sites. An attempt to prove these views directly by determining the solubility of the activator in ZnS has failed because of the small concentrations involved and the difficulty of separating the dissolved from the adhering activator.

If a phosphor has been excited, it contains electrons in the conduction band. In the model assumed by us (Fig. 5), the conduction band is a Zn^+ band; for each excited electron one Zn^{2+} ion is transformed into a Zn^+ ion. These Zn^+ ions are larger than Zn^{2+}, their size being of the same order as that of Cu^+[14]. But we have seen above that, if oxygen is present, ions larger than Zn^{2+} tend to occupy positions adjacent to it, forced to do so by the principle of volume compensation. Therefore we must expect that Zn^+ also associates with O^{2-}. In connection with the dual character of Zn^+ (it represents a monovalent zinc ion as well as a free electron), this has the following implications for the conductivity. In pure ZnS there is no reason why an excited electron should be on one particular Zn^{2+} ion (transforming this into a Zn^+ ion) rather than on another. Therefore the electron may move freely through the lattice, jumping from one Zn^{2+} to a neighboring one, and so on. When some of the S^{2-} is replaced by the smaller O^{2-}, however, the electron tends to remain on a Zn^{2+} next to O^{2-}, as it is in this position that the large Zn^+ which it forms is incorporated with the least repulsion from its neighbors. But this is just a different way of saying that O^{2-} forms an electron trap. On the other hand, we have seen that O^{2-} tends to associate itself with the activator ions. In this way the view that the glow peaks, found with phosphors containing oxygen are due to the oxygen itself, may be reconciled with the view that the traps essentially belong to the centers; the traps are actually oxygen traps but a number of them equal to the number of activator ions are situated near these ions. It will be these traps that are preferentially filled upon excitation.

The same reason which favors the association of activators and oxygen in the case of ZnS prevents the association of the activator and sulfur in the case of ZnO; the large activator ions and the large sulfur ions avoid each other. This explains why the Zn^+ band of ZnO-Zn is not in the least changed by the incorporation of sulfur ions, although both the variation in lattice constant and the concentration of foreign atoms is of the same order as in ZnS-xZnO.

The principles of compensation of charge and volume are obviously not restricted to ZnS and ZnO phosphors. The former principle has been used in formulating semiconductors [Verwey (27), Wagner (28), Hauffe (29)], while Wells (30) has used it in explaining the favorable effect of Na and K on CaS-Bi and BaS-Bi phosphors. Compensation of volume, on the other hand, is the factor causing foreign ions to concentrate near dislocations in metals (31). It may also account for the favorable effect of O^{2-} on bismuth-activated sulfides of the alkaline earth group (28). It must be emphasized, however, that oxygen also affects the properties of SrS-Cu (32), although Cu^+ is smaller than Sr^{2+}, a result which seems to contradict the explanation suggested in this paper.

[14] According to an estimation by Stockar (34), the radius of Zn^+ is 0.87 Å, against Cu^+, 0.90 Å; Ag^+, 1.18 Å; and Au^+, 1.29 Å.

Acknowledgments

The authors wish to express their appreciation to Th. P. J. Botden for measuring the spectral distributions, to W. Hoogenstraaten for measuring the glow curves, to L. J. M. van Weert for his determination of lattice constants, and finally to Dr. P. H. Dowling for editing this paper.

Any discussion of this paper will appear in a Discussion Section, to be published in the December 1952 issue of the Journal.

References

1. P. Lenard, *Ann. Physik.*, **31**, 661 (1910); Riedel de Haen, Netherlands Pat. 42603 (1936), U.S. Pat. 2,136,871 (1936); H. W. Leverenz, *RCA Rev.*, **7**, 199 (1946); A. A. Guntz, *Ann. chim.*, **5**, 157, 363 (1926).
2. G. F. J. Garlick, A. F. Wells, and M. H. F. Wilkins, *J. Chem. Phys.*, **17**, 399 (1949).
3. S. Rothschild, *Trans. Faraday Soc.*, **42**, 635 (1946).
4. A. L. Smith, *J. (and Trans.) Electrochem. Soc.*, **93**, 324 (1948).
5. F. A. Kroeger and J. E. Hellingman, *J. (and Trans.) Electrochem. Soc.*, **93**, 156 (1948).
6. E. Grillot and M. Bancie-Grillot, *Compt. rend.*, **231**, 966 (1950).
7. F. A. Kroeger, J. E. Hellingman, and N. W. Smit, *Physica*, **15**, 990 (1949).
8. F. A. Kroeger and N. W. Smit, *Physica*, **16**, 317 (1950).
9. F. A. Kroeger and J. Dikhoff, *Physica*, **16**, 297 (1950).
10. A. Schleede, *Chem. Ber.*, **1942**, 661.
11. R. Schenck, *Z. anorg. u. allgem. Chem.*, **148**, 351 (1925); K. Frank and K. Raithel, *Z. Physik.*, **126**, 377 (1949).
12. M. Billy and A. Berton, *Compt. rend.*, **206**, 1631, 1958 (1938);

C. F. Goodeve, *Trans. Faraday Soc.*, **33**, 340 (1937); J. H. Gisolf, *Trans. Faraday Soc.*, **35**, 171 (1939).
13. E. Mollwo, *Reichsber. Physik*, **1**, 1 (1944).
14. R. Faivre, *Ann. chim.* (11), **19**, 58 (1944).
15. E. Mollwo and F. Stöckmann, *Ann. phys.*, **3**, 223 (1948).
16. F. A. Kroeger, *Physica*, **7**, 1 (1940).
17. S. M. Thomsen, *J. Chem. Phys.*, **18**, 770 (1950).
18. L. Wöhler, F. Martin, and E. Schmidt, *Z. anorg. u. allgem. Chem.*, **127**, 277 (1923).
19. J. Prener, R. W. Mason, and R. Ward, *J. Am. Chem. Soc.*, **71**, 1803 (1949).
20. M. Schön, *Z. Physik*, **119**, 483 (1942); *Chem. Ber.*, **1942**, 544; *Ann. phys.* (3), **6**, 333 (1948); H. A. Klasens, *Nature*, **158**, 306 (1946).
21. F. A. Kroeger, "Some Aspects of the Luminescence of Solids," Chapter VI, Elsevier, New York-Amsterdam (1948).
22. N. R. Nail, F. Urbach, and D. Pearlman, *J. Optical Soc. Am.*, **39**, 690 (1949).
23. S. Roberts and F. E. Williams, *J. Optical Soc. Am.*, **40**, 516 (1950).
24. G. Höhler, *Ann. phys.* (6), **4**, 371 (1949); R. Seiwert, *Ann. phys.* (6), **6**, 241 (1949).
25. R. Tomaschek, *Chem. Ber.*, **1942**, 517; *Ann. Physik*, (4), **75**, 127 (1924); R., H. Tomaschek, *Ann. Physik.*, (4), **84**, 1047 (1927).
26. O. Deutschbein, *Ann. Physik.*, (5), **14**, 712 (1932); *Physik. Z.*, **33**, 874 (1932); *Z. Physik*, **77**, 489 (1932).
27. E. J. W. Verwey, P. W. Haayman, and F. C. Romeyn, *Chem. Weekblad*, **44**, 705 (1948); E. J. W. Verwey, *Bull. soc. chim. France*, **1949**, D122.; E. J. W. Verwey, P. W. Haayman, F. C. Romeyn, and G. W. van Oosterhout, *Philips Research Repts.*, **5**, 173 (1950).
28. C. Wagner, *J. Chem. Phys.*, **18**, 62 (1950).
29. K. Hauffe and A. L. Vierk, *Z. physik. Chem.*, **196**, 160 (1950).
30. A. F. Wells, Ministry of Home Security Report RC(C) 119 cited by G. F. J. Garlick in Reports on Progress in Physics, **12**, 48 (1948–1949).
31. A. H. Cottrell, Report on a conference on the strength of solids, Bristol 1947, published by the Physical Society, p. 30.
32. D. Pearlman, P. E. Goddard, and F. Urbach, *J. Optical Soc. Am.*, **39**, 695 (1949).
33. R. H. Bube, *Phys. Rev.*, **80**, 655 (1950).
34. H. Stockar, *Helv. Chim. Acta*, **33**, 1409 (1950).

Zinc-Magnesium Oxide and Zinc-Magnesium Sulfide Phosphors[1]

ARTHUR L. SMITH

Tube Department, Radio Corporation of America, Lancaster, Pennsylvania

ABSTRACT

Zinc-magnesium oxide phosphors were briefly investigated, and procedures developed for producing highly efficient phosphors containing no intentional additions of either activator or flux.

True solid solutions of zinc and magnesium sulfides exist up to at least 25 mole per cent magnesium sulfide. With silver or copper as an activating agent, a shift in luminescence to shorter wavelengths occurs as the magnesium sulfide content increases. With manganese activation, emission is not appreciably affected by the addition of magnesium sulfide. Efficiencies are good under both ultraviolet and electron excitation, and a long-duration phosphorescence can be obtained by electron excitation of the copper-activated materials. Lead, antimony, arsenic, and bismuth can also be utilized as activators to give efficient phosphors.

INTRODUCTION

The existence of solid solutions of zinc-magnesium oxide has been known for some time (1, 2). The MgO crystallizes in the cubic lattice of the NaCl type; ZnO crystallizes in the hexagonal lattice of the ZnO type. Because the lattice structure of MgS is also of the NaCl type, and that of ZnS is either cubic or hexagonal, it seemed very probable that a solid solution should exist in the sulfide system as well as in the oxide system.

This paper reports the work done to establish the existence of a system of zinc-magnesium sulfide luminescent materials. Although the system has not yet been studied in complete detail, particularly in the region of MgS concentrations above 25 mole per cent, it is worthy of further study not only for its practical applications, but also for the clues it might furnish to such questions as the efficacy of activators in various bases [Bi, Pb, Sb (3, 4) and As are efficient activators in MgS and in (Zn, Mg)S but in ZnS alone they function weakly (5, 6) or not at all when compared with Ag, Cu, or Mn] and in the part which lattice dimensions might have in determining the emission for a particular activator. (Mg causes a contraction of the ZnS lattice and shifts emission toward the blue; Cd expands the lattice and shifts it toward the red. The reverse is true in the alkaline-earth infrared-sensitive phosphors (7–9) wherein lattice contractions shift emission toward the red.)

PREPARATION OF PHOSPHORS

(Zn, Mg)O.—Commercial zinc oxide designated as "C. P., Dry Process" and luminescent-grade magnesium oxide are used as reactants. The requisite proportions are mixed by dry rolling for 24 hours. Firing is done in apparatus and by procedures similar to those already reported (10). The reducing gas (either hydrogen or carbon monoxide) is purified by passage through the usual reagents necessary to remove oxygen and water vapor.

The firing temperature range found most suitable is between 940°–1000°C. Time of firing in the reducing atmosphere is dependent on the gas used, being 5 to 15 minutes in hydrogen, and 45 to 60 minutes in carbon monoxide. Some reduction occurs below this temperature range, hence, if the samples are introduced under reducing conditions into the furnace, variations will occur due to the different time each sample requires to reach temperature equilibrium. For this reason they are brought to temperature equilibrium in an inert atmosphere, such as nitrogen. When the proper temperature is reached, the reducing gas is then introduced. The reducing treatment is then followed by a mild oxidizing treatment in which 0.1 per cent to 0.3 per cent by volume of oxygen is introduced with the nitrogen for a period of 5 to 20 minutes. Highest ultraviolet emission under electron excitation is obtained when this oxidizing treatment is followed by one in pure nitrogen for a further 15–20 minutes. The reasons for this sequence of atmosphere firings are imperfectly understood. All that is known is that if any is omitted, inferior phosphors result.

(Zn, Mg)S.—The zinc sulfide used is the luminescent grade designated commercially by RCA as 33-Z-19. Magnesium sulfide is introduced into the matrix in either of two ways, the simplest being the addition of previously-prepared magnesium sulfide obtained in luminescent grade from the Mallinckrodt Chemical Company. The second method uti-

[1] Manuscript received January 11, 1952. This paper prepared for delivery before the Washington Meeting, April 8 to 12, 1951.

lizes the preparative procedure discovered by Sarge (11) and further perfected by Russo (12). In this method, magnesium ammonium chloride is added to the zinc sulfide in such quantity that the proper Zn/Mg ratio is obtained after the requisite firing in hydrogen sulfide. This method is advantageous because the chloride is not only a reactant but a flux as well. The product is then the finished phosphor and requires no subsequent washing or further treatment.

Severe decomposition will occur if aqueous or alcoholic solutions are in contact with magnesium sulfide, hence dry methods of additions of activators and fluxes must be used. Uniform distribution of the very small amount of activator then becomes a problem. It can be successfully overcome if the activator is added to the flux which then serves as a

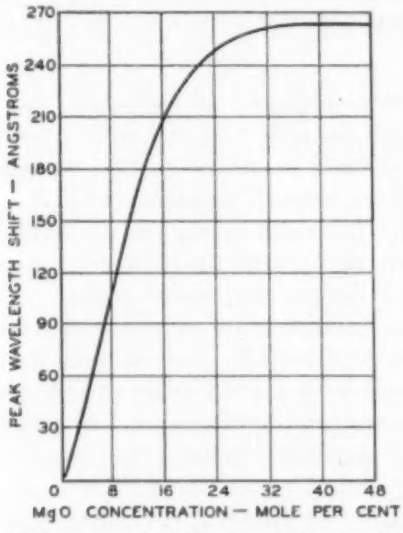

FIG. 1. Shift in wavelength of emission in visible region of (Zn, Mg)O phosphors with variation of MgO concentration.

dispersing medium. The activated flux is prepared by adding the requisite proportions of a soluble salt of the desired activator to the flux, dissolving them with a minimum of water, then evaporating to dryness at about 140°C. The resulting powder is then dry-rolled with the zinc sulfide for 24 hours to mix the ingredients thoroughly. The ZnS-MgS mixtures are fired at 980°C in purified nitrogen or in hydrogen sulfide if it is necessary to convert the magnesium chloride to sulfide. Some improvement in efficiency might be obtained if samples prepared in hydrogen sulfide are subsequently fired for one-half hour in sulfur dioxide (10). Time of firing is two to four hours for chloride conversion, or thirty minutes for the ZnS-MgS mixtures alone.

Method of measurement.—The phosphors were measured from the excited side by test techniques developed by Hardy and described in previous reports (13, 14).

RESULTS

(Zn, Mg)O.—Fig. 1 indicates the shift in peak wavelength of emission as the proportion of MgO in the phosphor is increased. The shape of the emission curve remains relatively unchanged as the shift toward shorter wavelengths occurs (Fig. 2). As in zinc oxide itself (15), an ultraviolet emission band is present. In this band, efficiency increases as the

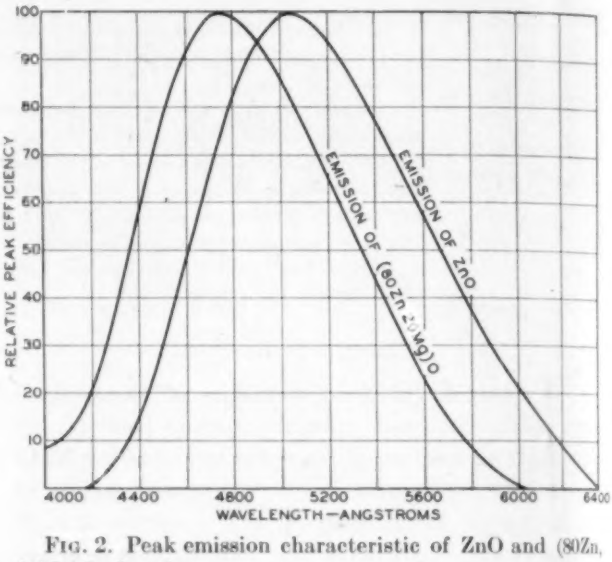

FIG. 2. Peak emission characteristic of ZnO and (80Zn, 20Mg)O phosphors.

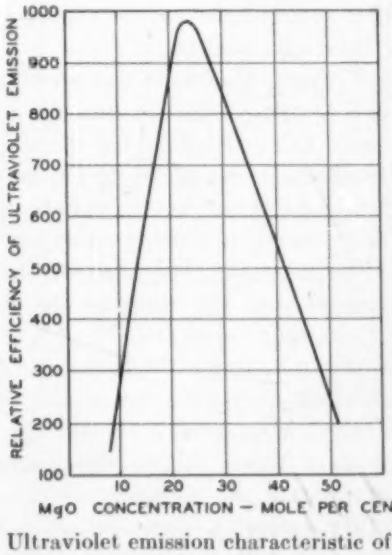

FIG. 3. Ultraviolet emission characteristic of (Zn, Mg)O phosphors of varying MgO concentrations.

magnesium oxide content approaches 25 mole per cent, and again rapidly decreases after this point (Fig. 3). It has not been determined whether this increase in output is a result of a broadening of the band or an increase in the peak output, or whether the peak wavelength of the ultraviolet emission band shifts in the same manner as the visible output. The peak efficiency of the visible band drops linearly with increasing MgO content and is about 75 per

cent of the efficiency of pure zinc oxide when the MgO concentration is 25 mole per cent.

X-ray diffraction analyses[2] show that true solid solutions of zinc and magnesium oxides occur at MgO concentrations up to 25 mole per cent. After this point, MgO begins to show as a distinct phase, and no further lattice contraction can be discerned. These analyses agree with the optical data which show that the shift in peak wavelength is very slight above 25 mole per cent (Fig. 1), at which point the ultraviolet emission is also at a maximum.

Like ZnO (16), the zinc-magnesium oxides appear to absorb their own emission in the ultraviolet region, but not quite to the same degree. Also, like ZnO (17), the solid solutions may be activated by sulfide ion which increases the efficiency of the visible band and at the same time decreases the efficiency of the ultraviolet emission band. A further

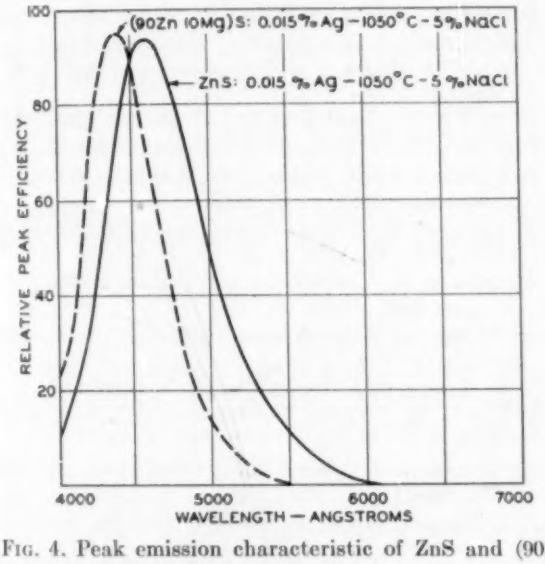

FIG. 4. Peak emission characteristic of ZnS and (90Zn, 10Mg)S phosphors with Ag activation.

similarity to zinc oxide (16, 18) can be found in the decay time, wherein the phosphorescence light level decreases to 30 per cent within 10^{-6} sec after the removal of the excitation source.

Unlike zinc oxide, for which the efficiency of the ultraviolet output depends to a considerable extent on the source of the oxide, these phosphors may be prepared with good efficiency from any good reagent grade of "dry-process" zinc oxide and luminescent grade of magnesium oxide.

(Zn, Mg)S.—The zinc magnesium sulfides were investigated chiefly in the region of magnesium sulfide concentrations up to 25 mole per cent, although spot checks were made for other concentrations. X-ray diffraction analysis shows that true solid solutions occur when the MgS concentration is up to 20 mole per cent. When a sample of the composition having 80 mole per cent ZnS and 20 mole per cent MgS is treated with water, no detectable hydrogen sulfide is found, a strong proof that no free MgS is present. A 50 mole per cent composition is not stable in water.

With either Ag or Cu activation, shifts toward shorter wavelengths are observed when increasing amounts of magnesium are used, as shown in Fig. 4 and 5. When MgS is added to mixtures of zinc sulfide-cadmium sulfide, the net effect on the emission characteristics is also a shift toward shorter

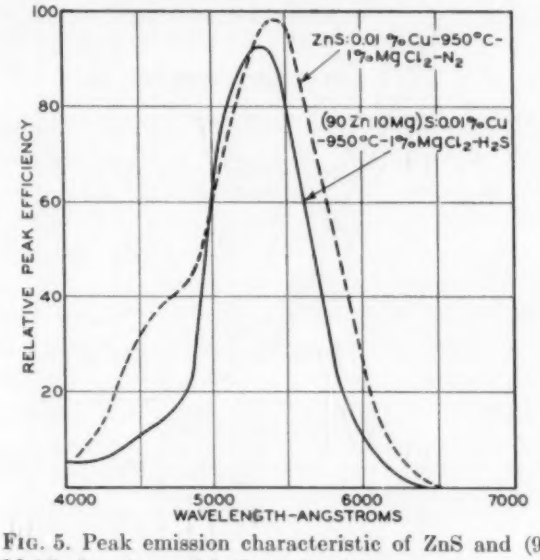

FIG. 5. Peak emission characteristic of ZnS and (90Zn, 10Mg)S phosphors with Cu activation.

TABLE I. *Influence of* MgS *on* (Zn, Cd)S:Cu

(Zn,CdS)/MgS mole ratio		Peak wavelength (Å)
(42Zn, 57Cd)S/MgS:	0.95/0.05	>7000
	0.9 /0.1	>7000
	0.8 /0.2	6650
	0.7 /0.3	5820
(86Zn, 14Cd)S/MgS:	0.95/0.05	5820
	0.9 /0.1	5600
	0.8 /0.2	4690
	0.7 /0.3	4620

wavelengths. The magnesium sulfide apparently cancels the influence of the added cadmium (Table I).

In general, the system follows the pattern of ZnS itself; the addition of nickel in small quantities decreases long-term phosphorescence; the activator pairs Pb-Mn, Cu-Mn, and Cu-Pb give rise to infrared-sensitive phosphors (5); copper gives rise to both a blue and a green band depending on concentration, the green band showing long-duration phosphorescence; high efficiency is obtained under both ultraviolet and electron excitation; a blue-emitting phosphor is obtained by "self-activation."

[2] Diffraction analyses done by A. D. Power, RCA, Harrison, New Jersey.

One major departure from the ZnS pattern is the long-duration phosphorescence induced by electron excitation of the copper-activated samples. Another interesting difference is the activating influence of lead, bismuth, arsenic, and antimony (Fig. 6). These activators have a much more pronounced influence on samples having a high content of magnesium than they do on zinc sulfide alone. These four activators function best when added in amounts

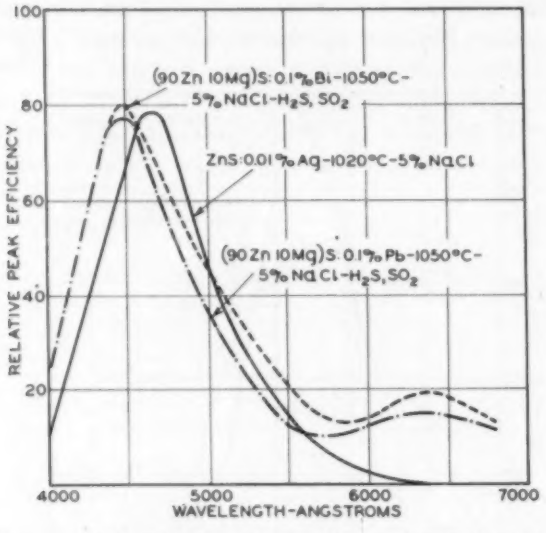

FIG. 6. Peak emission characteristic of ZnS:Ag, (90Zn, 10Mg)S:Pb and (90Zn, 10Mg)S:Bi phosphors

of about 0.01 weight per cent. The final concentration of these activators in the base has not been determined, but it must be lower than that added, since condensates on the cooler portions of the tube contain high concentrations of the activator. Firing under pressure should help in this determination.

Zinc-magnesium sulfide phosphors activated by Mn show an almost invariant emission curve, just as is the case with phosphors of zinc-cadmium sulfides, at least up to the point where free MgS cannot yet be detected; beyond this point shifts occur, but these are probably due to MgS:Mn present as a mechanical mixture.

ACKNOWLEDGMENTS

The assistance of the following is gratefully acknowledged: Dr. A. D. Power (RCA, Harrison, New Jersey) for the x-ray diffraction analyses; A. E. Hardy and R. F. Jefferies for optical measurements; and L. E. Whitmer for the preparation of some of these samples.

Any discussion of this paper will appear in a Discussion Section, to be published in the December 1952 issue of the JOURNAL.

REFERENCES

1. E. KORINTH AND G. MEDER, U. S. Pat. 2,028,980, Jan. 28, 1936.
2. L. J. REIMERT AND E. A. FATZINGER, U. S. Pat. 2,481,344, Sept. 6, 1949.
3. E. TIEDE AND A. SCHLEEDE, *Ann. Physik*, **62**, 573 (1922).
4. P. LENARD, F. SCHMIDT, AND R. TOMASCHEK, "Phosphoreszenz and Fluoreszenz," Handbuch Experimentalphysik, Parts 1 and 2, Akad. Verlag., Leipzig (1928).
5. G. R. FONDA, *J. Optical Soc. Am.*, **36**, 382 (1946).
6. J. S. PRENER, *J. Electrochem. Soc.*, **98**, 406 (1951).
7. A. L. SMITH, PH.D. Dissertation, Polytechnic Institute of Brooklyn (1946).
8. A. L. SMITH, R. E. ROSENSTEIN, AND R. WARD, *J. Am. Chem. Soc.*, **69**, 1725 (1947).
9. W. PRIMAK, H. KAUFMAN, AND R. WARD, *J. Am. Chem. Soc.*, **70**, 2043 (1948).
10. A. L. SMITH, *J. (and Trans.) Electrochem. Soc.*, **93**, 324 (1948).
11. T. W. SARGE, *U. S. Pat.* 2,358,661, Sept. 19, 1944.
12. V. RUSSO, M. S. Thesis, Polytechnic Institute of Brooklyn (1947).
13. A. L. SMITH, *J. (and Trans.) Electrochem. Soc.*, **96**, 287 (1949).
14. A. E. HARDY, *Trans. Electrochem. Soc.*, **91**, 221 (1947).
15. R. E. SHRADER AND H. W. LEVERENZ, *J. Optical Soc. Am.*, **37**, 939 (1947).
16. F. H. NICOLL, *J. Optical Soc. Am.*, **38**, 417 (1948).
17. S. M. THOMSEN, *J. Chem. Phys.*, **18**, 770 (1950).
18. H. W. LEVERENZ, "An Introduction to the Luminescence of Solids," p. 255, J. Wiley & Sons, Inc., New York (1950).

The Excitation Spectra of Various Silicate Phosphors[1]

ALEXANDER J. OSZY[2]

Sylvania Electric Products Inc., Bayside, Long Island, New York

ABSTRACT

A description is given of the excitation spectra of a number of silicate phosphors when irradiated by ultraviolet energy. Phosphors described are (*a*) manganese-activated zinc beryllium silicate, (*b*) lead- and manganese-activated calcium silicate, (*c*) barium silicate activated by lead, and (*d*) barium silicate activated by lead and modified by the substitution of magnesium. For the manganese-activated zinc beryllium silicates, the change of the excitation spectrum with the lattice constant is noted. For a number of the other phosphors, it is shown that the excitation spectra for the visible and ultraviolet bands are not the same. It is concluded that the mechanisms involved for the excitation of the two bands are different.

INTRODUCTION

In the development of a phosphor theory, a knowledge of the excitation spectrum of a phosphor is useful in calculating an energy level diagram of the system. The excitation spectrum combined with the absorption spectrum allows one to determine what part of the energy goes into radiative transitions. From the practical standpoint, the excitation spectrum can show whether further work would be profitable in the development of a new phosphor.

EXPERIMENTAL SETUP

In order to determine the excitation spectrum of a phosphor, the setup shown in Fig. 1 is used. Energy from a Beckman hydrogen lamp is monochromatized by a Beckman spectrophotometer and allowed to irradiate the sample. The sample consists of a thin layer of phosphor on one side of a quartz plaque or microscope slide. The fluorescence of the sample is measured with a multiplier phototube (Type 931-A or Type 1P22) and galvanometer. An optical glass filter placed between the fluorescent sample and the multiplier phototube absorbs any undesirable radiation. Where the spectral emission of the phosphor contains two bands, say an ultraviolet and a visible emission band, the excitation spectrum may be determined for each band by interposing the proper filter between the screen and the multiplier phototube. Typical of the Corning filters which have been used are: (*a*) #2412 for red emission bands; (*b*) #3060 plus #5030 for blue emission bands; and (*c*) #5970 alone, or #7380 plus #5840 for ultraviolet emission bands.

The ultraviolet output from the monochromator is determined with an Eppley thermopile, the output of which is amplified by a Perkin-Elmer D.C Breaker Amplifier, Model 53, and measured with a microammeter. The fluorescent response, as measured by the galvanometer, divided by the corresponding relative energy values of the ultraviolet radiation, as determined by the thermopile, gives the relative excitation spectrum of the phosphor. In taking the data, a constant slit width is used. Therefore, the band pass in terms of wave numbers varies. Since the excitation spectrum is a relative measurement, any decrease in the output of the hydrogen lamp does not affect the results provided that the spectral energy distribution (SED) does not change over the wavelength range of interest. In order to check the SED of the hydrogen lamp at regular intervals without having to use an elaborate thermopile setup, the hydrogen lamp response is determined with the Beckman "blue" photocell at the same time that the lamp is calibrated by the thermopile. At regular intervals thereafter, the hydrogen lamp is checked against the Beckman "blue" photocell to determine any relative SED changes and the proper correction applied. This, of course, assumes that the relative response of the cell has not changed during the interval.

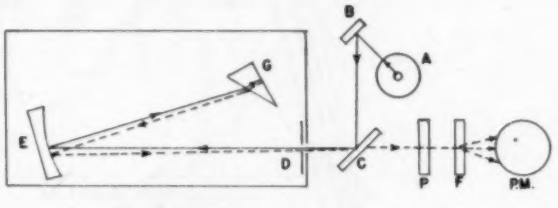

FIG. 1. Apparatus used to determine the excitation spectrum of phosphors.

EXCITATION SPECTRA OF ZINC BERYLLIUM SILICATES

The excitation spectra for a series of manganese-activated zinc beryllium silicates with varying per-

[1] Manuscript received October 15, 1951. This paper prepared for delivery before the Washington Meeting, April 8 to 12, 1951.

[2] Present address: Capehart-Farnsworth Corporation, Fort Wayne, Indiana.

centages of manganese are shown in Fig. 2. Increasing the manganese content shifts the excitation to lower wave numbers (i.e., longer wavelengths), which is what one would expect on the basis of the emission spectra which shift to lower wave numbers for increasing manganese content. Fig. 3 shows the excitation spectra for a series of manganese-activated zinc beryllium silicates with varying zinc to beryl-

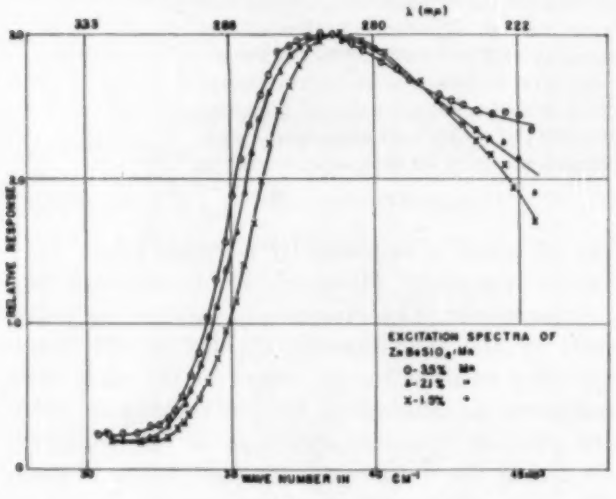

FIG. 2

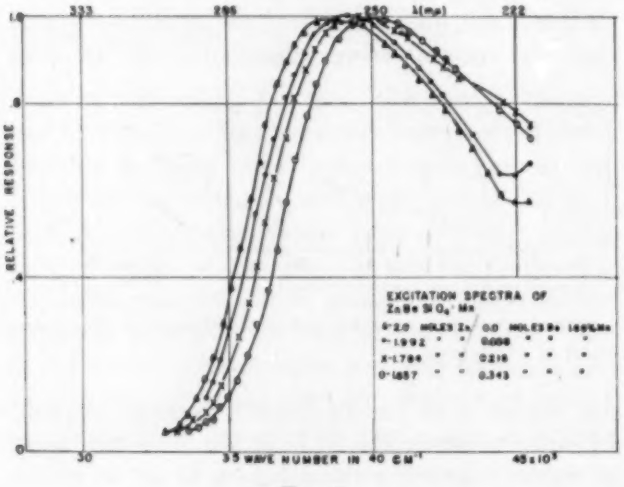

FIG. 3

lium ratios. Over the range covered by the data, increasing the Zn/Be ratio shifts the excitation curve to lower wave numbers. The peak of the various curves shifts from $40.3 \cdot 10^3$ cm^{-1} to $38.8 \cdot 10^3$ cm^{-1} (i.e., 2480 to 2570 Å). For the 2537 Å mercury line all members of this series of phosphors showed strong fluorescence. This, of course, is one of the reasons why the zinc beryllium silicates are such efficient phosphors when used in low-pressure mercury lamps.

The phosphors used to obtain the data for Fig. 2 and 3 all have a rhombohedral crystal structure similar to that of willemite, but there is a shift of the lattice constant due to the incorporation of beryllium and manganese. Fonda (1) and Kroeger (2) have shown that when beryllium orthosilicate is dissolved in zinc orthosilicate there is a contraction of the lattice, while the inclusion of manganese expands the lattice. Fig. 2 and 3 show that increasing the lattice constant shifts the excitation curve to lower wave numbers. However, for the emission spectra of $ZnBeSiO_4$:Mn, it is not possible to correlate the change in emission with the lattice constant. Increasing the amount of beryllium (decreasing the lattice constant) shifts the emission spectra from the green toward the red. A similar effect is obtained with increasing manganese (which increases the lattice constant). Thus, both a decrease and an

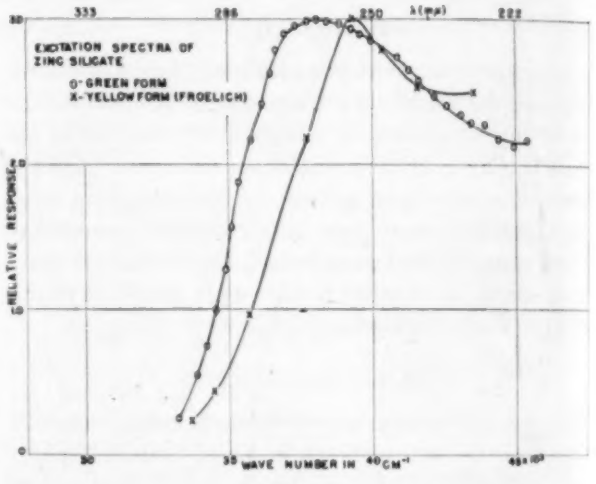

FIG. 4

increase of the lattice constant cause the emission curve to shift to lower wave numbers.

Reports have been given in the literature (3, 4) of three different modifications of manganese-activated zinc orthosilicate phosphors which luminesce green, yellow, and red, respectively. The crystal structures, as revealed by the x-ray patterns, are definitely different for the green and yellow modifications; the crystal structure of the red modification is still unsettled. The three modifications, according to Schleede (5), have identical excitation spectra. Fig. 4 shows the excitation spectrum of a green zinc orthosilicate, as well as the excitation spectrum obtained by Froelich (6) for the yellow form. These two sets of data do not support Schleede's claim.

The Excitation Spectra of Calcium Silicates

The excitation spectrum for a calcium metasilicate, lead- and manganese-activated phosphor is shown in Fig. 5. The data have been taken for both the red band and the ultraviolet band. The fact that

the two curves are not exactly identical shows that the SED of the phosphor varies slightly with exciting wavelength. This particular spectrum is for a sample to which had been added 0.011 moles manganese per mole of calcium (0.5 per cent by weight of calcium silicate), but the curves are identical up to 0.077 moles of added manganese per mole of calcium (3.7 per cent by weight of calcium silicate). One effect of increasing the manganese content is to cut down on the intensity of the ultraviolet (Pb) band. The sample containing zero moles of manganese did not have a red band since the red band is due to the manganese. The results given here agree with those of Froelich (7) who found the spectral sensitivity to be independent of the manganese con-

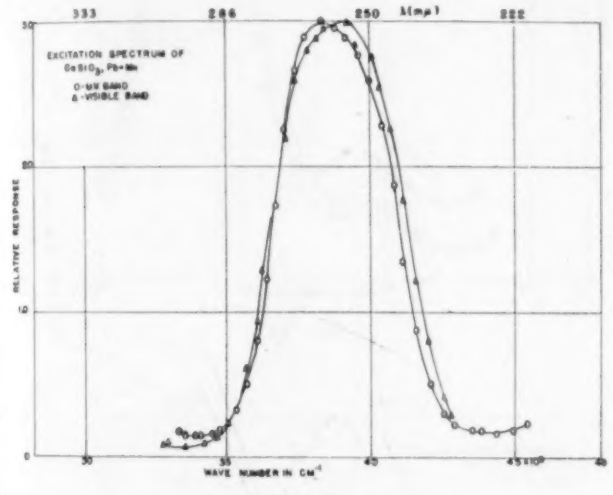

FIG. 5

centration for the range from zero to four per cent. Another sample was made by the addition of 0.165 moles of manganese per mole of calcium. It gave a similar curve for the red band. However, the results for the ultraviolet band were completely different. Since the data were not too accurate, no curve has been plotted. The general shape of the curve is such that this phosphor has a peak at $43 \cdot 10^3$ cm^{-1}, and a minimum at $41 \cdot 10^3$ cm^{-1} from which the curve rises slowly, reaching another peak at about $34 \cdot 10^3$ cm^{-1}. The manganese content of this sample was 7.8 per cent by weight of calcium silicate. There was one other change in this sample besides the increase in the manganese content. The lead addendum was increased from the 0.0035 mole of the previous samples to 0.0066 mole. Since the ultraviolet emission band is due to lead, the change in the excitation spectrum is undoubtedly due to the variation in the lead content.

Barium Silicates

For the remainder of this paper, data will be presented for both the ultraviolet and visible bands. It should be noted that in all cases the data for the ultraviolet band are at a higher wave number than the data for the visible band. This, of course, is what one would expect.

In Fig. 6 are shown the excitation spectra for the ultraviolet and visible bands, respectively, for three samples of lead-activated barium silicate. Going from left to right in both cases the samples are: barium

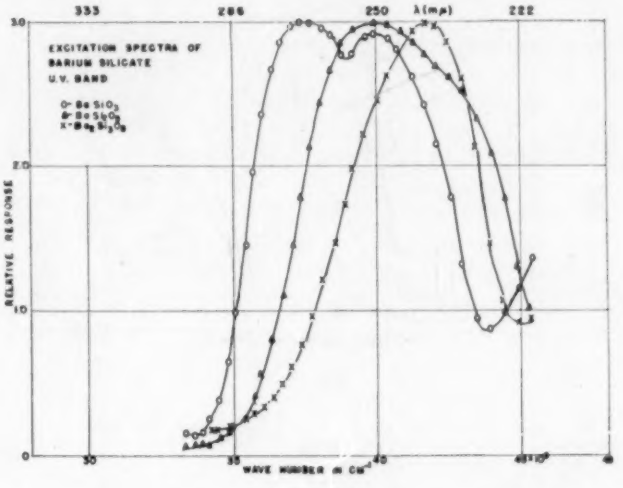

FIG. 6a

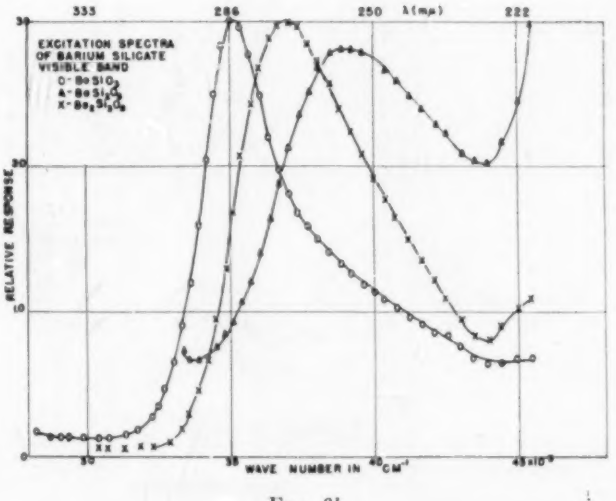

FIG. 6b

metasilicate ($BaSiO_3$), barium disilicate ($BaSi_2O_5$), and barium mesotrisilicate ($Ba_2Si_3O_8$). To form these three compounds, the ratio of silica to barium oxide is varied. Fig. 7 shows the excitation spectra for such a series. In these samples, the ratio of lead and barium is kept constant and the silica content varied. For the ultraviolet band the curves show that increasing silica gradually suppresses the low frequency peak, while for the visible band the peak gradually shifts to a higher frequency. Table I gives the crystal structure of these phosphors as determined by x-ray diffraction.

Earlier work on barium silicate ultraviolet phosphors has been reported by Clapp and Ginther (8), and by Butler (9). Recently, Butler and Cassanos (10) have described some lead-activated barium silicate phosphors in which the color is varied by introducing magnesium as a modifier. The excitation spectra of three of these phosphors listed as types I, III, and IV in the original paper are shown in Fig. 8. The x-ray data show type I to be a barium mesotrisilicate ($Ba_2Si_3O_8$). Butler and Cassanos in their paper refer to the crystal structure of the other two types as compound Z with some pattern A.

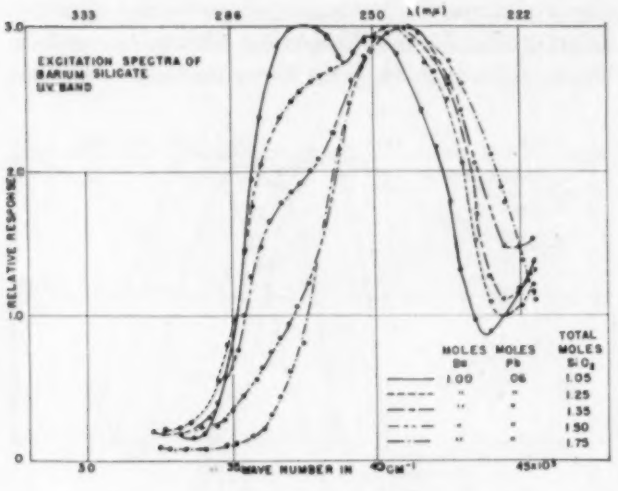

FIG. 7*a*

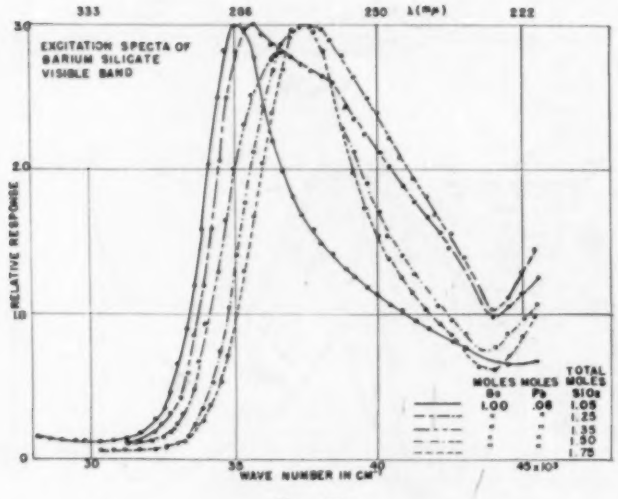

FIG. 7*b*

TABLE I

Composition in moles			X-ray identification
Ba	Pb	SiO_2	
1.0	0.06	1.05	$BaSiO_3$
1.0	0.06	1.25	$BaSiO_3$ + $Ba_2Si_3O_8$ (very weak)
1.0	0.06	1.35	$BaSiO_3$ + $Ba_2Si_3O_8$ (weak)
1.0	0.06	1.50	$Ba_2Si_3O_8$ + $BaSiO_3$ (very weak)
1.0	0.06	1.75	Compound "Y"*

* This compound has not as yet been identified.

For manganese-activated zinc beryllium silicate, Butler (11) has shown that the emission spectra may also be broken up into subbands. An attempt to determine the excitation spectra for these various subbands was unsuccessful. This was due to the large overlapping of the various subbands, which made it impossible to obtain and isolate each subband and still obtain sufficient response. However, Kroeger (2) states that the emission spectrum is independent of the manner of excitation and is identical for the various excitation regions. From this he concludes that all the overlapping emission bands of this phosphor must be excited by one and the same kind of center.

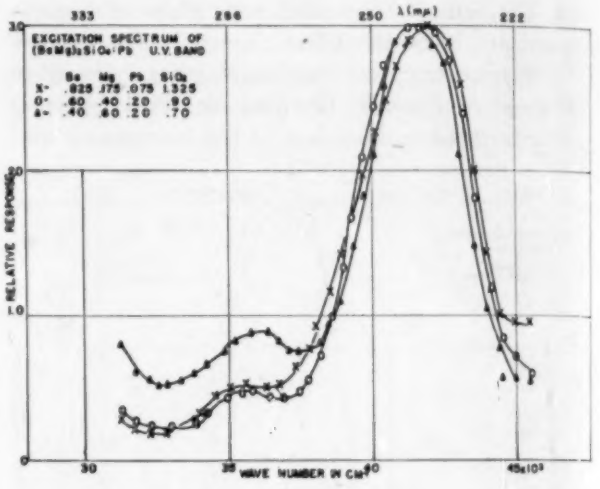
EXCITATION SPECTRUM OF (Ba Mg)₂ SiO₄ : Pb U.V. BAND
Ba Mg Pb SiO₂
X- .825 .175 .075 1.325
O- .60 .40 .20 .90
Δ- .40 .60 .20 .70
RELATIVE RESPONSE
WAVE NUMBER IN CM⁻¹

FIG. 8*a*

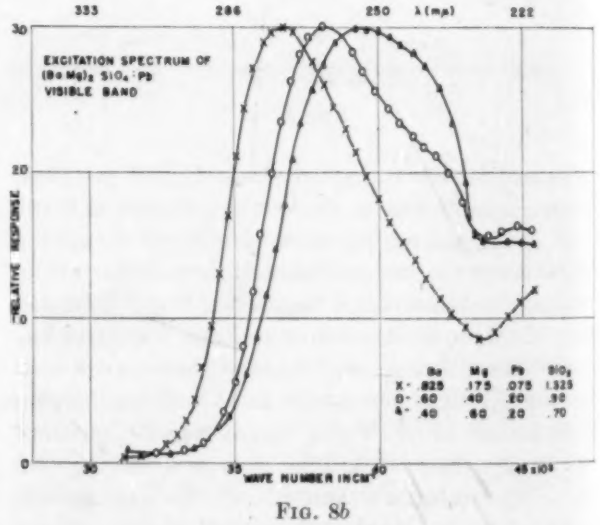
EXCITATION SPECTRUM OF (Ba Mg)₂ SiO₄ : Pb VISIBLE BAND
Ba Mg Pb SiO₂
X- .825 .175 .075 1.325
O- .60 .40 .20 .90
Δ- .40 .60 .20 .70
RELATIVE RESPONSE
WAVE NUMBER IN CM⁻¹

FIG. 8*b*

CONCLUSION

For the silicate phosphors studied which have two separate emission bands, it has been shown that the

excitation spectra of the two bands are different. This shows that the spectral energy distribution of that phosphor is a function of the exciting wavelength. But, more important, is the fact that it indicates that the mechanism for the excitation of each band is different.

Acknowledgments

The author wishes to express his thanks to Dr. K. H. Butler and Mr. A. B. Davis for supplying the phosphors, and to Mr. W. S. Romito for doing the calculations and taking some of the data.

Any discussion of this paper will appear in a Discussion Section, to be published in the December 1952 issue of the Journal.

References

1. G. R. Fonda, *J.* (*and Trans.*) *Electrochem. Soc.*, **95,** 304 (1949).
2. F. A. Kroeger, Dissertation, Amsterdam (1940).
3. H. P. Rooksby and A. H. McKeag, *Trans. Faraday Soc.*, **37,** 308 (1941).
4. G. R. Fonda, *J. Phys. Chem.*, **44,** 851 (1940).
5. P. Pringsheim, "Fluorescence and Phosphorescence," p. 612, Interscience Publishers, Inc., New York (1948).
6. H. C. Froelich, *J. Phys. Chem.*, **47,** 669 (1943).
7. H. C. Froelich, *J.* (*and Trans.*) *Electrochem. Soc.*, **93,** 101 (1948).
8. R. H. Clapp and R. J. Ginther, *J. Optical Soc. Am.*, **37,** 355 (1947).
9. K. H. Butler, *J.* (*and Trans.*) *Electrochem. Soc.*, **95,** 267 (1949).
10. K. H. Butler and J. G. Cassanos, *J. Electrochem. Soc.*, **97,** 83 (1950).
11. K. H. Butler *J.* (*and Trans.*) *Electrochem. Soc.*, **93,** 143 (1948).

Liquid Settled Luminescent Screens[1]

S. Pakswer and P. Intiso

Research Laboratory, The Rauland Corporation, Chicago, Illinois

ABSTRACT

A distinction is made in liquid settling of fluorescent particles in television tubes between "wet" adhesion, i.e., adhesion of particles during tilt, and "dry" adhesion, i.e., adhesion in the finished screen. Wet adhesion in H_2O, salt solutions, silicate solutions, and in a complete system, $Ba(NO_3)_2$ | silicate | H_2O, is discussed. An apparatus to measure dry adhesion is described and it is shown that dry adhesion increases suddenly when a definite total amount of silicate in the settling solution is reached. This amount of silicate is a function of the surface, suggesting a "mortar" action of the silica between the phosphor particles.

Introduction

At present, liquid settling is the most generally adopted method for preparing luminescent screens in cathode-ray tubes for television purposes. The general procedures have been described by Sadowsky (1). Edelberg and Hazel (2) and Stericker and Hazel (3) published results of their investigations on electrical and chemical effects that take place during the settling process. These authors gave a comprehensive theory of the scientific foundations of the settling technique. However, in our opinion, further developments of this theory are necessary to explain all observations made on different types of screen settling and to allow for better leads in the setting up of settling formulae.

Fundamentally, the settling of luminescent powders from a liquid on the face of a glass bulb is part of the question of the adhesion of microscopic particles to solid surfaces (4, 5). It was shown by von Buzagh that the same laws apply for adhesion of particles as can be recognized in the stability and coagulation of sols. All of the electrolytes which coagulate negatively charged sols increase the adhesion of negatively charged particles and those which act as peptizing agents lower the adhesion. Both the lyotropic ionic series and the Schulze-Hardy rules govern the action of these electrolytes. This covers the fundamentals of liquid settling; better understanding can be gained by further analysis of the procedure.

Experimental

Description of the Settling Process

The procedure is roughly as follows. A bulb is placed vertically, face down, on a tilting table or a conveyor belt, and a layer of water, which may contain a certain amount of salt, is introduced into the bulb. A suspension of the luminescent powder of exactly determined weight (total weight being proportional to screen surface) is mixed with a solution of potassium silicate and poured into the column of liquid. (Potassium silicate can also be added to the settling liquid, or salt to the suspension.) After a definite minimum time, the liquid is removed by decanting and the screen is dried in a stream of air or in vacuum.

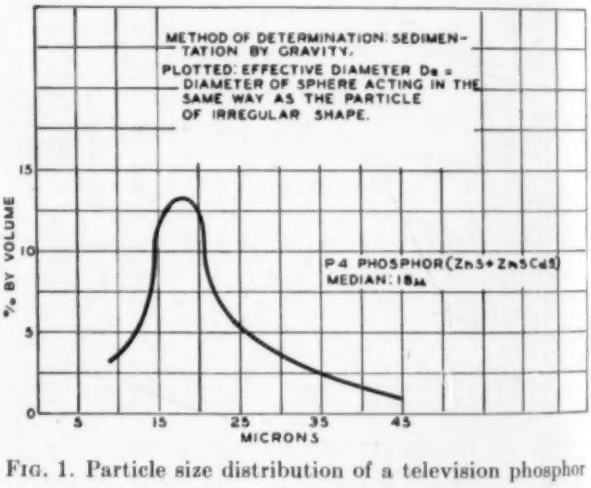

Fig. 1. Particle size distribution of a television phosphor

There are many variables in this process, such as particle size, particle size distribution, shape and "wettability" of the luminescent particles, chemical composition and concentration of the salt, amount of silicate in the solution, temperature of the solution, and settling time. In this report the settling properties of a standard mixture of ZnS and ZnSCdS for P4 luminescent screens will be discussed. The particle size distribution, measured by the method of Palo-Travis (6), is represented in Fig. 1.

Wet and Dry Adhesion

A better understanding of the settling process can be obtained if the requirements for the formation

[1] Manuscript received May 7, 1951. This paper prepared for delivery before the Detroit Meeting, October 9 to 12, 1951.

of a satisfactory screen are broken down in two parts. (*a*) The luminescent powder must adhere to the glass face sufficiently to allow the liquid to be poured off without disturbing the screen; this property will be called "wet" adhesion. (*b*) The luminescent powder when dried must have sufficient adhesion to withstand further processing and use. This requirement will be called "dry" adhesion.

The adhesion necessary to form satisfactory screens upon tilting is a criterion for wet adhesion in the preparation of luminescent screens. Since adhesion of a lesser degree is of no practical value, the methods for measuring wet adhesion, such as the "adhesion number method" and the "secondary angle of tilt" (4), could not be applied to this work. The measurements for wet adhesion consisted of screens being classified as satisfactory or unsatisfactory after the supernatant liquid was removed by tilting.

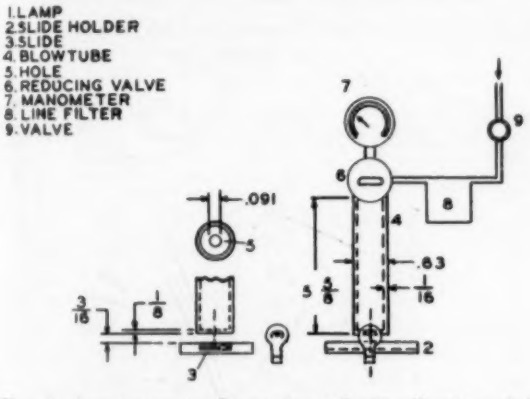

FIG. 2. Apparatus to determine "dry" adhesion of fluorescent screens.

"Dry" adhesion is measured according to the setup shown in Fig. 2. Several microscope slides are placed in a cutout bottom half of a television bulb; the screen is settled and, after a given settling time, the supernatant liquid is removed by siphoning. After a screened slide has been dried with filtered air, it is placed on a slide holder at a determined distance from the orifice of the blow tube as shown in Fig. 2. A jet of filtered air of variable pressure is blown onto the completed screen. The pressure at which particles are blown off from the glass plate is reproducible and is considered to be a measure of "dry" adhesion.

Adhesion of Phosphor Particles in Water

The complex system in a settling solution contains the powder and the glass surface, water, salt anion and cation, silicate, and potassium ions. To arrive at conclusions in this total system, it is necessary to examine the conditions in partial systems. The settling of luminescent powders in water (or organic liquids) will be considered first. It was observed that phosphors of small particle size, deposited on a horizontal surface, slid on standing under the influence of gravitation in pure water (2 ppm impurity) but did not slide in impure H_2O (110 ppm impurity). Phosphors of large particle size show less sliding. This observation is in line with von Buzagh's measurements. He found that the adhesion of particles in water first diminishes slightly with size and then goes up asymptotically. He explained this behavior as follows. In order to produce good adhesion, the solid parts of the particle and the glass wall must come in contact so that short-range London-van der Waals forces can keep the two parts together. In a liquid both the particles and the glass wall are covered with a solvated layer, the thickness of which is inversely proportional to the dielectric constant of the liquid. The thicker the solvated layer, the less strongly the particles adhere[2]. Fig. 3A is a drawing illustrating the phenomenon recognized by von Buzagh, that for thick solvate layers bigger particles

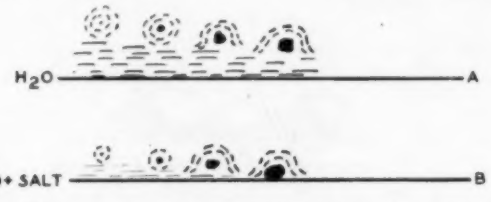

FIG. 3. Formation of solvate hulls responsible for "wet" adhesion.

have a better chance to come in closer contact with the surface and adhere better. Since the weight of large particles is greater, they may slide at large angles of tilt although they will not slide easily at small angles. It is not surprising, therefore, that the adhesion number method shows that only particles of medium size will adhere, and this is substantiated in screen settling experience. Since the formation of solvate hulls depends on the dielectric constant, alcohol should act better than water for settling, and acetone better than alcohol.

Adhesion of Phosphor Particles in Salt Solutions

According to this theory, addition of salt to water modifies the solvate hulls around the surfaces in the same way as it would in colloidal sols, that is, it decreases their thickness considerably. All observations concerning the formation of an electric double layer and parallelism or absence of parallelism in

[2] A very similar line of reasoning presented in a more mathematical and quantitative form is discussed by Verwey and Overbeek in their book "Theory of the Stability of Lyophobic Colloids." The words "electric double layer" could be substituted for "solvated layer." The balance of attractive and repulsive forces leads to a potential barrier (stability) or to an attraction throughout (instability ~ flocculation).

flocculation and ξ potential are applicable here. For our purpose it is possible to assume that adhesion and flocculation behave analogously. Thus, elements of the second group act in much smaller concentrations (about 1/100) than elements of the first group of the periodic system, and within the groups, the concentrations are regulated by the lyotropic series. The effect of Na_2SO_4 on the ξ potential of phosphor and glass is shown by Edelberg and Hazel; this effect should be expected from our analogy. It is to be suspected that anions will also exercise some effect especially at high concentrations. This influence of anion and cation in combinations on wet adhesion is shown by von Buzagh. He also shows that the adhesion number drops with rising concentration in NaOH, rises with concentration in KCl and $BaCl_2$, and has maxima and minima in $ThCl_4$. The influence of particle size in salt-water solutions is shown by Fig. 3B. It can be seen that adhesion is better with small particle sizes and worse with large particle sizes.

FIG. 4. Phosphor crystals held together by an intermediate layer.

Adhesion Due to Silicate-Mortar Action of the Silicate

For surfaces whose sign of charge is the same, the adhesion may be given by short range forces ($\approx 1/d^2$) acting between the solid particles at the points where they are in intimate contact. The highest adhesion would therefore be shown by cubic particles settled over a face on a flat surface. Spherical particles would have a lower adhesion. Luminescent particles of irregular shape (white planes in Fig. 4) would have only a partial adhesion because of lack of contact. Amorphous layers of silicate between the particles and the wall (black in Fig. 4) increase the adhesion when dry by acting as a "mortar."

To improve the dry adhesion (and also "wet" adhesion in mixed salt and silicate solutions, as will be explained later) it is current practice to add potassium silicate[3] to screening liquors. It is known that screens with low concentrations of potassium silicate alone cannot be made. At higher concentrations (about 6 per cent of solids) screens can be formed and even tilted, although the wet adhesion is not very good. When dried, the adhesion is strong. Edelberg and Hazel found that the ξ potential of the phosphor is raised by potassium silicate from -11 to -49 mv, and remains constant, whereas on the glass the ξ potential is raised from -57 to -78 mv and drops to -42 mv. Thus, at low concentration of silicate, phosphor particles are kept apart and away from the glass wall, as they would be in a sol. At higher concentration the adsorption of K^+ ions reduces the "peptizing" action of silicate.

[3] Potassium silicate made by the Philadelphia Quartz Company and sold as "Kasil #1" was used in the present tests.

Wet and Dry Adhesion in a Complete System, Water|Salt|Silicate

Salt alone does not give satisfactory dry adhesion, nor is the wet adhesion generally sufficient to tilt screens on tilt tables or conveyors. Dry adhesion with silicate alone is satisfactory, but wet adhesion is very poor. Certain combinations of salt and silicate give better results. Such conditions are illustrated in Tables I–IV and Fig. 5 and 6.

TABLE I. *"Dry" adhesion of settled screens*

3 grams of ZnS + ZnSCdS powder, avg size 16 μ; silicate + H_2O = 3000 cm³

Point in diagram Fig. 6	Settling time	cm³ $Ba(NO_3)_2$ 1.6% soln.	cm³ Kasil 1:4	lb pressure	
				For appearance of holes	For complete "blow-off"
1	10 min	35	50	—	6
1	4 hr	35	50	4	4
2	15 min	65	105	2	6
	overnight	30	2850	11–12	35
3	15 min	30	1200	8–19	>35
3	3 hr	30	1200	15	24
4	15 min	75	162	~11	23
5	20 min	40	162	8–17	18–35
6	2 hr	75	1200	6–12	33
7	15 min	75	125	4	6

In the tables and in Fig. 5 are shown results of measurements of dry adhesion made on screens settled from $Ba(NO_3)_2$|silicate solutions, with the apparatus shown in Fig. 2. In the tests of Table I, the ZnS+ZnSCdS television phosphor having the particle size distribution of Fig. 1 was used. The numbers in the first column correspond to the position of the points in the diagram Fig. 6. Curve 1 of Fig. 5 represents the data from Table I. For each point, 4 slides were settled, and about 4 "blow-off" tests were made on each slide. The values reported are average values of all readings, so that each point represents at least 16, and in some cases 32 or 48 readings, because most of the settlings were repeated several times. The readings were reproducible and consistent within 1 lb in the horizontal branches of the curves in Fig. 5. On the vertical branches the readings varied much more. This is quite understandable because this is a transition region in which seemingly two different processes are coexistent. For these reasons the multitude of data obtained were

not plotted individually. Instead, they are presented as curves which are closest to the average values. It can be seen that with low amounts of silicate dry adhesion has a low and constant value, then a sudden steep rise takes place followed by only a slight increase with still higher silicate quantities. The physical appearance of the "blow-off" changes: in the low silicate region the particles are blown off completely and separately; at higher quantities, the phosphor particles leave the plate as cohesive clumps or chunks. To investigate further the baffling phenomenon of the steep rise of dry adhesion, the tests were modified as follows:

TABLE II. *"Dry" adhesion of settled screens*

3 grams of ZnS + ZnSCdS powder, avg size 5 μ; silicate + H_2O = 3000 cm³

Point in diagram Fig. 6	Settling time	cm³ $Ba(NO_3)_2$ 1.6% soln.	cm³ Kasil 1:4	lb pressure	
				For appearance of holes	For complete "blow-off"
5	15 min	75	162	~4	8
	30 min	75	212	~5–11	14
	30 min	75	262	7–15	32
	15 min	75	100	2–4	8

TABLE III. *"Dry" adhesion of settled screens*

3 grams of ZnSCdS powder very coarse; silicate + H_2O = 3000 cm³

Settling time	cm³ $Ba(NO_3)_2$ 1.6% soln.	cm³ Kasil 1:4	lb pressure	
			For appearance of holes	For complete "blow-off"
min				
15	50	80	—	4
15	50	100	5	8
15	50	262	—	29
30	50	1200	—	36
20+	75	162	12	27
15	50	80	—	7
15	50	80	—	5
30	50	150	—	17
30	50	125	—	16
30	50	1200	—	35
30	60	162	—	26
30	100	162	—	20
30	25	162	—	23

TABLE IV. *"Dry" adhesion of settled screens*

4.6 grams of ZnS + ZnSCdS powder, avg size 16 μ; H_2O = 6000 cm³

Settling time	cm³ $Ba(NO_3)_2$ 1.6% soln.	cm³ Kasil 1:4	lb pressure	
			For appearance of holes	For complete "blow-off"
min				
25	90	162	—	8
30	90	250	—	30
28	90	200	—	15

In the tests shown in Table II and curve 2 of Fig. 5, a ZnS + ZnSCdS powder of smaller particle size (~5 μ avg) was used. It can be seen that again there is a steep rise, but at higher silicate quantities. In this case, the total surface available for adsorption was increased. For the tests of Table III and curve 3 of Fig. 5, a phosphorescent ZnSCdS of large particle size was used. This phosphor has less total surface than the powder of Table I and required somewhat less silicate for a steep rise. Finally, in Table IV, curve 4, settled screens of the same weight per cm² were settled in a larger container (surface of settled screen 1161 cm² against 706 cm² used previously), that is, the total weight of the powder was increased from 3.0 to 4.6 grams[4]; the volume of the

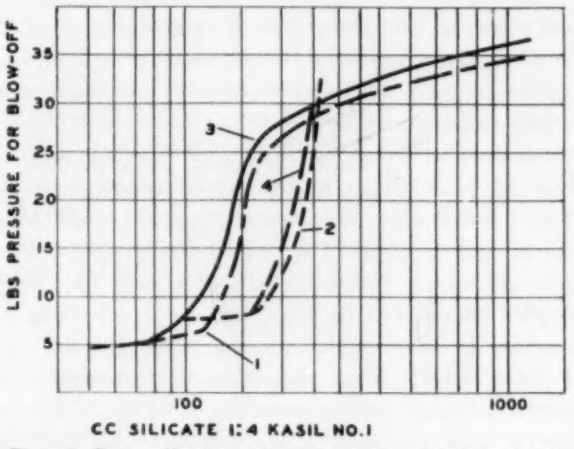

FIG. 5. Dry adhesion of phosphors settled in barium nitrate|silicate solutions.

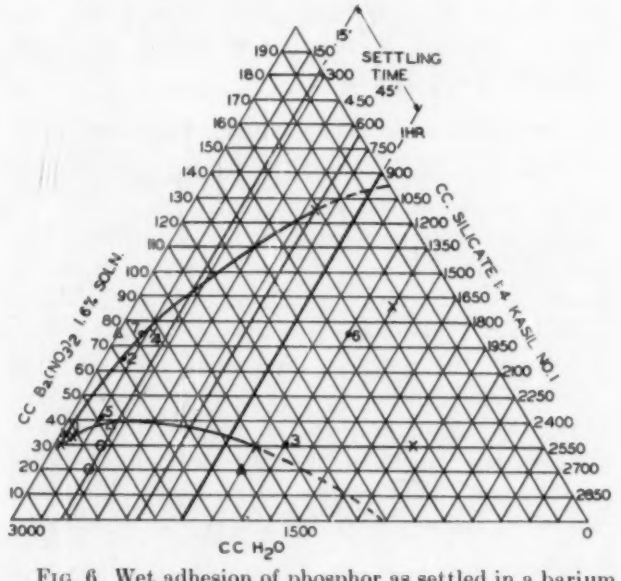

FIG. 6. Wet adhesion of phosphor as settled in a barium nitrate|silicate|water medium. ×—good wet adhesion; ○—no wet adhesion; Δ—borderline proportions; ●—points used in tests, Tables I–IV.

[4] These values are within 7 per cent error and sufficiently close for this type of work.

silicate-water solution was increased from 3000 to approximately 6000 cm³ and the amount of $Ba(NO_3)_2$, for optimum sticking in line with previous experience, from 75 to 90 cm³ of 1.6 per cent solution. It can be seen that the steep rise occurs at higher amounts of silicate but without corresponding increase in silicate concentration, and that the ratio of the cm³ silicate added in both cases to obtain the top point at the steep rise is almost equal to the ratio of the weights of the powder.

The picture obtained from dry adhesion tests would not be complete without settling tests corresponding to the wet adhesion. In Fig. 6 is shown a diagram of settlings in the $Ba(NO_3)_2$|silicate|water system based on a silicate-water volume of 3000 cm³. For all points inside the closed curve, the wet adhesion is above the minimum necessary for tilting. To the left, it can be seen that pure salt does not produce good enough adhesion, but the addition of very little silicate improves the wet adhesion enormously and such screens can be tilted in 10 minutes or less; increase of silicate increases the time which must elapse before the screen can be tilted.

In points above the curve, the salt and the silicate are present in such high concentrations that the silicate particles in solution coagulate (gel) and screening is not possible.

Interpretation of Experimental Results

These experimental results on dry and wet adhesion cannot at the present stage be traced to a simple picture of happenings in the complete system salt|silicate|water. One way of approach might be based on certain ideas on the stability of lyophobic colloids (7). It is conceivable that, at small amounts of silicate, the particles (and silica) deposit from "stable" suspensions with predominantly repulsive forces. At higher amounts of silicate, the suspensions become "unstable" with attraction forces being predominant. This picture could explain a sudden change in resistance of the screens to mechanical forces.

Another possibility of approach would be to assume that the powder particles and possibly the glass wall adsorb silicate molecules. They also adsorb ions which facilitate coagulation (or adhesion). The phosphor particles can adsorb a layer of a given maximum thickness if there is enough silicate present. The actual amount of the adsorbed silicate, the extent to which a silicate layer surrounding the particles has been formed, is determined by the total surface of the powder and the glass and by the total amount of silicate present and not by the silicate concentration. When little silicate is present, the adsorbed ions act in such a way that local bonds are formed between the silicate and the glass. These bonds may be of a chemical nature as shown by Stericker and Hazel. This explains the good wet adhesion, the short time necessary for bond formation, and the poor dry adhesion with the tendency of the powder to separate. When the layer surrounding the powder particles is completely saturated with silicate, the particles start to be bound one to another, possibly also by silicate bridges described by Stericker and Hazel. Because of this additional amount of silicate, longer settling time is necessary to obtain sufficient wet adhesion to allow the supernatant liquid to be decanted without affecting the screen. After drying, the additional silicate acts as a mortar between the particles producing better dry adhesion. This would be the optimum point for most practical purposes because it permits a more rugged treatment of the dry screen. From the data of Fig. 6 and Tables I to IV, adequate settling formulae can be calculated for any tube size and any particle size.

If the silicate content is increased beyond the point necessary for improved dry adhesion, screens have to be settled longer because the salt|silicate ratio has to be lowered to prevent gelling. That the dry adhesion is further improved with increasing amount of silicate can be explained by the appearance of a silicate membrane on top of the powder which forms from the drying solution after it has been siphoned or poured off and which acts as a "mortar."

From the standpoint of colloidal chemistry, there is included in the picture given above the action of an electrolyte on a protective agent. Such cases are known but as yet there does not seem to be a complete understanding of such processes; at the present stage it may be pure speculation to state whether the bridges formed in the solvate hulls by the precipitated protective agent are due to chemical bonds or to van der Waals adhesion.

Any discussion of this paper will appear in a Discussion Section, to be published in the December 1952 issue of the Journal.

REFERENCES

1. M. Sadowsky, *Trans. Electrochem. Soc.*, **95**, 112 (1949).
2. R. Edelberg and F. Hazel, *Trans. Electrochem. Soc.*, **96**, 13 (1949).
3. W. Stericker and F. Hazel, *J. Phys. & Colloid Chem.*, **54**, 1045 (1950).
4. A. von Buzagh, "Colloid Systems," The Technical Press, Ltd., London (1937); Kolloid-Z., **47**, 370 (1929); **51**, 105 and 230 (1930); **52**, 46 (1930); **76**, 2 (1936).
5. G. I. Fuks, V. M. Klychnikov, and E. Tsyganova, *Doklady Akad. Nauk S.S.S.R.*, **65**, 307 (1949).
6. Pierce M. Travis, *ASTM Bull.* (Jan. 1940).
7. E. J. W. Verwey and J. Th. G. Overbeek, "Theory of the Stability of Lyophobic Colloids," Elsevier, New York (1948).

The Mechanism of the Cathodic Hydrogen Evolution Reaction[1]

J. O'M. Bockris and E. C. Potter

Imperial College of Science, London, England

ABSTRACT

Some of the outstanding problems of concept and mechanism in the field of cathodic hydrogen evolution kinetics are discussed and clarified. A full derivation and correlation of kinetic equations which assume no mechanism reveals expressions for several parameters which take values specific to one or more mechanisms. The use of statistical methods of treatment of data proves indispensible in estimating the values of these parameters. A further method of ascertaining the mechanism of the hydrogen evolution reaction is to examine the kinetics of the individual reaction paths, so that the expected values of parameters common to all paths may be deduced. A number of mechanisms important in acid and alkaline solutions are thus treated, and are shown to be distinguishable experimentally. Using already published data, the actual conditions under which various reaction paths take place at mercury, silver, nickel, and smooth platinum cathodes are calculated. It is not only possible to compare these deduced data with observation, and thereby verify the occurrence of a particular reaction path, but also to demonstrate the impossibility of some mechanisms in specific cases. The recent advances which the foregoing methods have made possible are discussed in relation to data which have recently become available.

I. Introduction

The electrolytic evolution of hydrogen is generally chosen as the main subject of experimental and theoretical research in electrode kinetics because it was originally thought to be one of the simplest electrode reactions. This expectation has not been confirmed. However, work already done has emphasized the importance of the reaction, and its practical significance to studies in corrosion has stimulated further attempts to solve the problems discovered. In the following, some general equations of electrode kinetics are formulated and indicate the experimental methods best suited to mechanism determinations.

II. Some Difficulties of Technique and Concept

It is notoriously difficult to measure the velocity of an electrode reaction and the corresponding electrode potential with reproducibility. The best agreement obtained between workers in different laboratories is ± 8 mv on Hg and ± 20 mv on solid (e.g., Ni) cathodes.

Many different types of Tafel lines are reported in the literature. Some of these are collected in Fig. 1, from which it is seen that only the first and the last two represent forms which are free from vitiating influences. The principal vitiating factor in experimental work arises from minute traces of impurities in solution. For example, addition of only 10^{-10} gram moles/liter of As_2O_3, CS_2, CO, KCN, etc., detectably affect the electrode potential at a given current density at nickel cathodes (1). Reproducible results can only be obtained in solutions which have been purified by pre-electrolysis on to an auxiliary cathode (2). Use of this method involves laborious work to determine the amount of pre-electrolysis necessary for a given electrode and solution. The criterion by which the optimum conditions for pre-electrolysis are found is that passage of further coulombs at higher potentials makes no further difference to the experimental results. Even then, the initial state of the solution before purification may be difficult to reproduce so that sometimes less pre-electrolysis is necessary than at other times.

Many difficulties in preparing the surface of solid metals in a reproducible, clean state have caused most studies to be made on mercury. In one method (3) the electrode in wire form is heated in a stream of hydrogen to remove oxide films and sealed into a thin glass bulb containing pure hydrogen. After pre-electrolysis of the solution the bulb is broken by a glass probe thereby immersing the electrode in the purified and oxygen-free solution. A further possible method would be to heat the wire electrode electrically, e.g., inductively inside the cell, containing hydrogen, before placing it in solution.

In addition, a few difficulties connected with the general attitude of much past work to studies of the hydrogen evolution reaction may be mentioned. First, the difficulty of measuring the electrode poten-

[1] Manuscript received March 26, 1951. This paper prepared for delivery before the Washington Meeting, April 8 to 12, 1951.

tial, and the comparative ease of measuring the current, directed attention away from the fact that the problems connected with overpotential were purely kinetic, and that attention should be focused upon the current. Second, considerable attention has been paid to the determination of i_0, the current

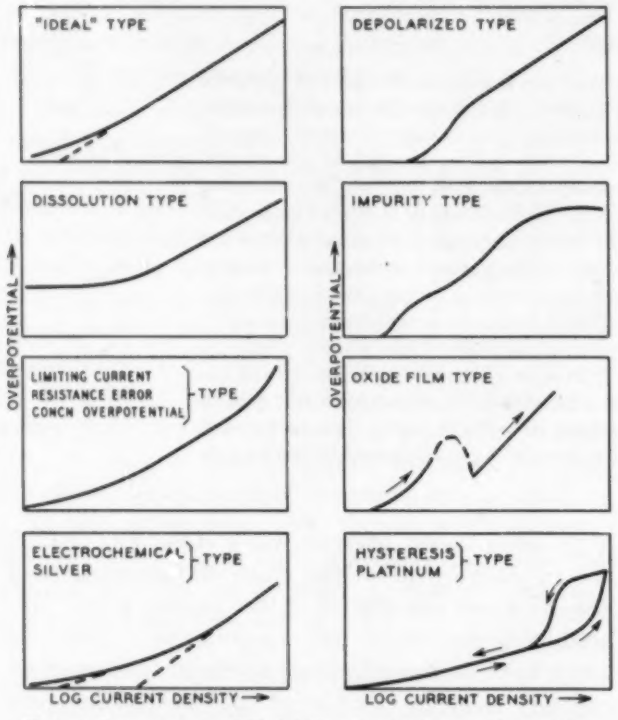

FIG. 1. Some types of Tafel line for hydrogen deposition

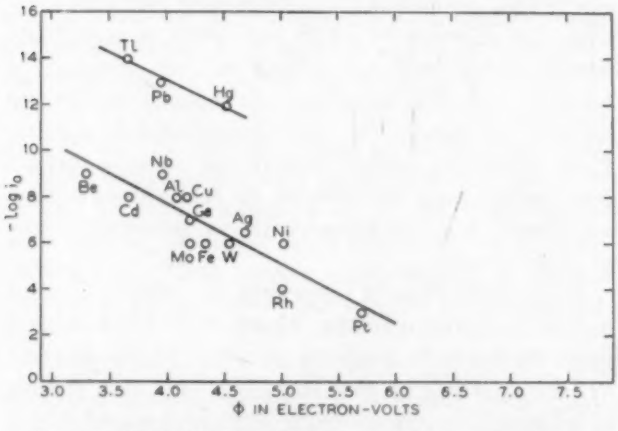

FIG. 2. Relationships between exchange current and thermionic work function for a number of cathodes.

passing in either direction at the electrode at the reversible potential, i.e., at zero overpotential.

Consider a complete galvanic cell at constant temperature consisting of a metal M (the cathode in a cell in which overpotential is measured) and a Pt electrode in the same solution as the metal M. There are three potential differences in the cell: V_M, that at the boundary M-solution; V_{Pt}, at the boundary Pt-solution; and X, the contact potential difference between the metals. If ΔV is a potential difference measured by means of a potentiometer connected to wires of composition M, then,

$$\Delta V = V_M - V_{Pt} + X.$$

Now, $X \doteq \Phi_M - \Phi_{Pt}$, where Φ_M and Φ_{Pt} are the work functions of the metals M and Pt respectively (neglecting the Peltier heat in the usual way). Hence,

$$V_M = \Delta V + V_{Pt} - \Phi_M + \Phi_{Pt}.$$

Or, if the experimental conditions are appropriate, so that ΔV represents a hydrogen overpotential,

$$V_M = \eta + V_{Pt} - \Phi_M + \Phi_{Pt} = \eta - \Phi_M + K, \quad (1)$$

where K is a constant potential difference for all cells in which hydrogen overpotential, η, is measured at the same pH and temperature. But also, the relation between current density, i_c, and potential, for a kinetic electrode process in which the reverse reaction can be neglected, is given (see below) by an equation of the form,

$$i_c = K_1 \exp\left[\frac{-\alpha V_M \mathbf{F}}{RT}\right]$$

where α and K_1 are constants and the pH is assumed to be constant. Thus,

$$i_c = K_1 \exp\left[\frac{-\alpha(\eta - \Phi_M + K)\mathbf{F}}{RT}\right]. \quad (2)$$

Therefore, if when $\eta = 0$, $i_c = i_0$, then,

$$i_0 = K_2 \exp\left[\frac{\alpha \Phi_M \mathbf{F}}{RT}\right], \quad (3)$$

where K_2 is a new constant.

A relation of type (3) is indeed observed, and is shown in Fig. 2. It follows, then, that the most appropriate potential at which to compare the rate of the hydrogen evolution reaction at various electrode materials is not the reversible hydrogen potential but the absolute zero of potential. In the absence of reliable knowledge of this, the potential of the charge-free surface appears to be the best reference potential.

Similar conclusions apply to the heat of activation, ΔH_0^*, which is usually quoted at the reversible hydrogen potential. However, measurements of i_0 and ΔH_0^* retain considerable relevance because they assist in distinguishing between various possible mechanisms of the electrode reactions.

Lastly, the rate of the evolution reaction depends upon the difference of two inner potentials ϕ, i.e., it depends upon a Galvani potential, where ϕ is defined by

$$\phi = \psi + \chi, \quad (4)$$

ψ being the Volta potential of a phase and χ the surface potential. The latter potential is strongly dependent upon the surface condition of a phase, and hence the overpotential at a given rate of reaction would depend sharply upon trace impurities.

III. Statistical Methods in Measurements of Hydrogen Electrode Kinetics

In order to observe with reasonable and known accuracy those of the theoretically important parameters in overpotential studies (e.g., temperature and concentration effects) which may vary little more than the reproducibility of the measurements, it is essential to replicate the observations and to apply statistical methods.

In applying the method of least squares to estimate the parameters of a Tafel line, those formulae should be employed which correspond to the current as the independent variable and the potential as the dependent variable. This means that the sums of squares of the *vertical* deviations of the experimental points from the computed Tafel line are minimized, and that, consequently, a prediction of potential at a stated current has the minimum possible error based on the original observations. Thus we have

$$a = \bar{y} - b\bar{x}, \tag{5}$$

and

$$b = \frac{n\Sigma xy - \Sigma x\Sigma y}{n\Sigma x^2 - (\Sigma x)^2} = \frac{N}{D}, \tag{6}$$

where x and y take the corresponding experimental values of log i_c and η, respectively, n is the number of pairs of observations, $\bar{y}$ is $(\Sigma y)/n$, and $\bar{x}$ is $(\Sigma x)/n$. The variances of the Tafel line parameters may be calculated from

$$V(b) = \frac{[n\Sigma y^2 - (\Sigma y)^2]D - N^2}{(n-2)D^2}, \tag{7}$$

$$V(a) = V(b)\,[D/n + \bar{x}^2], \tag{8}$$

and

$$V(\log i_0) = \frac{V(b)[D/n + (\log i_0 - \bar{x})^2]}{b^2}, \tag{9}$$

where $V(b)$, $V(a)$, and $V(\log i_0)$ are the respective variances of b, a, and log i_0, each with $n-2$ degrees of freedom.

When replication of observations is carried out, it is often desired to replace the population of Tafel lines so obtained by one mean line. The parameters of this line may be calculated by bulking the observations and applying (5) and (6), but the variances of these parameters cannot be found by applying equations (7) to (9) to such bulked data. In these circumstances the required variances are calculated from equations of the type,

$$V(\bar{p}) = \frac{\Sigma(p_j - \bar{p})^2}{n_T(n_T - 1)}, \tag{10}$$

where $V(\bar{p})$ = variance of $\bar{p}$,
p_j = the value of the parameter p of the j^{th} Tafel line,
$\bar{p} = (\Sigma p_j)/n$,
and n_T = number of Tafel lines in the population.

It can be shown that the relation between log i_0 and absolute temperature, T, is

$$\log i_0 = \log B - \frac{\Delta H_0^*}{2.303RT}, \tag{11}$$

where log B contains a temperature term, but is usually considered to be temperature independent over the ranges of temperature often used experimentally. It is evident from (11) that since log B is formally the value of log i_0 at infinite temperature, the value of log B is obtained by a long extrapolation of the observed relation. Also, since log i_0 is itself obtained by lengthy extrapolation of a Tafel line, it is not surprising that published values of log B show lack of agreement (4). In order to obtain the most probable values of ΔH_0^* and log B from the data, it is clear that by treating $1/T$ as the independent variable and log i_0 as the dependent variable, equations analogous to (5) to (8) can be applied.

The experimental accuracy which must be achieved to attain any desired limits of error in an estimate of log B may be calculated in the following way. The variance of log i_0, $V(\log i_0)$, is given with sufficient accuracy by

$$V(\log i_0) = \frac{V(m)D'}{n'}, \tag{12}$$

where $V(m)$ is the variance of m,
m is $\Delta H_0^*/2.303R$,
D' is the appropriate denominator corresponding to D, in (6),
and n' is the number of pairs of observations of log i_0 and $1/T$.

Also, the variance of log B, $V(\log B)$, is obtained from an equation analogous to (8) as,

$$V(\log B) = V(m)\,[D'/n' + \bar{\tau}^2], \tag{13}$$

where $\bar{\tau} = \Sigma\tau/n' = (\Sigma 1/T)/n'$. From (12) and (13) and noting by analogy to (6) that $D'/n' = \Sigma(\tau - \bar{\tau})^2$,

$$V(\log i_0) = \frac{V(\log B)\Sigma(\tau - \bar{\tau})^2}{\bar{\tau}^2 + \Sigma(\tau - \bar{\tau})^2}. \tag{14}$$

In order to use (14) numerically suppose that the values of τ are derived from the experimental

temperatures 0°, 10°, 20°, 30°, and 40°C, and furthermore, let it be arbitrarily decided that the maximum inaccuracy tolerable in log B corresponds to 95 per cent confidence limits of ± 0.5. Hence, assuming that the errors in log B are normally distributed, we have $3.18 \sqrt{V(\log B)} = 0.5$, where 3.18 is the value of Student's t for 3 degrees of freedom and the 0.05 probability level. Hence from (14) $V(\log i_0)$ is 0.000286. Now, from (6) and (9) it is seen,

$$V(\log i_0) = \frac{V(b)[(\log i_0 - \overline{\log i_c})^2 + \Sigma(\log i_c - \overline{\log i_c})^2]}{b^2} \quad (15)$$

where $\overline{\log i_c} = \bar{x}$. This equation may be applied to typical experimental data for the mercury cathode, which (reference shows) gives the most reproducible overpotential measurements. Let log i_c take the nine values, -7, -6.5, -6, $\cdots -3$, so that the value of $\overline{\log i_c}$ is -5.0. Taking b and log i_0 for the mercury cathode in aqueous acid solution as 0.115 volt and -12.0, respectively, and using the value for $V(\log i_0)$ calculated above, it is found that $V(b)$ is $0.0592 \cdot 10^{-6}$ (corresponding to 95% confidence limits in b of ± 0.0006 volt). Such an accuracy in estimating the slope of the Tafel line is unattainable even with modern techniques. This is evident since an error of only 1 mv in estimating the overpotential at 10^{-7} amp/cm^2 and a similar error in the opposite direction at 10^{-3} amp/cm^2 is sufficient to cause an inaccuracy of ± 0.0005 volt in b.

In a recent investigation using nickel cathodes (10) one twentieth of the experimental Tafel lines attained less than the above inaccuracy in slope, but the slope of the mean line of a population of Tafel lines could not be determined with an accuracy (95% confidence limits) greater than ± 0.004 volt. The 95 per cent confidence limits for log B were on the average ± 2.2, each limit being based on an average of 25 pairs of observations. It, therefore, appears that the quantity B is not a useful distinguishing criterion of reaction mechanism.

While variances (which should be quoted with their number of degrees of freedom) are independent of distribution of errors they are not readily assimilable as measures of error, and it is customary to assume (in the absence of evidence otherwise) that the distribution of errors is normal so that confidence limits may be quoted. Some caution is necessary here; for if it is assumed that the parameters b and log i_0 of the Tafel line have normal distribution of errors, then the errors in i_0 itself are not normally distributed. Consequently, the distribution of errors of λ which is calculable from i_0 (see later) is not normal, although it is unlikely that serious error would arise by assuming normality.

IV. General Equations

A. Current and Potential

Suppose that k_1 is the specific rate constant of an unspecified rate-determining step in the forward direction of a reaction (ions depositing). Then,

$$k_1 = \kappa \frac{kT}{h} \exp\left(-\frac{(\Delta G^*)_1}{RT}\right), \quad (16)$$

where $(\Delta G^*)_1$ is the standard free energy of the activated complex of the rate-determining step with respect to the initial state (here assumed to be λ gram ions of hydrogen ions constituting part of the monolayer adjacent to the electrode surface, often termed the Helmholtz double layer) of the reaction, where κ is the transmission coefficient, and where k and h have their usual meanings. Let a_I be the activity of H_3O^+ ions in the initial state. Then the forward velocity $\vec{v}$ is

$$\vec{v} = a_I k_1. \quad (17)$$

Also, the forward current is

$$\vec{i} = \vec{v}\lambda\mathbf{F}, \quad (18)$$

where λ is the number of electrons necessary so that one act of the rate-determining step can occur.

Suppose a potential difference $\Delta\phi_c$ is applied between the electrode and the initial state of the reaction. If this potential difference is positive it retards the flow of reactants over the energy barrier of the rate-determining step, i.e., it makes $(\Delta G^*)_1$ more positive. The potential difference increases $(\Delta G^*)_1$ by $\beta\lambda\mathbf{F}\Delta\phi_c$ where $\beta\Delta\phi_c$ is the potential difference through which the electrons pass before they reach the transition state. (Work done on the system *after* it has passed the transition state does not affect the velocity of the reaction.) Hence $0 < \beta < 1$. β varies with the reaction mechanism, and is a complex quantity, except in certain simple mechanisms. Thus, in the discharge reaction $H_3O^+ + e \rightarrow MH + H_2O$, $\beta = \frac{1}{2}$ if the energy barrier is symmetrical. General and limiting values of β are evaluated below for common mechanisms. From (16), (17), and (18),

$$\vec{i} = \kappa\lambda\mathbf{F} \frac{kT}{h} a_I \exp\left(-\frac{(\Delta G^*)_1 + \beta\lambda\Delta\phi_c\mathbf{F}}{RT}\right). \quad (19)$$

By a similar argument,

$$\overleftarrow{i} = \kappa\lambda\mathbf{F} \frac{kT}{h} a_P \exp \cdot \left(-\frac{(\Delta G^*)_2 - (1-\beta)\lambda\Delta\phi_c\mathbf{F}}{RT}\right), \quad (20)$$

where $(\Delta G^*)_2$ is the standard free energy of activation of the reverse reaction referred to the initial

state of this reaction, and a_F is the activity of the entities in this initial state.

If $\Delta\phi_e = \Delta\phi_r$, the reversible potential,

$$\vec{i} - \overleftarrow{i} = 0, \text{ where } \vec{i} = i_0 = \overleftarrow{i}. \tag{21}$$

From (19), (20), and (21) and since $\eta = \Delta\phi_e - \Delta\phi_r$,

$$\vec{i} = i_0 \exp\left(-\frac{\beta\lambda\eta\mathbf{F}}{RT}\right), \tag{22}$$

$$\overleftarrow{i} = i_0 \exp\left(+\frac{(1-\beta)\lambda\eta\mathbf{F}}{RT}\right), \tag{23}$$

$$\therefore i_c = \vec{i} - \overleftarrow{i} = i_0\left[\exp\left(-\frac{\beta\lambda\eta\mathbf{F}}{RT}\right) - \exp\left(\frac{(1-\beta)\lambda\eta\mathbf{F}}{RT}\right)\right]. \tag{24}$$

Equation (24) is the most general expression for the cathodic current, and represents a more fruitful form of the relationship than has been stated hitherto.

Special Case 1.—Relation between i_c and η at appreciable overpotentials (e.g., η more negative than about -75 mv, see special case 3).

Equation (24) becomes

$$i_c = i_0\left[\exp\left(-\frac{\beta\lambda\eta\mathbf{F}}{RT}\right)\right], \tag{25}$$

or

$$\eta = \frac{RT}{\beta\lambda\mathbf{F}} \ln i_0 - \frac{RT}{\beta\lambda\mathbf{F}} \ln i_c. \tag{26}$$

Equation (26) is Tafel's equation,

$$\eta = a - b \log i_c, \tag{27}$$

or

$$\eta = a - \frac{RT}{\alpha\mathbf{F}} \ln i_c \tag{28}$$

so that, comparing (26) and (27) and (28), it follows that:

$$a = \frac{RT}{\beta\lambda\mathbf{F}} \ln i_0, \tag{29}$$

$$b = \frac{2.303RT}{\beta\lambda\mathbf{F}}, \tag{30}$$

$$\alpha = \beta\lambda. \tag{31}$$

Equation (31) shows that α is a composite quantity, and need not be between 0 and 1 since β and λ can have maximum values of 1 and 2, respectively. Thus, the experimentally observed values of α of 2, which have been difficult to explain hitherto, are a special case of equation (31).

Special Case 2.—Relation between i_c and η at low overpotentials (e.g., η less negative than -20 mv).

By expanding exponentials, equation (24) becomes,

$$i_c = -\frac{\lambda i_0 \eta\mathbf{F}}{RT}. \tag{32}$$

Thus, i_c and η are linearly related at sufficiently low overpotentials. Also, from (32) and formally allowing for the possibility of $\partial i_c/\partial\eta$ depending on η,

$$\lambda = -\frac{RT}{\mathbf{F}i_0}\left(\frac{\partial i_c}{\partial\eta}\right)_{\eta\to 0}. \tag{33}$$

λ (see Ref. 21) can be termed the electron number of the reaction and is estimated experimentally by applying equation (33). As shown below, λ is a valuable diagnostic criterion of reaction mechanisms.

Special Case 3.—Relations connected with non-linearity between η and log i_c.

From (24),

$$i_c = i_0 \exp\left(-\frac{\beta\lambda\eta\mathbf{F}}{RT}\right)[1 - f], \tag{34}$$

where

$$f = \exp\left(\frac{\lambda\eta\mathbf{F}}{RT}\right). \tag{35}$$

When the departure of the Tafel line [see equation (27)] from linearity due to the reverse current in (20) is just detectable experimentally, then f is just distinguishable from zero, and $\eta = \eta_s$. The smallest detectable and significant value of f, i.e., f_s, depends on the experimental design, but, provided a minimum number of about five pairs of observations fall within a region about 0.025 volt on either side of η_s, it may be assumed that f_s is 0.05. Therefore, from (35),

$$f_s = 0.05 = \exp\left(\frac{\lambda\eta_s\mathbf{F}}{RT}\right); \tag{36}$$

or at 20°C with η_s expressed numerically in volts,

$$\lambda = \frac{0.075}{\eta_s}. \tag{37}$$

Equation (37) gives an alternative method of estimating λ experimentally and has not been previously described.

B. Potential and Time

1. *During Build-up of Overpotential*

For a completely polarisable electrode, the net constant cathodic current is the sum of the condenser (i') and faradaic (i'') currents:

$$i_c = i' + i''. \tag{38}$$

Let C be the differential capacity of the electrode-solution interface. Then,

$$-C\,d\eta_t = i'\,dt \tag{39}$$

where $d\eta_t$ and dt are infinitesimal changes in η_t and time, t, respectively. Let η_t and η_∞ be values of η at times $t = t$ and $t = \infty$, respectively. Since i'' is given by (24), then from (24), (38), and (39),

$$-\frac{Cd\eta_t}{dt} = i_c - i_0\left[\exp\left(-\frac{\beta\lambda\eta_t\mathbf{F}}{RT}\right) - \exp\left(\frac{(1-\beta)\lambda\eta_t\mathbf{F}}{RT}\right)\right]. \quad (40)$$

Special Case 1. $dC/d\eta = 0$; η_t more negative than -75 mv.

Equation (40) becomes

$$-\frac{Cd\eta_t}{dt} = i_c - i_0\left[\exp\left(-\frac{\beta\lambda\eta_t\mathbf{F}}{RT}\right)\right]. \quad (41)$$

Let

$$\frac{i''}{i_c} = f' \quad (42)$$

and suppose $f' < 0.05$ so that i'' is negligible in (38), then from (38) and (39),

$$i_c = -\frac{Cd\eta_t}{dt}. \quad (43)$$

Hence, from (42) and if $f' < 0.05$, $d\eta_t/dt$ is a constant. To find the region of overpotential in which this result is valid, we apply (38) which becomes $i_c = i''$ at $t = \infty$, so that from (25),

$$i_c = i_0\left[\exp\left(-\frac{\beta\lambda\eta_\infty\mathbf{F}}{RT}\right)\right]. \quad (44)$$

Also from (25),

$$i'' = i_0\left[\exp\left(-\frac{\beta\lambda\eta_t\mathbf{F}}{RT}\right)\right]. \quad (45)$$

Thus, from (42), (44), and (45),

$$f' = \exp\left(\frac{\beta\lambda(\eta_\infty - \eta_t)\mathbf{F}}{RT}\right). \quad (46)$$

For example, let $f' = 0.03$, then from (46), taking a typical value of $2.303RT/\beta\lambda\mathbf{F}$ from experiment as 0.12, $\eta_\infty - \eta_t = -0.15$, i.e., the relation of potential to time is linear [(43) is valid] to within 0.15 volt of the constant value η_∞.

Special Case 2. $dC/d\eta = 0$; η_∞ more negative than -75 mv; $(\eta_\infty - \eta_t)$ less negative than -20 mv.

Let $\eta_\infty - \eta_t = \Delta\eta$; at $t = t_1$, $\Delta\eta = \Delta\eta_1$ and at $t = t_2$, $\Delta\eta = \Delta\eta_2$. Hence, from (40) and (44),

$$\frac{d\eta_t}{dt} = -\frac{i_0}{C}\left[\exp\left(-\frac{\beta\lambda\eta_\infty\mathbf{F}}{RT}\right)\right]\cdot\left[1 - \exp\left(\frac{\beta\lambda\Delta\eta\mathbf{F}}{RT}\right)\right]. \quad (47)$$

Or, integrating between t_1 and t_2 and the corresponding values of $\Delta\eta$,

$$t_1 - t_2 = \frac{CRT}{i_0\beta\lambda\mathbf{F}}\left[\exp\frac{\beta\lambda\eta_\infty\mathbf{F}}{RT}\right]\ln(\Delta\eta_1 - \Delta\eta_2). \quad (48)$$

Equation (48) indicates that during the initial build-up of overpotential, η_t relatively rapidly reaches practically constant values. For example, with $2.303RT/\beta\lambda\mathbf{F} = 0.1$, the time required for overpotential to rise from within 10 mv to within 1 mv of η_∞ is the same as that required for the interval 1 mv to 0.1 mv from η_∞.

2. *During Decay*

(i) *Relations in which it is assumed that* $dC/d\eta = 0$.

From (41) with $i_c = 0$, and η_∞ more negative than -75 mv,

$$\frac{d\eta_t'}{dt} = \frac{i_0}{C}\left[\exp\left(-\frac{\beta\lambda\eta_t'\mathbf{F}}{RT}\right)\right], \quad (49)$$

where η_t' is the overpotential t seconds after the commencement of decay. Integrating,

$$t = \frac{CRT}{i_0\beta\lambda\mathbf{F}}\exp\left(\frac{\beta\lambda\eta_t'\mathbf{F}}{RT}\right) + \text{const.} \quad (50)$$

At $t = 0$, $\eta' = \eta_\infty$. Hence,

$$\text{Const.} = -\frac{CRT}{i_0\beta\lambda\mathbf{F}}\exp\left(\frac{\beta\lambda\eta_\infty\mathbf{F}}{RT}\right). \quad (51)$$

From (50) and (51),

$$t = \frac{CRT}{i_0\beta\lambda\mathbf{F}}\left[\exp\left(\frac{\beta\lambda\eta_t'\mathbf{F}}{RT}\right) - \exp\left(\frac{\beta\lambda\eta_\infty\mathbf{F}}{RT}\right)\right]. \quad (52)$$

Special Case 1. $\eta_t' = \eta_\infty - \Delta\eta'$, where $\Delta\eta'$ is less negative than -20 mv.

Using this condition in (52) yields

$$\exp\left(\frac{\beta\lambda\eta_\infty\mathbf{F}}{RT}\right)\left[\exp\left(-\frac{\beta\lambda\Delta\eta'\mathbf{F}}{RT}\right) - 1\right] = \frac{\beta\lambda\mathbf{F}i_0t}{CRT}. \quad (53)$$

Having regard to the condition for $\Delta\eta'$, (53) becomes

$$\Delta\eta' = -\frac{i_0t}{C}\exp\left(-\frac{\beta\lambda\eta_\infty\mathbf{F}}{RT}\right). \quad (54)$$

Equation (54) shows that the initial decay of overpotential is linear with time. Hence, linear extrapolations to zero time in the commutator method of measuring overpotential are valid under the above defined conditions.

Special Case 2. $\Delta\eta'$ more negative than approximately -50 mv (normal decay); η_t' more negative than -20 mv.

Applying this condition to (52), and thus neglecting $\exp(\beta\lambda\eta_\infty\mathbf{F})/RT$ gives,

$$t = \frac{CRT}{\beta\lambda\mathbf{F}i_0}\exp\left(\frac{\beta\lambda\eta_t'\mathbf{F}}{RT}\right). \quad (55)$$

$$\therefore\ \eta_t' = \frac{RT}{\beta\lambda\mathbf{F}}\ln t - \frac{RT}{\beta\lambda\mathbf{F}}\ln\frac{CRT}{\beta\lambda\mathbf{F}i_0}. \quad (56)$$

Hence from (56) and (30),

$$\frac{d\eta_t'}{d(\log t)} = \frac{2.303RT}{\beta\lambda\mathbf{F}} = b. \quad (57)$$

Equation (57) shows that overpotential decays logarithmically with time under the above conditions and that the slope of the logarithmic decay curve is the same as that of the corresponding Tafel line [cf. Butler (24)].

Special Case 3. η_t' less negative than -20 mv. From this condition, the faradaic current i'', is given by (32), also from (38), in which during decay $i_c = 0$, and using (39) it follows that

$$\frac{d\eta_t'}{dt} = -\frac{\lambda i_0\eta_t\mathbf{F}}{CRT}. \quad (58)$$

Integrating (58),

$$t = \frac{CRT}{\lambda i_0\mathbf{F}}\ln|\eta_t| + \text{const.} \quad (59)$$

Equation (59) shows that the decay curve of overpotential against time becomes asymptotic to the time axis, the relation being exponential. The equation may be used to find the differential capacity (25).

(ii) *Relations in which* $dC/d\eta = f(\eta)$.

During decay, $i'' = C\,d\eta_t'/dt$. Using this in (38) and (39) gives

$$-C\frac{d\eta_t}{dt} = i_c - C\frac{d\eta_t'}{dt}. \quad (60)$$

or

$$C = \frac{i_c}{\left(\frac{d\eta_t'}{dt}\right) - \left(\frac{d\eta_t}{dt}\right)}, \quad (61)$$

where the values of C, $d\eta_t'/dt$, and $d\eta_t/dt$ refer to the same overpotential η.

Further, if (54) is applied to infinitesimal changes during decay,

$$\left(\frac{d\eta'}{dt}\right)_{\eta_t} = -\frac{i_0}{C}\exp\left(-\frac{\beta\lambda\mathbf{F}\eta_t'}{RT}\right), \quad (62)$$

so that

$$\ln C = \ln i_0 - \frac{\beta\lambda\mathbf{F}\eta_t'}{RT} - \ln\left(\frac{d\eta_t'}{dt}\right)_{\eta_t}. \quad (63)$$

Equation (61) enables estimates of differential capacity obtained from the build-up of overpotential to be corrected for faradaic current from observations of the corresponding decay curve (22). The differential capacity may be obtained from the decay curve by application of (63), it being also necessary to know the values of b and $\log i_0$ of the corresponding Tafel line.

C. *Current and Temperature*[2]

From (19) and (21),

$$i_0 = \kappa\lambda\mathbf{F}\frac{kT}{h}a_I\exp\left(-\frac{(\Delta G^*)_1 + \beta\lambda\Delta\phi_r\mathbf{F}}{RT}\right), \quad (64)$$

$$\therefore\quad i_0 = \kappa\lambda\mathbf{F}\frac{kT}{h}a_I\exp\left(-\frac{(\Delta G_0^*)_1}{RT}\right), \quad (65)$$

where $(\Delta G_0^*)_1$ is the standard free energy of activation for the forward direction of the rate-determining step at the reversible potential. Hence,

$$i_0 = B\exp\left(-\frac{\Delta H_0^*}{RT}\right), \quad (66)$$

where

$$B = \kappa\lambda\mathbf{F}\frac{kT}{h}a_I\exp\left(\frac{\Delta S_0^*}{R}\right), \quad (67)$$

and ΔH_0^* and ΔS_0^* are respectively the heat and entropy of activation corresponding to $(\Delta G_0^*)_1$. Assuming ΔH_0^* and ΔS_0^* are not temperature dependent, and that over small ranges of temperature B is constant, the plot of $\ln i_0$ against $1/T$ has a slope of $-\Delta H_0^*/R$.

Further, when η is more negative than -75 mv, (25) and (66) give

$$i_c = B\exp\left(-\frac{\Delta H_0^* + \beta\lambda\eta\mathbf{F}}{RT}\right). \quad (68)$$

Hence, taking B and $\beta\lambda$ as temperature independent,

$$\left(\frac{\partial(\ln i_c)}{\partial T}\right)_\eta = \frac{\Delta H_0^* + \beta\lambda\eta\mathbf{F}}{RT^2}. \quad (69)$$

From (26), and with conditions assumed as for (69),

$$\left(\frac{\partial\eta}{\partial(\ln i_c)}\right)_T = -\frac{RT}{\beta\lambda\mathbf{F}}. \quad (70)$$

From (69) and (70) it follows that

$$\left(\frac{\partial\eta}{\partial T}\right)_{i_c} = -\frac{\Delta H_0^* + \beta\lambda\eta\mathbf{F}}{\beta\lambda\mathbf{F}T}. \quad (71)$$

[2] Other relations between current and temperature have been given by Agar (23).

V. Possible Reaction Paths of the Hydrogen Evolution Reaction[3]

A. *Source of Proton is* H_3O^+

The possible paths are (M being a metal atom):

$$\begin{aligned} &H_3O^+ + e \xrightarrow{\text{slow}} MH + H_2O \\ &MH + MH \xrightarrow{\text{fast}} 2M + H_2 \end{aligned} \quad (A)$$

$$\begin{aligned} &H_3O^+ + e \xrightarrow{\text{fast}} MH + H_2O \\ &MH + MH \xrightarrow{\text{slow}} 2M + H_2 \end{aligned} \quad (B)$$

$$\begin{aligned} &H_3O^+ + e \xrightarrow{\text{slow}} MH + H_2O \\ &H_3O^+ + MH + e \xrightarrow{\text{fast}} H_2 + H_2O \end{aligned} \quad (C)$$

$$\begin{aligned} &H_3O^+ + e \xrightarrow{\text{fast}} MH + H_2O \\ &H_3O^+ + MH + e \xrightarrow{\text{slow}} H_2 + H_2O \end{aligned} \quad (D)$$

B. *Source of Proton is* H_2O

$$\begin{aligned} &H_2O + e \xrightarrow{\text{slow}} MH + OH^- \\ &MH + MH \xrightarrow{\text{fast}} H_2 + 2M \end{aligned} \quad (E)$$

$$\begin{aligned} &H_2O + e \xrightarrow{\text{fast}} MH + OH^- \\ &MH + MH \xrightarrow{\text{slow}} H_2 + 2M \end{aligned} \quad (F)$$

$$\begin{aligned} &H_2O + e \xrightarrow{\text{slow}} MH + OH^- \\ &H_2O + MH + e \xrightarrow{\text{fast}} H_2 + OH^- + M \end{aligned} \quad (G)$$

$$\begin{aligned} &H_2O + e \xrightarrow{\text{fast}} MH + OH^- \\ &H_2O + MH + e \xrightarrow{\text{slow}} H_2 + OH^- + M \end{aligned} \quad (H)$$

In alkaline solution it is also possible that the metal M_1^{z+} ion discharge is an intermediate step in the evolution reaction.

$$\begin{aligned} &M_1^{z+} + ze \xrightarrow{\text{slow}} M_1 \\ &M_1 + zH_2O \xrightarrow{\text{fast}} M_1^{z+} + zH + zOH^- \\ &MH + MH \xrightarrow{\text{fast}} H_2 + 2M \end{aligned} \quad (I)$$

$$\begin{aligned} &M_1^{z+} + ze \xrightarrow{\text{fast}} M_1 \\ &M_1 + zH_2O \xrightarrow{\text{slow}} M_1^{z+} + zH + zOH^- \\ &MH + MH \xrightarrow{\text{fast}} H_2 + 2M \end{aligned} \quad (J)$$

$$\begin{aligned} &M_1^{z+} + ze \xrightarrow{\text{fast}} M_1 \\ &M_1 + zH_2O \xrightarrow{\text{fast}} M_1^{z+} + zH + zOH^- \\ &MH + MH \xrightarrow{\text{slow}} H_2 + 2M \end{aligned} \quad (K)$$

[3] The reaction paths suggested are by no means exhaustive, e.g., it is possible that the discharge of hydroxonium ions may occur with an electrochemical desorption involving water, i.e., $H_2O + MH + e \rightarrow H_2 + OH^- + M$.

$$\begin{aligned} &M_1^{z+} + ze \xrightarrow{\text{slow}} M_1 \\ &M_1 + zH_2O \xrightarrow{\text{fast}} M_1^{z+} + zH + zOH^- \\ &H_2O + M_1H + e \xrightarrow{\text{fast}} H_2 + OH^- + M_1 \end{aligned} \quad (L)$$

$$\begin{aligned} &M_1^{z+} + ze \xrightarrow{\text{fast}} M_1 \\ &M_1 + zH_2O \xrightarrow{\text{slow}} M_1^{z+} + zH + zOH^- \\ &H_2O + M_1H + e \xrightarrow{\text{fast}} H_2 + OH^- + M_1 \end{aligned} \quad (M)$$

$$\begin{aligned} &M_1^{z+} + ze \xrightarrow{\text{fast}} M_1 \\ &M_1 + zH_2O \xrightarrow{\text{fast}} M_1^{z+} + zH + zOH^- \\ &H_2O + M_1H + e \xrightarrow{\text{slow}} H_2 + OH^- + M_1 \end{aligned} \quad (N)$$

The kinetics may be complicated by the presence of: (*a*) simultaneous reactions in which, say, two desorptive reactions proceed at the same velocity in the steady state; (*b*) dual reactions in which two stages in the evolution have virtually the same energy barrier (to within, say, 3 kcal); (*c*) linked reactions, where the energy barriers of various steps are of appreciably different heights, but the kinetics of the overall process depend upon the heights of two or more energy barriers.

It has been shown recently that discharge from water molecules in acid solutions is improbable (5). Hence, reactions *E* to *N* are likely only in alkaline solutions. The reactions *A* to *D* are the best known and the most reliable material exists by which their kinetics, developed below, may be compared with experiment. A, B, and D are commonly termed: The Slow Discharge, Atomic Hydrogen, and Electrochemical Mechanisms of the electrolytic evolution of hydrogen, respectively.

VI. The Kinetics of Specific Reaction Paths

The most important reaction paths will be considered here in some detail. It will be assumed that the adsorption of hydrogen upon the electrode is governed by a Langmuir isotherm and that the velocity of the reverse desorption reaction may be neglected at potentials not near the reversible hydrogen potential.

A. *The Source of the Protons is* H_3O^+ *and the Atomic Hydrogen Reaction is Desorptive (Paths A and B)*

1. *General Kinetic Equations*

The reactions and velocities v_1, v_2, v_3 to be considered are:

$$H_3O^+ + e \xrightarrow{v_1} MH, \quad (72)$$

$$MH \xrightarrow{v_2} H_3O^+ + e, \quad (73)$$

and

$$MH + MH \xrightarrow{v_3} H_2 + 2M \qquad (74)$$

Let a_{H^+} be the activity of hydrogen ions in the electrical double layer in gram equivalents per liter[4]; a_H be the activity of hydrogen atoms on the electrode surface in gram atoms per cm^2; and x be the fraction of the surface covered with adsorbed hydrogen (x is more rigorously defined as the fraction of the available surface covered). Then $a_H = 10^{-9}\,x$ if there are 10^{15} free spaces for adsorption per cm^2, of the electrode surface, and assuming the activity coefficient of the adsorbed hydrogen is unity it follows,

$$v_1 = k_1\, a_{H^+}(1 - x)\, \exp\left(-\frac{\Delta\phi \mathbf{F}}{2RT}\right), \qquad (75)$$

$$v_2 = k_2\, 10^{-9}\, x \exp\left(\frac{\Delta\phi \mathbf{F}}{2RT}\right), \qquad (76)$$

and

$$v_3 = k_3\, 10^{-18} x^2, \qquad (77)$$

where k_1, k_2, k_3 are specific reaction velocities, and the energy barrier of the discharge reaction is assumed to be symmetrical. $\Delta\phi = (\Delta\phi_c - \zeta)$ where $\Delta\phi_c$ is the inner potential difference of cathode and solution and ζ is the potential difference between the bulk of the solution and the plane passing through the center of the ions adjacent to the cathode surface.

In the steady state,

$$v_1 - v_2 - 2v_3 = 0. \qquad (78)$$

Solving (75), (76), (77), and (78) for x gives the real solution:

$$x = \frac{-(a_1 + a_2) + \sqrt{(a_1 + a_2)^2 + 8a_1 a_3}}{4a_3} \qquad (79)$$

where

$$a_1 = k_1 a_{H^+} \exp\left(-\frac{\Delta\phi \mathbf{F}}{2RT}\right), \qquad (80)$$

$$a_2 = 10^{-9} k_2 \exp\left(\frac{\Delta\phi \mathbf{F}}{2RT}\right), \qquad (81)$$

and

$$a_3 = 10^{-18} k_3. \qquad (82)$$

The current is, therefore,

$$i_c = 2\mathbf{F}v_3 = 2\mathbf{F}10^{-18} k_3 x^2 = 2\mathbf{F}a_3 x^2 \qquad (83)$$

$$= \frac{\mathbf{F}}{8a_3}\left[-(a_1 + a_2) + \sqrt{(a_1 + a_2)^2 + 8a_1 a_3}\right]^2. \qquad (84)$$

[4] For ease of representation the suffix H_3O^+ is replaced by H^+.

2. *Kinetics when Discharge is Rate-Determining (Path A)*

(i) *General condition for slow discharge mechanism.*—The condition is

$$10(a_1 + a_2) < a_3, \qquad (85)$$

where the factor 10 is an arbitrary limit of significance. The use of the terms "a" in the condition rather than the "k" terms provides for the possibility of changes of mechanism occurring on varying potential or hydrogen ion concentration. The linking of a_1 and a_2 by a positive sign in the condition is clear, since, by the nature of the reactions concerned, a decrease in a_2 increases x, thereby decreasing a_1 and increasing a_3: that is, a decrease in a_2 increases the probability of the slow discharge mechanism, as shown by the condition (85) above.

(ii) *Coverage of surface.*—From (85) and provided $(a_1 + a_2)^2 > 10a_2(a_2 + a_1)$, i.e.,

$$a_1 > 9a_2, \qquad (86)$$

it is easy to show that $8a_1a_3 > (a_1 + a_2)^2$. Hence using this condition in (79) it follows

$$x = \sqrt{\frac{a_1}{2a_3}}. \qquad (87)$$

(iii) *Tafel line.*—From (80), (83), and (87) it follows

$$i_c = \mathbf{F}k_1 a_{H^+} \exp\left(-\frac{\Delta\phi \mathbf{F}}{2RT}\right). \qquad (88)$$

Hence from (27), (29), and (30) for the slow discharge mechanism,

$$\alpha = 0.5; \qquad (89)$$

and, since $\lambda = 1$,

$$\beta = 0.5. \qquad (90)$$

(iv) *Effect of* pH *in pure dilute acid solution.*—Assuming that the Stern model of the electrical double layer prevails at the metal-solution interface, that the solution is dilute, that specific adsorption of ions is absent, and that the interfacial potential conditions are more than about 0.3 volts from those of the electrocapillary maximum, the following equations may be validly used,

$$a_{H^+} = (a_{H^+})_B \exp\left(\frac{-\zeta \mathbf{F}}{RT}\right), \qquad (91)$$

$$\Delta\phi_c = \Delta\phi_r + \eta, \qquad (92)$$

$$\Delta\phi_r = \frac{RT}{\mathbf{F}} \ln (a_{H^+})_B, \qquad (93)$$

and

$$\zeta = \text{Const.} + \frac{RT}{\mathbf{F}} \ln (a_{H^+})_B, \qquad (94)$$

where $(a_{H^+})_B$ is the activity of hydrogen ions in the bulk of the solution. Using these equations in (88) it is found that $\eta = \text{Const.} - \frac{2RT}{F} \ln i_c$. Therefore, overpotential is independent of the *p*H of the solution with the above mechanism under the conditions (85) and (86).

(v) *Effect of* p*H in the presence of excess neutral salt.*—In the presence of excess neutral salt (e.g., $LaCl_3$) ζ decreases to a constant value near zero. Under these conditions (91), (92), (93), and (94) may be combined to

$$\eta = \text{Const.} - \frac{2RT}{F} \ln i_c + \frac{RT}{F} \ln (a_{H^+})_B. \quad (95)$$

Equation (95) shows that under the above conditions (85) and (86), overpotential should decrease numerically by 58 mv at 20°C upon decreasing the *p*H of the solution by one unit.

(vi) *Effect of neutral salt at constant* p*H.*—From (88), (92), (93), and (94), and considering $(a_{H^+})_B$ as constant,

$$\eta = \text{Const.} - \frac{2RT}{F} \ln i_c - \zeta. \quad (96)$$

Since on addition of neutral salt to the electrolyte ζ becomes more positive and approaches zero, overpotential increases numerically.

3. *Kinetics when Atomic Combination is Rate-Determining (Path B)*

(i) *General condition for atomic hydrogen mechanism.*—Comparing with (85), the condition is

$$10a_3 < a_1 + a_2. \quad (97)$$

(ii) *Coverage of surface.*—Using condition (97) and also the condition

$$9a_2 < a_1, \quad (98)$$

and also since $\sqrt{1+n} = 1 + \frac{1}{2}n$ where n is small, it follows

$$x = \frac{a_1}{a_1 + a_2}. \quad (99)$$

(iii) *Tafel line.*—From (80), (81), (82), (83), and (99),

$$i_c = 2F10^{-18}k_3 \left[\frac{a_1}{a_1 + a_2}\right]^2 = 2Fk_3 10^{-18} \left[\frac{1}{1 + \frac{k_2 10^{-9}}{k_1 a_{H^+}} \exp\left(\frac{\Delta\phi F}{RT}\right)}\right]^2. \quad (100)$$

Evaluation of $\frac{d(\Delta\phi)}{d(\ln i_c)}$ yields

$$\frac{d(\Delta\phi)}{d(\ln i_c)} = -\frac{b}{2.303} = \frac{1 + \frac{k_2 10^{-9}}{k_1 a_{H^+}} \exp\left(\frac{\Delta\phi F}{RT}\right)}{\frac{2Fk_2 10^{-9}}{RTk_1 a_{H^+}} \exp\left(\frac{\Delta\phi F}{RT}\right)}. \quad (101)$$

Hence values of α and, therefore, of β are complex functions of potential, and can be calculated from (101) by the use of (29) and (30), taking λ as 2. Two important limiting conditions arise from (101).

Limiting condition 1:

$$\text{If} \quad \frac{k_2 10^{-9}}{k_1 a_{H^+}} \exp\left(\frac{\Delta\phi F}{RT}\right) > 10, \quad (102)$$

$$b = \frac{2.303RT}{2F} = 0.029 \quad \text{at} \quad 20°\text{C}. \quad (103)$$

Therefore,

$$\alpha = 2 \text{ and } \beta = 1, \text{ as } \lambda = 2 \quad (104)$$

Limiting condition 2:

If $\Delta\phi$ tends to $-\infty$,

$$b \to \infty, \quad (105)$$

so that

$$\alpha \to 0, \quad \text{and } \beta \to 0. \quad (106)$$

The forms of (100) corresponding to (103) and (105) are, respectively,

$$i_c = 2Fk_3 \left[\frac{k_1 a_{H^+}}{k_2}\right]^2 \exp\left(-\frac{2\Delta\phi F}{RT}\right), \quad (107)$$

and

$$i_c = 2Fk_3 10^{-18}. \quad (108)$$

Equation (108) clearly indicates the limiting current caused by the atomic combination reaction.

(iv) *Effect of* p*H in pure dilute acid solution.*—Using (91), (92), and (93) in (107) it follows

$$\eta = \text{Const.} - \frac{RT}{2F} \ln i_c. \quad (109)$$

Equation (109) indicates that with the above mechanism overpotential is independent of the *p*H of the solution. It is evident from (108) that the magnitude of the limiting current is independent of *p*H.

(v) *Effect of* p*H in the presence of excess neutral salt.*—Equation (109) shows that η is independent of ζ and, therefore, is independent of *p*H in the presence of excess neutral salt. Equation (108) shows that the limiting current is independent of the presence of neutral salt.

(vi) *Effect of neutral salt at constant pH.* η is unaffected by the presence of neutral salt (see 109).

4. *Minimum Coverage of Cathode by Hydrogen for Atomic Combination to be Desorptive*

From (16), (77), and (83),

$$i_c = 2F \frac{kT}{h} 10^{-18} x^2, \quad (110)$$

if $(\Delta G^*)_1$ is taken as zero to give a maximum velocity of combination, $\kappa = 1$, and k_1 in (16) is identified

with k_3 in (83). Hence, the least possible coverage for the atomic hydrogen reaction to maintain a current density of i_c amp/cm^2 is given by

$$x = 10^9 \sqrt{\frac{i_c h}{2\mathbf{F}kT}}. \qquad (111)$$

B. *The Source of Protons is* H_3O^+ *and the Electrochemical Reaction is Desorptive (Paths C and D)*

1. *General Kinetic Equations*

The reactions and velocities to be considered are

$$H_3O^+ + e \xrightarrow{v_1} MH, \qquad (72)$$

$$MH \xrightarrow{v_2} H_3O^+ + e, \qquad (73)$$

and

$$H_3O^+ + MH + e \xrightarrow{v_4} H_2. \qquad (112)$$

v_1 and v_2 are given by (75) and (76). v_4 is given by

$$v_4 = k_4 10^{-9} a_{H^+} x \exp\left(-\frac{\Delta\phi\mathbf{F}}{2RT}\right). \qquad (113)$$

The steady state value of x yielded by reasoning analogous to that leading to (79) is

$$x = \frac{a_1}{a_1 + a_2 + a_4}, \qquad (114)$$

where

$$a_4 = k_4 10^{-9} a_{H^+} \exp\left(-\frac{\Delta\phi\mathbf{F}}{2RT}\right). \qquad (115)$$

The current is, therefore,

$$i_c = \frac{2\mathbf{F}k_1k_4 10^{-9}(a_{H^+})^2 \exp\left(-\frac{\Delta\phi\mathbf{F}}{2RT}\right)}{(k_1 + k_4 10^{-9})a_{H^+} + k_2 10^{-9} \exp\left(\frac{\Delta\phi\mathbf{F}}{RT}\right)}. \qquad (116)$$

From (116),

$$\frac{d(\Delta\phi)}{d(\ln i_c)} = \frac{1 + \frac{k_2 10^{-9}}{(k_1 + k_4 10^{-9})a_{H^+}} \exp\left(\frac{\Delta\phi\mathbf{F}}{RT}\right)}{\frac{-\mathbf{F}}{2RT}\left[1 + \frac{k_2 10^{-9}}{(k_1 + k_4 10^{-9})a_{H^+}} \exp\left(\frac{\Delta\phi\mathbf{F}}{RT}\right)\right] - \left[\frac{\mathbf{F}k_2 10^{-9}}{(k_1 + k_4 10^{-9})a_{H^+}RT} \exp\left(\frac{\Delta\phi\mathbf{F}}{RT}\right)\right]}. \qquad (117)$$

2. *Kinetics when Discharge is Rate-Determining (Path C)*

(i) *General condition for slow discharge mechanism.*—The condition is

$$10(a_1 + a_2) < a_4. \qquad (118)$$

(ii) *Coverage of surface.*—Utilizing (118) in (114), and also from (80) and (115),

$$x = a_1/a_4 = k_1/10^{-9}k_4. \qquad (119)$$

(iii) *Tafel line.*—Condition (118) utilized in (116) gives,

$$i_c = 2\mathbf{F}k_1 a_{H^+} \exp\left(-\frac{\Delta\phi\mathbf{F}}{2RT}\right), \qquad (120)$$

which relation is very similar to that found for a rate-determining discharge reaction followed by an atomic hydrogen desorption step. Hence, $\alpha = 0.5$ and $\beta = \frac{1}{4}$ as $\lambda = 2$.

(iv) *Effect of* pH *in pure dilute acid solution*, (v) *effect of* pH *in presence of excess neutral salt*, and (vi) *effect of neutral salt at constant* pH.—These three effects are as already given in Section A, 2.

3. *Kinetics when Electrochemical Step is Rate-Determining (Path D)*

(i) *General condition for electrochemical mechanism.*—The condition is

$$10a_4 < a_1 + a_2. \qquad (121)$$

(ii) *Coverage of surface.*—Special case (*a*)

$$10a_1 < a_2. \qquad (122)$$

From (114), (121), and (122),

$$x = a_1/a_2. \qquad (123)$$

Special case (*b*)

$$10a_2 < a_1. \qquad (124)$$

From (114), (121), and (124),

$$x \simeq 1. \qquad (125)$$

(iii) *Tafel line.*—Special case (*a*). Conditions (121) and (122). From (116),

$$i_c = 2\mathbf{F}\frac{k_1}{k_2}k_3(a_{H^+})^2 \exp\left(-\frac{3\Delta\phi\mathbf{F}}{2RT}\right). \qquad (126)$$

From (27), (29), and (30) it follows that

$$\alpha = 3/2 \qquad (127)$$

$$\text{as } \lambda = 2, \quad \beta = 3/4. \qquad (128)$$

(iv*a*) *Effect of* pH *in pure dilute acid solution.*—Using (91), (92), (93), and (94) in (126) it follows

$$\eta = \text{Const.} - \frac{2RT}{3\mathbf{F}} \ln i_c. \qquad (129)$$

Hence with the above mechanism under the above conditions overpotential is independent of the pH of the solution.

(v*a*) *Effect of* pH *in the presence of excess neutral salt.*—From (91), (92), (93), and (126) and as $\zeta \to 0$ it follows that:

$$\eta = \text{Const.} - \frac{2RT}{3\mathbf{F}} \ln i_c + \frac{RT}{3\mathbf{F}} \ln (a_{H^+})_B. \qquad (130)$$

Equation (130) shows that under the above condition overpotential decreases numerically by 19 mv at 20°C upon decreasing the *p*H of the solution by one unit.

(via) *Effect of neutral salt at constant* pH.—From (91), (92), (93), and (126) and considering $(a_{H^+})_s$ as constant,

$$\eta = \text{Const.} - \frac{2RT}{3\mathbf{F}} \ln i_v - \zeta/3. \quad (131)$$

Hence, as ζ becomes more positive and approaches zero on addition of neutral salt, overpotential increases numerically.

(iiib) *Tafel line.*—Special case (*b*). Conditions (121) and (124). From (116),

$$i_c = 2\mathbf{F}k_3 a_{H^+} 10^{-9} \exp\left(-\frac{\Delta\phi\mathbf{F}}{2RT}\right). \quad (132)$$

From (27), (29), and (30) it follows that

$$\alpha = 0.5 \quad (133)$$

$$\text{as } \lambda = 2, \qquad \beta = 1/4. \quad (134)$$

(ivb) *Effect of* pH *in pure dilute acid solution,* (vb) *effect of* pH *in the presence of excess neutral salt,* (vib) *effect of neutral salt at constant* pH.—Consideration of (91), (92), (93), and (132) shows that the above three effects are as already given in Section A, 2.

C. *The Source of the Protons is Water and a Metal Cation Takes Part in the Reaction: A Special Case*

Reference to the reaction paths *E* to *N* indicates that many more possibilities exist for the mechanism of the evolution of hydrogen when the source of the protons is water than when it is the hydroxonium ion. Since little data as yet exist with which comparison may be made, the kinetics of these schemes will be formulated here only in one special case. It has been recently shown by Bockris and Watson (6) that the evolution of hydrogen at mercury cathodes from aqueous alkaline solutions involves the alkali or alkaline earth metal cation. Hence, the possibilities in this case are:

$$M^{z+} + ze \xrightarrow{\text{slow}} M/Hg \quad (a)$$

$$M/Hg + zH_2O \xrightarrow{\text{fast}} M^{z+} + zHgH + zOH^- \quad (b)$$

or,

$$M^{z+} + ze \xrightarrow{\text{fast}} M/Hg \quad (c)$$

$$M/Hg \xrightarrow{\text{fast}} M^{z+} + ze \quad (d)$$

$$M/Hg + zH_2O \xrightarrow{\text{slow}} M^{z+} + zHgH + zOH^- \quad (e)$$

In both reaction schemes desorption of hydrogen may occur by means of the reactions,

$$HgH + HgH \rightarrow H_2 + 2Hg \quad (f)$$

$$H_2O + HgH + e \rightarrow H_2 + OH^-. \quad (g)$$

It is improbable that reaction (*a*) occurs because evidence is available (7) that alkali metal deposition occurs on Hg without being accompanied by an appreciable overpotential. Reaction scheme *cdef* will, therefore, be formulated. It can be shown that very similar results are obtained for the scheme *cdeg* (6).

Let v_5 be the velocity of reaction *c*, v_6 that of *d*, v_7 that of *e*, and v_8 that of *f*. Let x_1 be the fraction of the surface of mercury covered with alkali metal atoms in the steady state and x_2 be the similar fraction for hydrogen atoms. Then,

$$v_5 = k_5 a_{H^+}(1 - x_1 - x_2) \exp\left(-\frac{z\Delta\phi\mathbf{F}}{2RT}\right), \quad (135)$$

$$v_6 = k_6 10^{-9} x_1 \exp\left(\frac{z\Delta\phi\mathbf{F}}{2RT}\right), \quad (136)$$

$$v_7 = k_7 (10^{-9} x_1)^{\frac{1}{2}} a_{H_2O}, \quad (137)$$

where x_1 is raised to the power $\frac{1}{2}$ in accordance with the experimental data of Jofa and Pechkovskaya (8) on the velocity of reaction between potassium amalgam and water. a_{H_2O} is the activity of water, and k_5–k_7 are velocity constants.

At low and medium current densities, $1 \gg x_1, x_2$. Also, in the steady state,

$$v_5 - v_6 - v_7 = 0, \quad (138)$$

$$v_7 - v_8 = 0. \quad (139)$$

According to the mechanism suggested,

$$k_5 a_{H^+} \exp\left(-\frac{z\Delta\phi\mathbf{F}}{2RT}\right) \gg k_7 10^{-9/2} a_{H_2O} \ll k_6 10^{-9} \exp\left(\frac{z\Delta\phi\mathbf{F}}{2RT}\right). \quad (140)$$

From (140) by an argument similar to that used in the derivation of (88), one obtains

$$i_c = \mathbf{F}k_7 \left(\frac{k_5}{k_6}\right)^{\frac{1}{2}} a_{H_2O}(a_{M^{z+}})^{\frac{1}{2}} \exp\left(-\frac{z\Delta\phi\mathbf{F}}{2RT}\right). \quad (141)$$

But,

$$\frac{k_5}{k_6} = \exp\left(-\frac{(\Delta G_1^*)_5 - (\Delta G_2^*)_5}{RT}\right) = \exp\left(-\frac{\Delta G_5}{RT}\right), \quad (142)$$

where ΔG_5 is the standard free energy change in reaction (*c*). Because the departure from irreversibility in (135) and (136) is small it follows that approximately,

$$\Delta G_5 = -ze_0'\mathbf{F}, \quad (143)$$

where e_0' is the reversible electrode potential for the alkali metal concerned at unit activity in mercury. Hence, from (141) and (142) and (143),

$$i_c = z\mathbf{F}a_{H_2O}\,(a_{M^{z+}})^{\frac{1}{2}}\,k_7 \exp\left(\frac{z\mathbf{F}}{2RT}\,[e_0' - \Delta\phi]\right). \quad (144)$$

A reasonably good value of e_0' can be obtained from the emf of a reversible amalgam electrode of the type M amalgam/M^{z+} ions at unit activity. If it is assumed that the interaction energy between M and Hg is included in e_0', and that it is constant over a small change of activity, then the electrode potential e_a is given by

$$e_a = e_0' + \frac{RT}{\mathbf{F}} \ln \frac{1}{C_M}, \quad (145)$$

where C_M = concentration of alkali metal M in Hg. From (145), knowing e_a experimentally, e_0' is found.

VII. Discussion of Mechanism at Hg, Ag, Ni, and Pt Cathodes

A. *Table of Distinguishing Criteria*

These are given in Table I which is based upon the general results to be found in Sections IV and VI.

B. *Numerical Calculations*

1. *General Remarks and Preliminary Calculations*

The results of calculations presented here are to be regarded as of order accuracy only. This is due to (*i*) the approximation involved both in the equations themselves and in the method of numerical application (e.g., calculation of reversible electrode potential, see below), and (*ii*) the inaccuracy of some of the experimental and theoretical data. The following results are intended to be exemplifying rather than exhaustive (e.g., throughout, the concentration of hydroxonium ions in the electrical double layer has been taken to be 10^{-1} gram equivalents per liter and no quantitative examination has been made of the effect of variation of concentration).

Evaluation of terms such as $\exp(\Delta\phi_r\mathbf{F})/RT$ has been made by expressing $\Delta\phi_r$ as the potential of the reversible hydrogen electrode with respect to the electrocapillary maximum of the metal concerned. The approximations involved in this procedure, involving the neglect of the potential difference at the interface due to adsorbed solvent dipoles, should be recognized; in comparison of rates on various metals, this error is less serious because it is

TABLE I. *Characteristics of various mechanisms of cathodic hydrogen evolution*

Characteristic of mechanism		Conditions for application		λ	With symmetrical energy barrier		$\left[\frac{\partial\eta}{\partial(\ln a_{H^+})_B}\right]_{T,i}$‡		Neutral salt effect at constant pH
					α	β	Pure soln.	+ Excess neutral salt	
Acid solution mechanisms	Slow discharge Fast atomic H (*A*)	$10(a_1 + a_2) < a_3$ $9a_2 < a_1$		1	½	½	Nil	$\frac{1-\gamma}{\gamma} \cdot \frac{RT}{\mathbf{F}}$	η more neg.
	Slow atomic H Fast discharge (*B*)	$10a_3 < a_1 + a_2$ $9a_2 < a_1$		2	2	1	Nil	Nil	Nil
	Slow discharge Fast electrochemical (*C*)	$10(a_1 + a_2) < a_4$		2	½	½	Nil	$\frac{1-\gamma}{\gamma} \cdot \frac{RT}{\mathbf{F}}$	η more neg.
	Slow electrochemical	$a_1 + a_2 > 10a_4$	$a_2 > 10a_1$	2	⅔	⅓	Nil	$\frac{1-\gamma}{1+\gamma} \cdot \frac{RT}{\mathbf{F}}$	η more neg.
	Fast discharge (*D*)		$a_1 > 10a_2$	2	½	½	Nil	$\frac{1-\gamma}{\gamma} \cdot \frac{RT}{\mathbf{F}}$	η more neg.
Alkaline solution mechanisms	Slow discharge from H_2O with either fast atomic H (*E*) or fast electrochemical from H_3O^+ (*G*)	Analogous to mechanisms with discharge from H_3O^+		1	½	½	$\frac{-2RT}{\mathbf{F}}$	$\frac{-RT}{\mathbf{F}}$	η more pos.
	Slow M/H_2O reaction Fast M^{z+} discharge Fast atomic H (*J*)	$a_1 > 10a_7 < a_4$		z	$\frac{z}{2}$	½	$\frac{-RT}{\mathbf{F}} + \frac{RT}{z\mathbf{F}} \cdot \frac{\partial \ln(a_{M^{z+}})_E}{\partial \ln(a_{H^+})_B}$ If $\gamma = 0.5$	$\frac{-RT}{\mathbf{F}}$	Nil

γ = Barrier disymmetry factor = Fraction of potential assisting forward direction of rate-determining step.
* Assuming univalent alkali metal ion.
‡ Assuming that relation $\zeta = \text{const} \pm \frac{RT}{\mathbf{F}} \ln (a_{H^+})_B$ is valid.

reasonable to assume that the dipole contributions are approximately the same at different metals.

The terms ΔG_1^*, ΔG_2^*, ΔG_3^*, and ΔG_4^* (where ΔG^* is a standard free energy of activation; 1 and 2 refer respectively to the forward and reverse directions of the discharge of hydroxonium ions; and 3 and 4 refer respectively to the forward atomic hydrogen and electrochemical desorption steps) have been obtained as follows. ΔG_1^* and ΔG_2^* have been taken from calculations by Parsons (26) of the energetics of the discharge reaction[5]. ΔG_3^* (for the atomic hydrogen desorption) will be shown below to have a value of approximately zero. ΔG_4^* (for the electrochemical desorption) cannot yet be calculated even with sufficient accuracy for the present purposes; k_n, where $n = 1$, 2, or 3 depending on the reaction concerned, has been calculated from ΔG_n^* by means of the equation,

$$k_n = \frac{kT}{h} \exp\left(-\frac{\Delta G_n^*}{RT}\right). \qquad (146)$$

TABLE II. *Certain numerical quantities at 20°C*

Cathode	Log i_0 ($a_{H^+} = 0.1$)	Reversible H potential referred to electrocapillary maximum volts	ΔG_1^* kcal	Log k_1	ΔG_2^* kcal	Log k_2	k_1/k_2
Hg	−12	+0.20	38	−15.5	23.2	−4.5	−11.0
Ag	−7	−0.046	31	−10.3	23.9	−5.0	− 5.3
Ni	−6	−0.30†	31	−10.3	23.6	−4.7	− 5.6

† Value obtained from interpolation of an observed relation between Φ and the potential of the electrocapillary maximum for a number of metals.

TABLE III. *Potential conditions for slow discharge mechanism (Path A) at 20°C*

Cathode	Condition (85): Overpotential in volts	Condition (86): Overpotential in volts
Hg	More positive than −1.4	More negative than −0.43
Ag	More positive than −0.54	All values satisfy condition
Ni	More positive than −0.29	All values satisfy condition

TABLE IV. *Surface coverage with hydrogen at various overpotentials (Path A)*

Cathode	Overpotential (volts)	−0.1	−0.3	−0.5	−0.7	−1.0	−1.5
Hg	Coverage x	$10^{-6.2}$	$10^{-5.4}$	$10^{-4.5}$	$10^{-3.4}$	$10^{-2.4}$	Satd.
Ag	Coverage x	$10^{-3.6}$	$10^{-1.7}$	$10^{-0.9}$	Satd. surface		
Ni	Coverage x	$10^{-1.5}$	$10^{-0.8}$	Saturated surface			

[5] All numerical values quoted in following sections hence depend upon the accuracy of these very approximate calculations, except for values calculated here concerning platinum.

Table II gives numerical values of some of the quantities used in the following calculations.

2. *Potential Conditions for Applicability of Slow Discharge Mechanism (Path A)*

The two conditions to be satisfied for (88) to apply are (85) and (86). Numerical application of these conditions gives the results of Table III.

3. *Coverage of Surface (x) for Slow Discharge Mechanism (Path A)*

Table IV gives the surface coverages at various overpotentials obtained by applying equation (87) at 20°C.

4. *The Value of ΔG_3^* for Atomic Hydrogen Desorption*

For smooth Pt cathodes the observed experimental slope of the Tafel line at current densities of about 10^{-2} − 10^{0} amp/cm^2 indicates that the atomic hydrogen mechanism is rate-determining. The limiting current density for this mechanism is found to be 30 amp/cm^2 in 1N aqueous acid solution (13). Substituting in (146) it follows that,

$$\Delta G_3^* = -2.5 \text{ kcal approx.}$$
$$k_3 = 10^{14.2}.$$

The correct value of ΔG_3^* can therefore be taken as about 0 kcal, the corresponding value of k_3 being $10^{12.8}$ at ordinary temperature. With the approach of saturation appreciable departures from ideality among the hydrogen atoms on the surface are likely to occur. Hence, the reaction may be somewhat slower than indicated by the value of ΔG_3^*. A low value of ΔG_3^* would be expected because the reaction concerned is a surface radical reaction. To a first approximation it is assumed that ΔG_3^* (and also k_3) are the same for all cathodes.

5. *The Value of k_1/k_2 for* Pt *Cathodes*

Utilizing the above determined value of ΔG_3^* (or k_3) in (100), (80), and (81) referred to the special case of the exchange current i_0 so that $\eta = 0$, it follows that

$$k_1/k_2 = 10^{-14.4}.$$

6. *Calculation of the Course of the Tafel Line for the* Pt *Cathode*

Substituting the above obtained values[6] for k_3 and k_1/k_2 in (100) gives the complete Tafel equa-

[6] In this calculation the experimental value of k_3 i.e. $10^{14.2}$, has been used in order that the limiting current shall appear at 30 amp/cm^2. If the value of $k_3 = kT/h = 10^{13.8}$ is used the limiting current appears at 1 amp/cm^2. In either case the form of the calculated Tafel line remains the same. The values of log i_0 and the reversible hydrogen potential referred to the electrocapillary maximum have been taken as −3, and +0.28 volts, respectively.

tion for hydrogen evolution from aqueous 0.1*N* HCl. The two limiting slopes deduced in (103) and (105) are shown (see Fig. 3).

7. *Minimum Coverage of Cathode by Hydrogen for the Atomic Hydrogen Mechanism to be Desorptive*

The required minimum coverage is obtained from (111) as a function of current and is given in Table V.

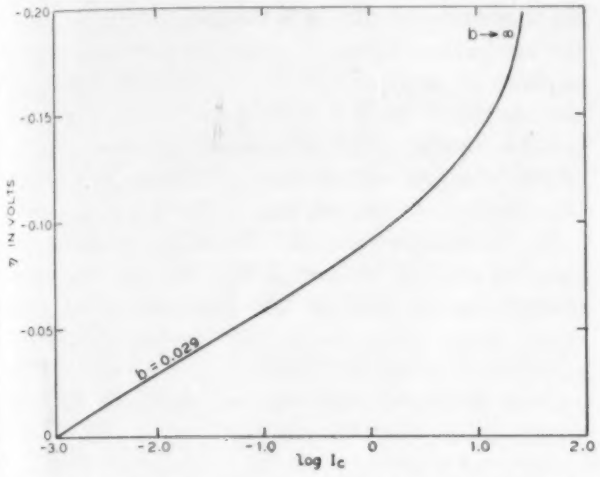

FIG. 3. Calculated course of Tafel line for the smooth platinum cathode in 0.1*N* HCl at 20°C (assuming path B is rate determining).

TABLE V. *Minimum coverage for atomic hydrogen desorption*

i_c amp/cm²	x
10^{-12}	10^{-6}
10^{-9}	$10^{-4.5}$
10^{-6}	10^{-3}
10^{-3}	$10^{-1.5}$
1	1 (satd. surface)
10	Saturated surface

TABLE VI. *Potential conditions for atomic hydrogen mechanism (Path B) at 20°C*

Cathode	Condition (97) Overpotential in volts	Condition (98) Overpotential in volts
Hg	More negative than −1.65	More positive than −0.43
Ag	More negative than −0.78	All values satisfy condition
Ni	More negative than −0.64	All values satisfy condition

8. *Potential Conditions for Applicability of Atomic Hydrogen Mechanism (Path B)*

The two conditions to be satisfied for (100) to apply are (97) and (98). Numerical application of these conditions gives the results of Table VI. For smooth platinum cathodes, the use of the experimental values of k_1/k_2 in condition (97) shows that for the atomic hydrogen mechanism to apply at $\eta = 0$, k_1 must be $> 10^{-6.8}$.

9. *Conditions for Applicability of Slow Discharge Mechanism (Path C)*

The condition to satisfy for (120) to apply is (118). However, in this case it is not possible to calculate sufficiently accurate values of k_4 or ΔG_4^* for potential conditions to be found. Limiting values for k_4 and ΔG_4^* when Path C is rate-determining have therefore been calculated and are given in Table VII.

Calculations of ΔG_4^* by statistical mechanical means are complex and have only been attempted by Conway (9) in the case of Ag. He finds $(\Delta G_4^*)_{Ag} \simeq$ 9 kcal, in which case, therefore, discharge would be rate-determining if the desorption were electrochemical.

TABLE VII. *Limiting values of k_4 and ΔG_4^* for Path C to be rate-determining at 20°C*

Cathode	k_4 limit for Path C, Rate-determining	ΔG_4^* limit for Path C, Rate-determining
Hg	When η more negative than −0.43 volt k_4 must be $> 10^{-5.5}$	When η more negative than −0.43 volt ΔG_4^* must be < 24 kcal
Ag	k_4 must be $> 10^{-0.3}$ at all overpotentials	ΔG_4^* must be < 17 kcal at all overpotentials
Ni	As for Ag	As for Ag

TABLE VIII. *Maximum values of surface coverage for Path C to be rate-determining*

Cathode	Maximum value of x
Hg	10^{-1} at overpotentials more negative than −0.43 volt
Ag	10^{-1} at all overpotentials
Ni	As for Ag

10. *Coverage of Surface for Slow Discharge Mechanism (Path C)*

The coverage x is given by (119), and by using the limiting values of k_4 given in Table VII a maximum value of x can be calculated (see Table VIII).

11. *Conditions for Applicability of Electrochemical Mechanism (Path D)*

The condition to satisfy for Path D to be rate-determining is (121), but since k_4 and ΔG_4^* are not known accurately, Table IX gives limiting values of these quantities (cf. Subsection 9).

12. *Potential Conditions for Applicability of $\alpha = \frac{3}{2}$ and $\alpha = \frac{1}{2}$ when Path D is Rate-Determining*

The condition to be satisfied for α to have values of $\frac{3}{2}$ and $\frac{1}{2}$ are, respectively, (122) and (124). The potential conditions appropriate to both values of α are given in Table X.

13. *Coverage of Surface for Electrochemical Mechanism (Path D)*

The required coverage is found from (114) neglecting a_4 and is as follows:

Hg: Surface saturated at overpotentials more negative than −0.37 volt,

Ag: } Surface saturated at all overpotentials.
Ni: }

C. *Estimate of Rate-Determining Reactions at* Hg, Ag, Ni, *and* Pt *Cathodes According to Evidence at present Available*

1. *Mercury*

(i) *In Acid Solution.*—The value of $\alpha = \frac{1}{2}$ shows that the mechanism must be *A*, *C*, or *D*. At low current densities the velocity of the atomic combination is too great for mechanism *D* to occur (see Section VII, B, 11). It is therefore highly improbable that this mechanism occurs at all on mercury because a change to it at higher current densities would involve a change in the value of i_0 and this is not observed. Further, according to the conclusion of Section (VII, B, 13), if *D* were operative, the surface of the mercury would be saturated with adsorbed hydrogen at all potentials accessible to experiment, and this is contrary to evidence concerning the variation of the interfacial tension of mercury-solution interfaces with *p*H (11). According to the results of Section (VII, B, 12), mechanism *D* with a value of $\alpha = \frac{3}{2}$ would occur up to an overpotential of −0.3 volt (corresponding to a current density of about 10^{-9} amp/cm^2) if electrochemical desorption were the rate-determining reaction. Measurements in this current density region have been made (12) and do indeed show an increase in the value of α. Here, however, the continuous increase of α with decreasing current density probably indicates the presence of slight trace impurities in the mercury used (to which traces the kinetics of the electrode reaction would be very sensitive at the very low current densities involved).

TABLE IX. *Limiting values of k_4 and ΔG_4^* for Path D to be rate-determining at 20°C*

Cathode	k_4 limit for Path *D*, Rate-determining	ΔG_4^* limit for Path *D*, Rate-determining
Hg	When η more negative than −0.43 volt k_4 must be $< 10^{-7.5}$	When η more negative than −0.43 volt ΔG_4^* must be > 27 kcal
Ag	k_4 must be $< 10^{-2.3}$ at all overpotentials	ΔG_4^* must be > 20 kcal at all overpotentials
Ni	As for Ag	As for Ag

TABLE X

Cathode	Condition for $\alpha = 3/2$	Condition for $\alpha = 1/2$
Hg	η more positive than −0.32 volt	η more negative than −0.43 volt
Ag	No value of η	All values of η
Ni	No value of η	All values of η

The mechanism is hence probably *A* or *C*. According to the results of Sections (VII, B, 4 and 8), the mechanism cannot be *A* above a current density of about 30 amp/cm^2 and below about 10^{-8} amp/cm^2, outside which limits it must therefore be *C*. It is not possible to distinguish at present between *A* and *C* at intermediate current densities although for both the rate-determining reaction is the discharge step.

(ii) *In alkaline solution.*—As shown in the special case worked out in Section (VI, 6), the rate-determining reaction here is the combination of alkali metal atoms with water. An implication of this mechanism is that it would give rise to a limiting current density at high current densities, but this aspect is as yet unexamined.

2. *Silver in Acid Solution*

The value of α (9, 13) shows that the mechanism must be *A*, *C*, or *D*. The results of Section (VII, B, 2) show that mechanism *A* cannot occur at overpotentials more negative than −0.54 volt, and furthermore is unlikely at high current densities since no limiting current is detectable up to current densities of 150 amp/cm^2 (13). If the mechanism is *D*, Section (VII, B, 12) shows that α must equal $\frac{1}{2}$ as is observed. A determination of λ (14) yields the value 1 which favors mechanism *A*; and statistical mechanical calculations by Conway (9) have shown that ΔG_4^* is about 9 kcal, whereas for mechanism *D* to occur ΔG_4^* must be >20 kcal. Effect of *p*H is complex but can be brought into better accord with *A* or *C* if Stern's equations for the dependence of electrokinetic potential on concentration are developed fully.

3. *Nickel*

(i) *In acid solution.*—The value of α shows that the mechanism must be *A*, *C*, or *D* (9, 10, 15). Determination of λ is difficult since the Tafel line is of the dissolution type (see Fig. 1) and at intermediate current densities in strongly acid solutions ($>N/2$) the dissolution of the metal partially obscures *p*H and salt effects. Azzam and Bockris have shown (13) that a limiting current occurs at about 1 amp/cm^2 which supports mechanism *A*. The absence of *p*H effects at concentrations below $N/100$ also supports this mechanism. The results of Section

(VII, B, 2) show that mechanism *A* cannot take place at overpotentials more negative than −0.3 volt, and it is interesting to note that the Tafel line begins to attain a limiting current at about this potential when measurements are made using a fresh cathode surface (10).

(ii) *In alkaline solution.*—The coefficient α is $\frac{1}{2}$ and λ is observed to be 1 (10), which indicates that mechanism *E* or *G* is operative. This is confirmed by the interpretation of the observed *p*H effects.

4. *Smooth Platinum in Acid Solution*

The value of α at intermediate current densities indicates that the mechanism is *B* (16). The mechanism at current densities above the limiting current density may be *C* or *D*, but is probably *D* owing to the saturation of the surface with adsorbed hydrogen at the limiting current density.

VIII. Summary of Some Recent Advances

The controversy concerning the value of *b* in the Tafel equation now seems resolved experimentally as follows. If the solutions are pure, *b* is not (except transiently at a limiting current) greater than about 0.13, i.e., $\beta > 0.45/\lambda$. This fact confirms that the energy barrier for the discharge reaction is usually nearly symmetrical and is in accordance with the equations formulated in Section (VI). Higher values of *b* are probably connected with a distortion of the energy barrier (the position of the transition state complex being displaced toward the electrode) due to the specific adsorption of poisons on the electrode.

The realization of the use of λ as a distinguishing criterion of mechanism, and its intensive statistical application, has made available a criterion of greater power than previously existed.

Knowledge of ΔH_0^* and the potential of the electrocapillary maximum aid application of the quantitative conditions established above.

In recent years, it has been suggested (17) that prototropic transfer of hydrogen from water in the solution to water adsorbed on the electrode, and also (18) that the atomic hydrogen desorption replaced at higher current densities by electrochemical desorption are the main rate-determining reactions to be considered for the hydrogen evolution reaction. Evidence in favor of the first was based mainly upon the constancy of the factor *B* for various electrolyte concentrations and for a few metals. Consideration of (67) shows that the first requirement would be expected for any mechanism, however, and it has in any case been shown in an earlier section of this paper that a sufficiently accurate experimental determination of *B* is prohibitively difficult [see also Butler (19)]. In order that the prototropic transfer theory can yield a satisfactory theory of *p*H effects and of reversible electrode potentials an unusual structure of the double layer has to be assumed (20). Forecasts made upon this basis of similarities between hydrogen and oxygen overpotentials have also not been confirmed (27). The second theory (18) suffers the fundamental disadvantage that it involves the formulation of the kinetic processes at working hydrogen electrodes in terms of equations applicable only under equilibrium conditions; it is impotent in indicating expected *p*H and salt effects; and the explanation suggested for different values of *b* is based on experimental results which are not in accord with those obtained using very pure solutions.

Lastly, a quantitative, statistical mechanical formulation of the discharge reaction from both hydroxonium ions and water has recently been made (5). This work indicates rates of the discharge reaction in good accord with those experimentally observed on the two electrode materials considered (Hg and Ni). There also appears to be only a very small probability that discharge can proceed from water molecules in acid solution.

Acknowledgment

Thanks are due to Dr. R. Parsons for critical discussion and to Dr. R. G. H. Watson for verification of the numerical calculations.

Any discussion of this paper will appear in a Discussion Section, to be published in the December 1952 issue of the Journal.

REFERENCES

1. J. O'M. Bockris and B. E. Conway, *Trans. Faraday Soc.*, **45**, 989 (1949).
2. A. M. Azzam, J. O'M. Bockris, B. E. Conway, and H. Rosenberg, *Trans. Faraday Soc.*, **46**, 918 (1950).
3. J. O'M. Bockris and B. E. Conway, *J. Sci. Instruments*, **25**, 283 (1948).
4. J. O'M. Bockris, *Chem. Revs.*, **3**, 561 (1948).
5. R. Parsons and J. O'M. Bockris, *Trans. Faraday Soc.*, **47**, 914 (1951).
6. J. O'M. Bockris and R. G. H. Watson, *J. chim. phys.*, **49**, 1 (1952).
7. J. Heyrovsky, *Disc. Faraday Soc.*, **1**, 212 (1947).
8. J. Jofa and Z. B. Pechkovskaya, *Doklady Akad. Nauk. S.S.S.R.*, **59**, 265 (1948).
9. B. E. Conway, Thesis, University of London (1949).
10. J. O'M. Bockris and E. C. Potter, *J. Chem Phys.*, March (1952).
11. A. N. Frumkin, *Acta Physicochim. U.R.S.S.*, **18**, 23 (1943).
12. F. P. Bowden and K. E. W. Grew, *Disc. Faraday Soc.*, **1**, 86 (1947).
13. A. M. Azzam and J. O'M. Bockris, *Nature*, **165**, 403 (1950).

14. E. C. Potter, Unpublished results.
15. P. Lukovtsev, S. Lewina, and A. N. Frumkin, *Acta Physicochim. U.R.S.S.*, **11**, 21 (1939).
16. A. M. Azzam, Thesis, University of London (1949).
17. H. Eyring, S. Glasstone, and K. J. Laidler, *J. Chem. Phys.*, **7**, 1053 (1939).
18. A. Hickling and F. W. Salt, *Trans. Faraday Soc.*, **38**, 474 (1942).
19. J. A. V. Butler, *J. Chem. Phys.*, **9**, 279 (1941).
20. G. E. Kimball, S. Glasstone, and A. Glassner, *J. Chem. Phys.*, **9**, 91 (1941).
21. J. Horiuti and M. Ikusima, *Proc. Imp. Acad. Tokyo*, **15**, 39 (1939).
22. B. Kabanov and J. Jofa, *Acta Physicochim. U.R.S.S.*, **10**, 616 (1939).
23. J. N. Agar, *Disc. Faraday Soc.*, **1**, 81 (1947).
24. J. A. V. Butler, *Trans. Faraday Soc.*, **28**, 379 (1932).
25. P. Lukovtsev and S. Lewina, *J. Phys. Chem. U.S.S.R.*, **21**, 599 (1947).
26. R. Parsons, *Z. Elektrochem.*, **55**, 111 (1951).
27. A. Hickling and S. Hill, *Disc. Faraday Soc.*, **1**, 236 (1947).